

**BIOPHYSICAL INVESTIGATION OF THE EFFECTS OF ANTIOXIDANTS ON
NORMAL AND DIABETIC RAT BONE TISSUES AT MOLECULAR LEVEL**

A THESIS SUBMITTED TO
THE GRADUATE SCHOOL OF NATURAL AND APPLIED SCIENCES
OF
MIDDLE EAST TECHNICAL UNIVERSITY

BY

HANDAN BOYAR

IN PARTIAL FULFILLMENT OF THE REQUIREMENTS FOR THE DEGREE
OF
DOCTOR OF PHILOSOPHY
IN
BIOLOGY

JUNE 2004

Approval of the Graduate School of Natural and Applied Sciences

Prof. Dr. Canan ÖZGEN
Director

I certify that this thesis satisfies all the requirements as a thesis for the degree of Doctor of Philosophy.

Prof. Dr. Semra KOCABIYIK
Head of the Department

This is to certify that we have read this thesis and that in our opinion it is fully adequate, in scope and quality, as a thesis for the degree of Doctor of Philosophy.

Prof. Dr. Feride SEVERCAN
Supervisor

Examining committee members

Prof. Dr. Meral YÜCEL (METU, BIOCHEM.) _____

Prof. Dr. Belma TURAN (ANKARA UNIV., BIOPHYS.) _____

Prof. Dr. Mesude İŞCAN (METU, BIOCHEM.) _____

Prof. Dr. Nuhan PURALI (HACETTEPE UNIV., BIOPHYS.) _____

Prof. Dr. Feride SEVERCAN (METU, BIO.) _____

I hereby declare that all information in this document has been obtained and presented in accordance with academic rules and ethical conduct. I also declare that, as required by these rules and conduct, I have fully cited and referenced all material and results that are not original to this work.

Handan BOYAR

Signature:

ABSTRACT

BIOPHYSICAL INVESTIGATION OF THE EFFECTS OF ANTIOXIDANTS ON NORMAL AND DIABETIC RAT BONE TISSUES AT MOLECULAR LEVEL

Boyar, Handan

Ph.D., Department of Biology

Supervisor: Prof. Dr. Feride Severcan

June 2004, 148 pages

In the first part of this study, the effect of diabetes mellitus on the long bones (femur and tibia) of the streptozocin induced diabetic rats and the effect of selenium (Se) treatment on these bones are investigated at molecular level by Fourier transform infrared (FTIR) spectroscopy, light and electron microscopy. In the second part of this study, the effect of selenium and vitamin E deficiency or selenium toxicity on rat bones have been studied by FTIR spectroscopy.

The results of the first part of the present study revealed that the changes observed in the mineral and matrix phases of diabetic bones, briefly, the increase in the mineral crystal size, the decrease in the acid phosphate and carbonate content, the increase in the ratio of pyridinoline [Pyr] cross-links to dihydroxylysinonorleucine [DHLNL] cross-links present in collagen I of the bone tissue as well as the increase in the lipid to protein ratio of the matrix are quite similar to those seen in osteoporotic patients and animal models and confirms the evidence of diabetic osteoporosis. Histologic studies carried out with light and electron microscopy supported these findings. FTIR spectroscopic analysis revealed that sodium selenite treatment had some restoring effects on the deviated properties of the microstructure of diabetic bones.

The results of the second part of this study revealed that the deficiency of selenium led to increase in the crystal size of the bone minerals, decreases in acid phosphate and labile carbonate content and increase in the Pyr to DHLNL ratio as in the case of diabetic bones. These results can be indicative of the importance of selenium in glucose metabolism. The results of Se excess group are similar to those of Se deficient group except that toxic amount of selenium led to increase in the relative amount of acid phosphate. This can affect the pH of the mineral environment and lead to deformation of the bone tissue. It can be concluded from FTIR spectroscopic and light microscopic findings that both antioxidant deficient and excess diets cause almost similar defects in the mineral matrix phases of rat long bones.

Overall results may reflect the importance of antioxidants for human life and if they are used in proper amounts they can be preventive for the complications of diabetes seen in bones as well as other organs. However, further investigations are necessary for the therapeutic usage of selenium, since the treatment of control group rat femurs with sodium selenite led to some structural defects.

Keywords: Diabetes Mellitus, Bone, Antioxidant, FTIR Spectroscopy, Microscopy

ÖZ

ANTİOKSİDANLARIN NORMAL VE DİYABETİK SİÇAN KEMİK DOKULARINA ETKİLERİNİN MOLEKÜLER DÜZEYDE BİYOFİZİKSEL OLARAK ARAŞTIRILMASI

Boyar, Handan
Doktora, Biyoloji Bölümü
Tez Danışmanı; Prof. Dr. Feride Sevencan

Haziran 2004, 148 sayfa

Bu çalışmanın ilk kısmında; diabetes mellitus ve selenyum tedavisinin, streptozotosin muamelesi ile diyabet oluşturulmuş sıçanların uzun kemikleri (femur ve tibia) üzerine etkileri Fourier Dönüşüm Kızıl Ötesi (FTIR) spektroskopisi, ışık ve elektron mikroskopları ile moleküler düzeyde incelenmiştir. Çalışmanın ikinci bölümünde ise, selenyum ve vitamin E eksikliği ya da selenyum toksisitesinin sıçan kemikleri üzerine etkileri FTIR spektroskopisi ile çalışılmıştır.

Çalışmanın ilk kısmında; diyabetik sıçan kemiklerinin mineral ve matriks kısımlarında değişiklikler gözlenmiştir. Bu değişiklikler kısaca, mineral kristal büyüklüğünde artış, asit fosfat ve karbonat içeriğinde azalma, kemik dokunun kollajen I kısmında bulunan payridinolinin (Pyr) çapraz bağının dihidroksilizinonorlösin (DHLNL) çapraz bağına oranında artış, ve bununla birlikte kemik dokunun matriks kısmı için lipidin proteine oranında artış osteoporotik hastalarda ve hayvan modellerindeki sonuçla oldukça benzerdir. Bu sonuçlar, diyabetik osteoporozisin varlığını kanıtlamaktadır. Ayrıca ışık ve elektron mikroskopları ile yapılan histolojik çalışmalar da söz konusu sonuçları desteklemektedir. FTIR spektroskopisi analizlerinden sodyum selenit tedavisinin diyabetik kemiklerin anormal özellik gösteren mikroyapılarında bazı onarıcı etkilere sahip olduğu ortaya çıkmıştır.

Çalışmanın ikinci kısmından elde edilen sonuçlar göstermiştir ki; selenyum eksikliği kemik minerallerinin kristal büyüklüğünde artışa, asit fosfat ve kararsız karbonat miktarında azalmaya, payridinolinin dihidroksilizinonrlösine oranında ise artışa sebep olmaktadır. Bu sonuçlar selenyumun glikoz metabolizmasındaki önemini bir göstergesi olabilir. Selenyum fazlalığı gösteren grubun sonuçlarının, selenyumun toksik etkisinin asit fosfat artışına sebep olması dışında selenyum eksikliği sonuçları ile benzer olduğu ortaya çıkmıştır. Bu olay kemik dokunun deform olmasına ve asidik özelliğinin değişmesine neden olabilir. FTIR spektroskopisi, ışık ve elektron mikroskobu çalışmalarından elde edilen bulgulara göre; antioksidan bakımından eksik ve fazla günlük besin içi uzun kemiklerinin mineral kısmında benzer anormalliklere neden olmaktadır.

Elde edilen bütün sonuçlar antioksidanların insan yaşamı için önemini ve eğer uygun miktarlarda kullanılırsa, diyabet hastalığının kemiklerde ve ayrıca diğer organlarda neden olacağı komplikasyonları önleyebilme potansiyeline sahip olabileceklerini gösterebilir. Fakat, sodyum selenit muamele edilmiş kontrol grubu içi femur kemiklerinde bazı yapısal bozukluklar gözlemediğinden konuya ilgili ileri düzeyde çalışmalar selenyumun tedavi amaçlı kullanımı için gereklidir.

Anahtar kelimeler: Diabetes Mellitus, Kemik, Antioksidan, FTIR Spektroskopisi, Mikroskopi

To my parents, Gülseren-Suat BOYAR

ACKNOWLEDGEMENTS

I would like to express my deepest gratitude to my supervisor Prof. Dr. Feride SEVERCAN for her valuable guidance, patience, encouragement and supervision throughout this thesis study.

I am thankful to Prof. Dr. Belma TURAN and Prof. Dr. Mesude İŞCAN for their guidance and valuable suggestions during this study.

I would like to thank to Ankara University Medical Faculty Department of Biophysics members, under the supervision of Prof. Dr. Belma TURAN, for the preparation of bone samples that which were used in this study.

I would like to extend my thanks to Ankara University Medical Faculty Department of Histology and Embryology for the light and electron microscopic analysis of the bone samples used in this study.

I would like to thank Assoc. Prof. Dr Engin ÖZDAŞ and his assistant Bora KALKAN for the x-ray diffraction analysis of bone samples.

I am also thankful to Prof Dr. Meral YÜCEL and Prof. Dr. Nuhan PURALI for their suggestions, criticism and guidance.

Many thanks go to Prof Dr. Mete SEVERCAN for his patience and helps throughout my Msc. and PhD. thesis studies.

I would like to thank Graduate School of Natural and Applied Sciences for the support they provided (Project Number BAP (AFP)-2001-07-02-00-75) and Republic of Turkey Prime-Ministry State Planning Organisation, for their funding through several projects.

Special thanks to my parents Gülseren-Suat BOYAR for their endless patience, support and understanding during my studies.

My special thanks also go to Sevgi GÖRGÜLÜ, Banu AKKAŞ, Dr. Neslihan Toyran AL-OTAIBI, Dr. Güvenç GÖRGÜLÜ and Havva DİNÇ for their helps, support and friendship during my studies.

I would like to thank all my lab-mates in Molecular Biophysics Laboratory for their supports and friendship.

Many thanks go to my brother Hakan BOYAR and his family for their encouragement during my study.

My gratitude also go to Education Specialist Şevki KARACA in Educational Research and Development Directorate of Ministry of National Education for his continuous supports and encouragements throughout this study.

I would like to extend my thanks to Republic of Turkey Prime-Ministry State Planning Organisation European Union Education and Youth Programmes Center President Nuri BİRTEK for his support and understanding during the preparation of this thesis.

Handan BOYAR

TABLE OF CONTENTS

ABSTRACT	iv
ÖZ	vi
DEDICATION	viii
ACKNOWLEDGEMENTS	ix
TABLE OF CONTENTS	xi
LIST OF TABLES	xiv
LIST OF FIGURES	xvi
LIST OF ABBREVIATIONS	xix

CHAPTER

1. INTRODUCTION	1
1.1. Structure of Bone.....	1
1.1.1 Bone as an Organ: Macroscopic Organization	1
1.1.2. Bone as a Tissue: Microscopic Organization)	4
1.1.2.1. Bone Mineral and Matrix	4
1.1.2.2. Cellular Organizations within the Bone Matrix	8
1.1.3 Mineral Formation in Bone Tissue.....	10
1.2 Diabetes Mellitus.....	11
1.2.1 Insulin and Diabetes Mellitus.....	11
1.2.2 Experimental Models of Diabetes	14
1.2.2.1 Chemical Diabetes.....	14
1.2.3 Mechanisms Involved in Diabetic Bone Loss	15
1.3 Selenium	17
1.3.1 Basic Features of Selenium	17
1.3.2 Selenium Chemistry	18
1.3.3 Selenium Deficiency and Toxicity in Human Population.....	18
1.3.4 Effects of Selenium on Glucose Metabolism and Diabetes	21

1.4 Infrared Spectroscopy	23
1.4.1 The Basic Theory of Light Absorption by Molecules	23
1.4.2 Basis of Infrared Spectroscopy	25
1.4.3 Fourier Transform Infrared (FTIR) Spectroscopy	28
1.4.4 Advantages of Fourier Transform Infrared Spectroscopy	29
1.5 Scope and Aim of the Study	30
2. MATERIALS AND METHODS.....	32
2.1 Reagents	32
2.2 Preparation of Experimental Animals	32
2.2.1 Diabetes Induction and Selenium Treatment for Diabetes and Control Group Rats.....	32
2.2.1.1 Formation of Control Group.....	33
2.2.1.2 Formation of Streptozotocin-Induced Diabetic Group.....	33
2.2.1.3 Formation of Selenium Treated Diabetic Group.....	34
2.2.1.4 Formation of Selenium Treated Control Group	34
2.2.2 Induction of Selenium Deficiency and Toxicity.....	34
2.2.2.1 Contents of Diets and Feeding Procedure of Animals	35
2.3 FTIR Spectroscopic Measurements	35
2.3.1 Preparation of Control, Diabetic and Se Treated Control and Diabetic Bone Samples.....	35
2.3.2 Preparation of Bone Samples Taken from Selenium and Vitamin E Deficient and Selenium Excess Group Rats	36
2.4 Data Analysis	36
2.5 X-ray Diffraction Analysis	39
2.6 Light Microscopy Analysis.....	39
2.7 Electron Microscopy Analysis.....	40
2.8 Statistics	40
3. RESULTS	41
3.1 General Findings Related with the Animals	41
3.1.1. Effects of Sodium Selenite Treatment on Body Weight and Blood Glucose Levels of Control and Experimental Group Rats.....	41

3.1.2 Effects of Antioxidant Deficiency and Excess on Some of the Physical and Biochemical Characteristics of Rats	44
3.2 FTIR Spectroscopic Investigation of Bone Samples.....	45
3.2.1 FTIR Spectroscopic Analysis to Determine the Effects of Selenium on Diabetic Bone Samples.....	51
3.2.1.1 ν_4 Phosphate Bending Region	51
3.2.1.2 ν_1 , ν_3 Phosphate Stretching Region	55
3.2.1.3 ν_2 Carbonate (CO_3^{2-}) Region	62
3.2.1.4 Amide I Region	65
3.2.1.5 Mineral to Matrix and Carbonate to Phosphate Ratios	68
3.2.1.6 C-H Stretching Region	69
3.3 FTIR Spectroscopic Investigation of Bone Samples Taken From Selenium and Vitamin E Deficient or Selenium Excess and Vitamin E Adequate Group Rats	77
3.3.1 ν_4 Phosphate Bending Region	77
3.3.2 ν_1 , ν_3 Phosphate Stretching Region.....	79
3.3.3 ν_2 Carbonate (CO_3^{2-}) Region	80
3.3.4 Amide I Region.....	82
3.3.5 Mineral to Matrix and Carbonate to Phosphate Ratios	84
3.4 Powder X-Ray Diffraction Analysis of Normal, Diabetic and Selenium Treated Normal and Diabetic Rat Bone Samples.....	84
3.5 Light and Electron Microscopic Investigation of Control, Diabetic and Selenium Treated Control and Diabetic Group Rat Bone Ultra-structures	89
3.5.1 Light Microscopic Investigations	89
3.5.2 Electron Microscopic Investigations	92
3.6 Light Microscopic Investigation of Rat Bones Fed on Antioxidant Deficient and Excess Diet	96
4. DISCUSSION	98
5. CONCLUSION	114
REFERENCES	116
CURRICULUM VITAE.....	142

LIST OF TABLES

TABLE

1. The body weights for control (C), diabetes (D), diabetes + Se (DS) and control + Se (CS) groups	43
2. The blood glucose levels (mg/dl) for control, diabetes, diabetes + Se and control + Se groups	43
3. The effects of dietary selenium and vitamin E on body weight and plasma selenium and vitamin E contents.....	44
4. Major absorptions in FTIR spectrum of synthetic highly crystalline hydroxyapatite and/or of rat bone tissue in the 4000-400 cm ⁻¹ region.....	47
5. The partial peak areas of each of the five sub-bands calculated from the curve-fitting analysis results of the ν_4 PO ₄ ³⁻ bending band	54
6. Peak areas of sub-bands obtained from curve-fitting analysis of the ν_1 , ν_3 phosphate stretching region of the FTIR spectra for the femurs and the tibias of control and experimental groups.....	58
7. Crystal sizes of control, diabetes, diabetes + Se and control + Se group femurs and tibias	61
8. ν_2 CO ₃ ²⁻ spectral region curve-fitting analysis results.....	64
9. 1660 : 1690 ratio calculated from curve-fit spectra of control, diabetes, diabetes + Se and control + Se group femurs and tibias	67
10. Mineral to matrix ratios calculated for the femurs and tibias of control, diabetes, diabetes + Se and control + Se groups	68
11. Carbonate to phosphate ratios calculated for the femurs and tibias of control, diabetes, diabetes + Se and control + Se groups	69
12. Lipid to protein ratios calculated for the femurs and tibias of control, diabetes, diabetes + Se and control + Se groups.....	73

13. Lipid to protein ratios calculated from the curve-fitting analysis of FTIR spectra of the femurs and tibias of control, diabetes, diabetes + Se and control + Se (CS) groups	77
14. The mean partial peak areas obtained from curve-fitting analysis of the ν_4 PO_4^{3-} bending region of the FTIR spectra of femurs and tibias of control, Se and vitamin E deficient and Se excess, vitamin E adequate group rats.	79
15. The mean crystal size (\AA) values obtained from the curve-fitting analysis of the ν_1 , ν_3 PO_4^{3-} stretching ($900\text{-}1200 \text{ cm}^{-1}$) region.....	80
16. For control, deficient and excess groups, the partial areas obtained from curve-fitting analysis of the FTIR spectra in the ν_2 carbonate region.....	81
17. The variations in $1660 : 1690$ ratios for the femurs and tibias of control, deficient and excess group rats	83
18. Mineral : matrix and carbonate : phosphate ratios for the femurs and the tibias of the control, Se and vitamin E deficient, Se excess, vitamin E adequate group rats.	84
19. Mineral crystal sizes calculated by using Scherrer equation for the femurs and tibias of control, diabetes, diabetes + Se and control + Se groups	89

LIST OF FIGURES

FIGURE

1. The skeletal system of the rat	2
2. Structure of long bones	3
3. The structure of the pyridinoline and pyrrole cross	6
4. A schematic representation of an osteoblast cell.....	8
5. A schematic representation of an osteoclast celldrews	10
6. Typical energy-level diagram.....	25
7. Stretching and bending vibrations	26
8. Symmetric and asymmetric stretching vibrations.....	26
9. Types of bending vibrations	27
10. Out-of-plane bending and in-plane bending vibrations.....	27
11. The components of an FTIR spectrometer.....	29
12. Variation of body weights within the experimental period.....	42
13. Variation of blood glucose levels within the experimental period.....	42
14. Typical FTIR spectrum of hydroxyapatite and of a normal rat femur in 4000-435 cm ⁻¹ spectral region	46
15. Typical FTIR spectrum of hydroxyapatite and of a normal rat femur in 1800 - 435 cm ⁻¹ spectral region	49
16. Curve-fitting analysis of the $\nu_4 \text{PO}_4^{3-}$ bending region	52
17. The means of partial peak areas obtained from curve-fitting analysis of the $\nu_4 \text{PO}_4^{3-}$ bending region.....	53

18. Typical FTIR spectrum of rat femur in PO_4^{3-} stretching spectral region.....	56
19. Bar diagram illustrating mean of crystal sizes of control, diabetes, diabetes + Se and control + Se group femurs and tibias.....	61
20. Comparison of the spectra of poorly crystalline control and experimental group femurs, with highly crystalline synthetic hydroxyapatite in phosphate stretching region (900-1200 cm^{-1}).....	62
21. Curve-fitting analysis of the $\nu_2 \text{CO}_3^{2-}$ region (850-890 cm^{-1}).....	63
22. A typical FTIR spectrum of ground rat femur in the Amide I region and its underlying sub-bands obtained from curve-fitting analysis	66
23. Comparison of the 1660 to 1690 cm^{-1} peak area ratio for the femurs and tibias of control, diabetes, diabetes + Se and control + Se group rats.....	67
24. FTIR spectra in 2800-3050 cm^{-1} spectral region for control and experimental group rat femurs.....	70
25. For control group rat tibias the average FTIR spectra in the C-H stretching region	71
26. Comparison of the lipid to protein (CH_2 symmetric stretching to CH_3 symmetric stretching) ratio for the femurs and tibias of control, diabetes, diabetes + Se (DS) and control + Se (CS) group.....	72
27. The average second derivative spectra for the tibias of control and experimental groups in the C-H stretching region	74
28. A typical curve-fit spectrum and the best fitted individual component bands of the control group rat femur in 2810-3000 cm^{-1} region.....	75
29. For control, diabetes, diabetes + Se and control + Se group femurs and tibias, relative lipid to protein ratio (CH_2 symmetric stretching to CH_3 symmetric stretching) sub-bands obtained from curve-fitting analysis of FTIR spectra in the C-H stretching region.....	76
30. The results of the curve-fitting analysis of the FTIR spectra in ν_4 phosphate bending region for the femurs and the tibias from control, Se and vitamin E deficient and Se excess, vitamin E adequate group rats.....	78
31. ν_2 carbonate region curve-fitting analysis results for control, deficient and excess group rat bones.....	81
32. Comparison of the 1660:1690 ratio for the femurs and tibias of control, deficient and excess group rats.....	83

33. X-ray diffraction pattern of highly crystalline synthetic hydroxyapatite	85
34. X-ray diffraction pattern of poorly crystalline control group rat femur.....	86
35. Comparison of powder x-ray diffraction patterns for highly crystalline synthetic hydroxyapatite and poorly crystalline control group rat femur.....	87
36. Comparison of powder x-ray diffraction patterns in the 002 reflection for highly crystalline synthetic hydroxyapatite and poorly crystalline control and diabetes group rat femurs.....	88
37. Light micrograph of a section taken from control group rat	90
38. Light micrograph of a section taken from diabetic group rat	91
39. Light micrograph of a section taken from sodium selenite treated diabetic group rat	91
40. Light micrograph of bone section taken from sodium selenite treated control group rat	92
41. Electronmicrograph of a bone section taken from control group rat	93
42. Electronmicrograph of a bone section taken from diabetic group rat.....	94
43. Electronmicrograph of bone section taken from sodium selenite treated diabetic group rat	95
44. Electronmicrograph of a bone section taken from sodium selenite treated control group rat	95
45. Light micrograph of: femur and tibia of the control group; femur and tibia of the deficient group and femur and tibia of the excess group	97

LIST OF ABBREVIATIONS

AGE	Advanced Glycation End Products
DHLNL	Dihydroxylysinonorleucine
DM	Diabetes Mellitus
FTIR	Fourier Transform Infrared Spectroscopy
HA	Hydroxyapatite
IDDM	Insulin-Dependent Diabetes Mellitus
NIDDM	Noninsulin-Dependent Diabetes Mellitus
Pyr	Pyridinoline
Se	Selenium
STZ	Streptozotocin
XRD	X-Ray Diffraction

CHAPTER 1

INTRODUCTION

In this study the effects of ultra trace element selenium as an antioxidant on diabetic rat bones and the effects of selenium and vitamin E deficiency and selenium toxicity on rat bones were reported at molecular level via Fourier transform infrared (FTIR) spectroscopy and the results were supported by other techniques such as light and electron microscopy, and x-ray diffraction. In this chapter a detailed preliminary survey including structural properties of bone, diabetes mellitus, place of antioxidants in normal bones and diabetic bone complications, structural and functional properties of selenium in health and disease and basis of infrared spectroscopy has been conducted.

1.1 Structure of Bone

1.1.1 Bone as an Organ: Macroscopic Organization

Anatomically two types of bones can be distinguished in the skeleton: flat bones (e.g. skull bones, mandible) and long bones (e.g. tibia, femur, humerus, etc.) (Figure 1).

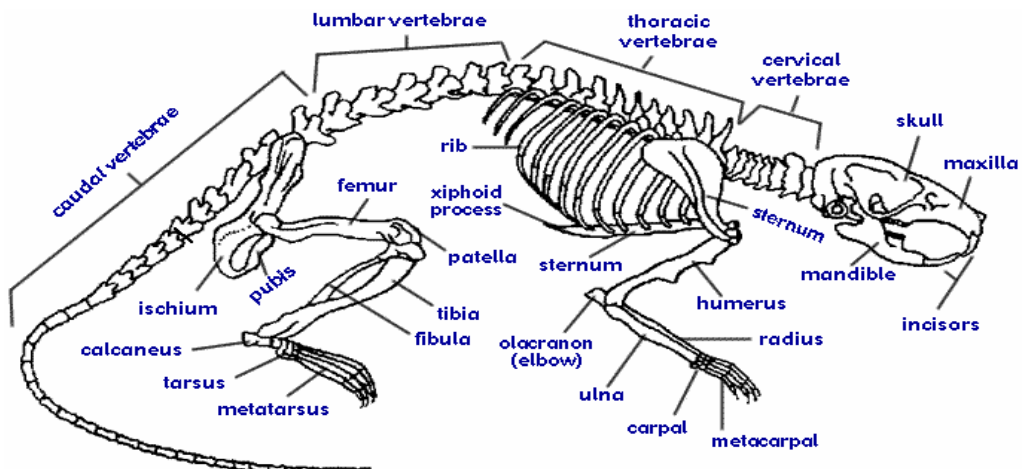


Figure 1. The skeletal system of the rat.
www.biologycorner.com/bio3/rat_external.html.

External examination of a long bone (Figure 2) shows two wider extremities (*the epiphysis*), a more or less cylindrical tube in the middle (*the midshaft or diaphysis*), and a developmental zone between them (*the metaphysis*). In a growing long bone, the epiphysis and the metaphysis, which originate from two independent ossification centers, are separated by a layer of cartilage, the *epiphyseal cartilage* (also called *growth plate*). This layer of proliferative cells and expanding cartilage matrix is responsible for the longitudinal growth of bones; it becomes entirely calcified and remodeled and replaced by bone by the end of the growth period. The external part of the bones is formed by a thick and dense layer of calcified tissue, the *cortex* (compact bone), which in the diaphysis, encloses the medullary cavity where the *hematopoietic* bone marrow is housed. Toward the metaphysis and the epiphysis, the cortex becomes progressively thinner, and the internal space is filled with a network of thin, calcified trabeculae; this is the *cancellous* bone, also named spongy or *trabecular* bone. The spaces enclosed by these thin trabeculae also are filled with hematopoietic bone marrow.

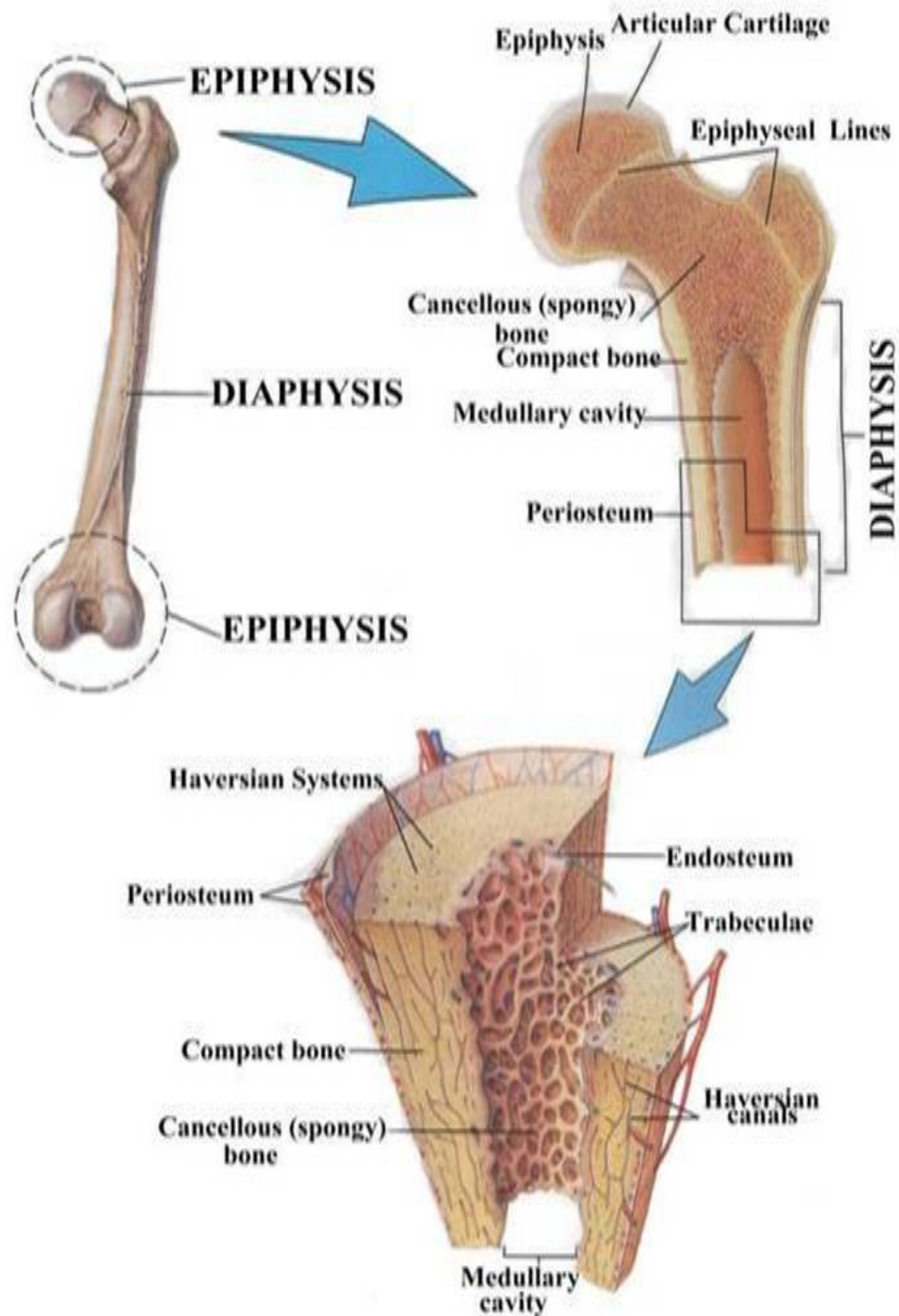


Figure 2. Structure of long bones: **A)** The right femur seen from the posterior. **B)** Section through an adult long bone **C)** Internal features of a part of a long bone (Seeley *et al.*, 1996).

and are in continuity with the medullary cavity of the diaphysis. The bone surfaces at the epiphysis that take part in the joint are covered with a layer of *articular cartilage* that does not calcify (Baron, 1999).

There are two bone surfaces at which the bone is in contact with the soft tissues: an external surface (the periosteal surface) and an internal surface (the endosteal surface). These surfaces are lined with osteogenic cells organized in layers, the *periosteum* and the *endosteum* (Figure 2).

1.1.2 Bone as a Tissue: Microscopic Organization

1.1.2.1 Bone Mineral and Matrix

Mature bone consists of 60-70 % mineral. The remainder organic matrix consists of collagen, noncollagenous proteins and lipids (Walters *et al.*, 1990). Poorly crystalline hydroxyapatite is the major mineral component of bone and other physiologically calcified tissues. Stoichiometric calcium hydroxyapatite, $\text{Ca}_{10}(\text{PO}_4)_6(\text{OH})_2$, in its most common form, occurs as a hexagonally packed crystal. Apatite from biological tissues is carbonate substituted, ~5-6 % by weight, leading to a nonstoichiometric apatite mineral (Pleshko *et al.*, 1991). In organic matrix of bone tissue, some 85-90 % of the protein consists of type I collagen (Termine and Robey, 1996, Banse *et al.*, 2002). Spindle-or plate-shaped crystals of hydroxyapatite are found on the collagen fibers, within them, and in the ground substance. In bone tissue, the ground substance is primarily composed of glycoproteins and proteoglycans. These highly anionic complexes have a high ion-binding capacity and are thought to play an important part in the calcification process and the fixation of hydroxyapatite crystals to the collagen fibers. The relative amounts and properties of both the mineral and the organic matrix influence the behavior of the structure. The collagen fibers provide the structural strength of bone while the hydroxyapatite confers rigidity on that structure.

Bone collagen consists of two α_1 and one α_2 polypeptide chains in a triple helical structure. The helical conformation of each chain is dependent on the fact that every third residue is a glycine (Gly) and that the sequence is rich in proline. A larger side chain than Gly would prevent the close contact of the three chains. About half of the proline side chains are hydroxylated; the resulting residue is hydroxyproline. The structure is stabilised by hydrogen bonds between the backbone amide of a Gly residue and the backbone carbonyl of residue X, where the sequence is represented by a repeat of -Gly-X-Y- (Bailey *et al.*, 1998).

Alpha chains in a single collagen monomer are approximately 1000 amino acids in length. Therefore, the collagen monomer as a uniform, semi-rigid asymmetric rod is about 296 nm in length and 14 Å in diameter (Veis, 1997). In a bone tissue, collagen molecules are arranged head-to-tail, with a 35 nm gap. Charged and uncharged residues are found to be periodically clustered along the sequence of collagen I every 234 residues, which is equivalent to 67 nm.

The ends of each rod have short extensions, which are not in the triple-helix conformation. These end-regions or *telopeptides*, different at the amino and carboxyl termini of each rod, are crucial in the formation of the intermolecular *cross-linkages*, which stabilize the fibrils and increase their tensile strength. The covalent cross-linkages between N- and C- telopeptides and their respective helix region receptors on adjacent molecules suggest a permanence of the mature fibril (Veis, 1997).

The formation of specific cross-links is controlled enzymatically through the hydroxylation of specific lysine residues and their subsequent enzymatic conversion to aldehydes. The cross-links are formed between an enzymatically induced lysyl aldehyde in the telopeptide and a specific hydroxylysine residue in the helical region. Bone collagen has a specific cross-link profile due to the high degree of lysyl hydroxylation in the telopeptide, whereas that in the triple helix is low. At present, seven major collagen cross-links have been established as naturally occurring intermolecular cross-links. They are:

- 1- Dehydrodihydroxylysinoornithine (deH-DHNL)
- 2- Dehydrohydroxylysinoornithine (deH-HNL)
- 3- Dehydrohistidinohydroxymerodesmosine (deH-HHMD)
- 4- Pyridinoline (Pyr)
- 5- Deoxypyridinoline (d-Pyr)
- 6- Pyrrole
- 7- Histidinohydroxylysinoornithine (HHL).

The first three are sodiumborohydride (NaBH_4) reducible. Their reduced forms are DHNL, HNL and HHMD, respectively. The rest are nonreducible compounds (Yamauchi, 1996). With increasing age, reducible divalent DHNL is converted to the nonreducible trivalent *hydroxylsyl* and *lysylpyridinolines* and *pyrroles* (Figure 3).

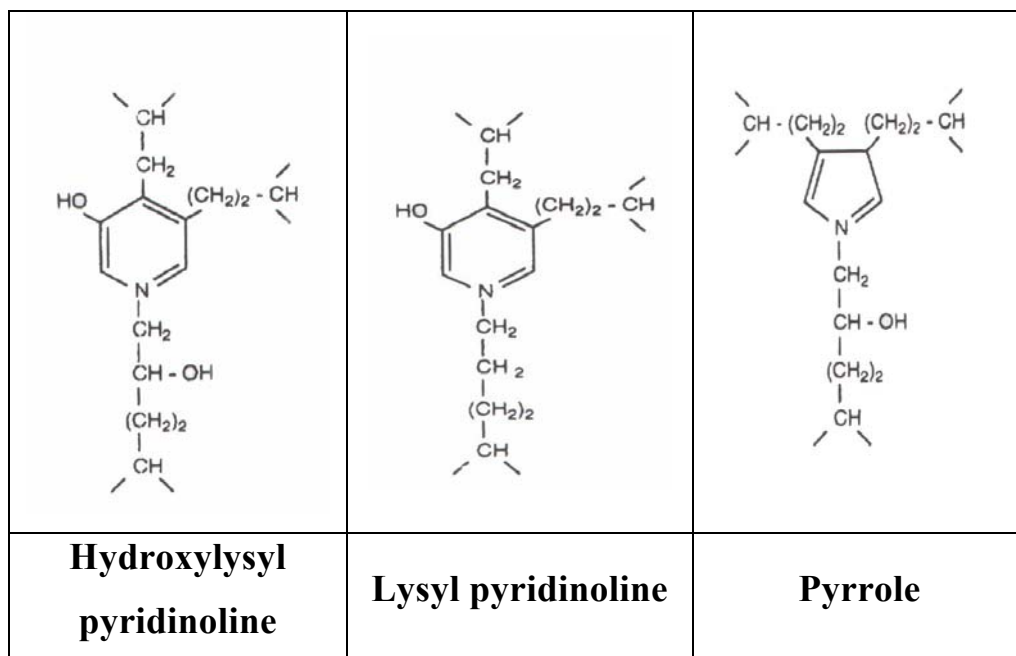


Figure 3. The structure of the pyridinoline and pyrrole cross-links. A) Hydroxylsyl pyridinoline (HL-Pyr); B) Lysyl pyridinoline (L-Pyr); C) Pyrrole (Knott and Bailey, 1998).

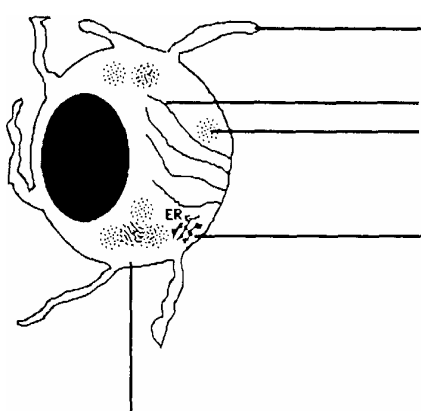
Formation of pyrrole rather than pyridinoline depends on reduced lysine hydroxylation, including both specific triple helix lysine and telopeptide lysine. The pyrrole cross-links predominate at the N-terminus of the molecule, whereas the pyridinoline predominates at the C-terminus (Banse *et al.*, 2002) and pyrrole forms interfibrillar cross-link and pyridinoline forms intrafibrillar cross-link. The mechanical properties of bone correlate with the pyrrole content rather than the pyridinoline content (Knott *et al.*, 1995).

The non-enzymatic reaction of collagen with glucose also leads to formation of intermolecular cross-links. This process is called as glycation. Glycation can affect the properties of collagen in a number of ways such as, its optimal biomechanical functioning, the alteration of its charge profile. Therefore, its interaction with cells and glycated collagen can act as an oxidizing agent (Bailey *et al.*, 1998). The early glycation products are reversible and do not accumulate. In non-mineralizing tissues, since collagen is a long-lived protein, these cross-links may undergo a series of reactions that result in formation of advanced glycation end products (AGEs). Bone tissue turns over relatively quickly, therefore, AGEs do not accumulate with age to the same extent as seen in skin, tendon and other non-mineralizing tissues (Knott and Bailey, 1998).

The preferential orientation of the collagen fibers alternates in adult bone from layer to layer, giving to the bone a typical *lamellar* structure. This fiber organization allows the highest density of collagen per unit volume of the tissue. During development and fracture healing, or in tumors and some metabolic bone diseases, the bone formation is very rapid. Therefore, there is no preferential organization of the collagen fibers. In that case they are not so tightly packed and found in somewhat randomly oriented bundles: this type of bone is called *woven* bone, as opposed to *lamellar* bone (Baron, 1999).

1.1.2.2 Cellular Organizations within the Bone Matrix

The structure of bone is maintained by a delicate relationship between the osteoblast and osteoclast; the former is associated with bone formation, the latter with bone resorption. The osteoblast is the bone-lining cell responsible for the production of the matrix constituents, such as collagen and ground substance (Figure 4).



PROCESSES FOR CELL TO CELL COMMUNICATION

**MICROFILAMENTS
ALKALINE PHOSPHATASE**

MATRIX PROTEINS
Collagen (predominantly type I) Non-collagen proteins e.g. osteocalcin, proteoglycans, osteonectin.

FACTORS WHICH STIMULATE MATRIX SYNTHESIS

- **Skeletal growth factor**
- **Bone morphogenetic protein**
- **Prostaglandin E2**
- **Interleukin I**

Figure 4. A schematic representation of an osteoblast cell (Watrous and Andrews, 1989).

Osteoblasts never appear or function individually but are always found in clusters of cuboidal cells along the bone surface (~100 to 400 cells per bone-forming site). At the light-microscope level, the osteoblast is characterized by a round nucleus at the base of the cell (opposite the bone surface), a strongly basophilic cytoplasm,

and a prominent Golgi complex located between the nucleus and the apex of the cell (Baron, 1999). Ultrastructural examination of osteoblasts reveals cytoplasmic microtubules, tight cell junctions and numerous radially directed cell processes containing parallel bundles of microfilaments (Weinger and Holtrop, 1974). These features suggest that cell-to-cell communication exists in bone. Osteoblasts produce alkaline phosphatase and extracellular matrix proteins. These proteins consist of collagen and a variety of noncollagen proteins. Osteocalcin or bone Gla (gamma-carboxyglutamic acid) protein constitutes 10 % to 20 % of the noncollagen matrix proteins (Gundberg *et al.*, 1984). Osteocalcin changes its conformation in the presence of calcium, binds strongly to hydroxyapatite and inhibits the formation of hydroxyapatite from amorphous calcium phosphate (Watrous and Andrews, 1989).

Osteocytes are osteoblasts that have become embedded in mineralized matrix with bone growth. Osteoblasts and osteocytes synthesize matrix proteoglycans with small chains consisting primarily of chondroitin sulfate and lesser amounts of dermatan sulfate, heparan sulfate, and hyaluronic acid (Hunter *et al.*, 1983). It has been suggested that for mineralization of the matrix to occur, a reduction in the amount of proteoglycans in the cartilage matrix is necessary. Several phosphoproteins also exist in the bone matrix. As an example osteonectin binds to and links both hydroxyapatite and collagen (Watrous and Andrews, 1989).

The *osteoclast* is the bone-lining cell responsible for bone resorption. It is a giant multinucleated cell, containing 4 to 20 nuclei (Figure 5). It is usually found in contact with a calcified bone surface and within a lacuna (Howship's lacunae) that is the result of its own resorptive activity. It is possible to find up to four or five osteoclasts in the same resorptive site, but there are usually only one or two. Under the light microscope, the nuclei appear to vary within the same cell: some are round and euchromatic, and some are irregular in contour and heterochromatic, possibly reflecting the asynchronous fusion of mononuclear precursors. The cytoplasm is "foamy" with many vacuoles (Baron, 1999).



Figure 5. A schematic representation of an osteoclast cell (Watrous and Andrews, 1989).

Characteristic ultrastructural features of osteoclasts are the abundant Golgi complexes characteristically disposed around each nucleus, the mitochondria, and the transport vesicles loaded with lysosomal enzymes. The most prominent features of the osteoclasts are, however, the deep foldings of the plasma membrane in the area facing the bone matrix: the *ruffled border* in the center is surrounded by a ring of contractile proteins (sealing zone) that serve to attach the cell to the bone surface, thus sealing off the subosteoclastic bone-resorbing compartment (Baron, 1999).

1.1.3 Mineral Formation in Bone Tissue

In the epiphyseal growth plate of long bones, mineralization is restricted to the longitudinal septal cartilage matrix into which matrix vesicles are dispersed selectively as clustures. These vesicles are the initial site of apatite mineral deposition. During phase I of mineralization, intravesicular calcium concentration

is increased by its affinity for lipids of the vesicle membrane interior. Phosphatase (e.g. alkaline phosphatase, pyrophosphatase or adenosine triphosphatase) at the vesicle membrane acts upon ester phosphate of matrix or vesicle fluid to produce a local increase in phosphate (PO_4^{3-}) in the vicinity of the vesicle membrane. This results in initial deposition of calcium and phosphate near the membrane. With accumulation and growth, intravesicular crystals are exposed to the extravesicular environment. Phase 2 of mineralization begins with exposure of performed apatite crystals to extravesicular fluid, which, in normal animals, is supersaturated with respect to apatite, enabling further crystal proliferation. Once the calcification cascade is begun, matrix vesicles are no longer needed to support mineralization and are consumed by the advancing mineralization front in which performed crystals serve as nuclei for the formation of new crystals.

In mineralizing and mineralized hydroxyapatite containing tissues, complexed acidic phospholipids exist in the membranes as components of proteolipids and act as hydroxyapatite nucleators (Raggio *et al.*, 1986, Boskey *et al.*, 1988). They are composed, in order of decreasing molar content, of calcium, phosphatidylserine, phosphatidylinositol, inorganic phosphate and other acidic phospholipids (Boskey and Posner, 1976). 1,25-dihydroxy vitamin D can stimulate the formation of phosphatidylserine other acidic phospholipids (Boskey *et al.*, 1988). Therefore, the rate of crystal proliferation is promoted by the availability of Ca^{2+} , PO_4^{3-} and also by the presence of collagen whereas, it is retarded by naturally occurring inhibitors of mineralization such as proteoglycans and several noncollagenous calcium-binding proteins of bone including osteocalcin, phosphoproteins, osteonectin and α -2HS glycoproteins (Anderson, 1989).

1.2. Diabetes Mellitus

1.2.1. Insulin and Diabetes Mellitus

Insulin, a peptide hormone, is secreted by the β -cells in response to a rise in blood glucose levels. Insulin or agents that can mimic its action are necessary to

promote the entry of glucose into tissues where the glucose can either be converted into energy or stored for later use. In addition to glucose uptake, insulin regulates a variety of other metabolic responses, including facilitating entry of amino acids into cells for the production of cellular proteins, increasing precursors for nucleic acid synthesis, transporting critical cellular ions, stimulating Na^+/K^+ ATPase as well as controlling the expression of a number of genes (Stapleton, 2000). Insulin also regulates the transcription of the genes for several key enzymes associated with carbohydrate and fatty acid metabolism (O'Brien and Granner, 1996). Glycogen synthase (Shepherd, *et al.*, 1995), glucokinase (Magnuson *et al.*, 1989), phosphoenolpyruvate carboxykinase (PEPCK) (Short *et al.*, 1986, O'Brien *et al.*, 1990), fatty acid synthase (Stapleton *et al.*, 1990, Moustaid *et al.*, 1994) and glucose-6-phosphate dehydrogenase (Wagle *et al.*, 1998), key enzymes in glycogen synthesis, glycolysis, gluconeogenesis, fatty acid biosynthesis and pentose phosphate pathway, respectively, have been targets of the studies with regard to insulin action. The lack of critical concentrations of circulating insulin or the ability of insulin to function properly leads to the onset of diabetes mellitus (DM). In the untreated state, DM is recognized by chronic elevation of glucose in the blood. The high concentration of blood glucose and other biochemical abnormalities results from a deficiency in β -cells of endocrine pancreas and/or from a sub-sensitivity to insulin in target cells. Although there are several diseases and syndromes associated with hyperglycemia, it has been traditional to classify all forms of diabetes as either insulin-dependent (IDDM) or noninsulin-dependent (NIDDM) on functional grounds (Öztürk *et al.*, 1996). IDDM usually begins before the age of 40, often in childhood and adolescence.

Characteristically, the plasma insulin is low or immeasurable, because a total deficiency in pancreatic β -cells has occurred in IDDM due to the T cell-mediated destruction of pancreatic β -cells. Moreover, glucagon level is elevated, but it can be suppressible with insulin. This type of diabetes is not responsive to the treatment with oral antidiabetic drugs. Therefore, insulin therapy is always

required for patients with IDDM. Autoimmune reactions seem to be quite possible for the pancreatic β -cell destruction, and the activation of cytokines such as interleukin-1 (IL-1) and tumor necrosis factor (TNF) may play an important role in this process (Mandrup-Poulsen, 1990, Rabinovitch and Baquerizo, 1990).

NIDDM usually begins in middle life or after. Symptoms begin more gradually than in IDDM and the diagnosis is frequently made when an asymptomatic person is found to have elevated plasma glucose on routine laboratory examination. In contrast to IDDM, plasma insulin levels are normal to high in absolute terms, although they are lower than predicted for the level of the plasma glucose, i.e., relative insulin deficiency is present. Insulin resistance seen in NIDDM involves both a decreased number of insulin receptors in target tissues and a postreceptor defect that has not been well identified, yet. Changes in the insulin receptor tyrosine kinase activity (Slieker *et al.*, 1990; Block *et al.*, 1991) and/or insulin sensitive glucose transporter (Garvey *et al.*, 1989, Strout *et al.*, 1990) may be the responsible mechanism(s) for the subsensitivity of target cells to insulin. Although this type of diabetes is responsive to the treatment with oral antidiabetic drugs, in further stages of the disease the combination of oral antidiabetic drugs with insulin has been found to be clinically useful for the treatment of NIDDM (Simpson *et al.*, 1990).

The metabolic disturbances of DM cause chronic, irreversible damage to vital organs and systems. Several complications, such as neuropathy, cardiomyopathy, angiopathy and nephropathy may be deleterious for diabetic patients and the development of these complications has been shown to confer an increased incidence of morbidity and mortality of diabetic patients.

Diabetic bone disease was recognized at the beginning of the 20th century. In the last quarter of that century several studies reported decreased bone mass in IDDM patients (Hamlin, 1975, Levin *et al.*, 1976, Rosenbloom *et al.*, 1977, Santiago *et al.*, 1977, McNair *et al.*, 1979a, 1981, Frazer *et al.*, 1981, Shore *et al.*, 1981,

Wiske *et al.*, 1982, Hui *et al.* 1985, Hough, 1987, Auwerx *et al.*, 1988, Giacca *et al.*, 1988, Leon, *et al.*, 1989). Those patients often suffered from an increased incidence of traumatic bone fractures (Lewis *et al.*, 1976), possibly relating to their high incidence of osteoporosis. Diabetes mellitus is known as one of the major causes of secondary osteopenia (Okuna *et al.*, 1991) and the degree of osteopenia depends on the quality of diabetic control (McNair *et al.*, 1979a). However, conflicting findings have been reported in patients with NIDDM, who showed evidence of decreased, normal or increased skeletal mass (Meema and Meema, 1967, Levin *et al.*, 1976, Deleeuw and Abs, 1977; El Miedany *et al.*, 1999, Kao, 2003). In these patients increased adipose tissue in connection with the frequently seen overweight yields metabolically active steroid hormones, insulin related growth factors that may stimulate bone formation.

The decrease in bone mass observed in diabetes is not necessarily due to insulin deficiency itself as diabetes is frequently associated with other risk factors for osteoporosis. Animal diabetes studies are therefore more appropriate for evaluating possible pathogenic mechanisms. Several experimental models of diabetes have been used to understand the etiology of diabetes mellitus, and also to investigate the mechanisms involved in diabetic complications (Bell and Hye, 1983, Tomlinson *et al.*, 1992). In the following section, the experimental models of diabetes will be briefly discussed.

1.2.2. Experimental Models of Diabetes

The following methodologies have been used to understand the etiology of DM and to investigate the mechanisms involved in diabetic complications: surgical, chemical, spontaneous and viral diabetes. Here chemical diabetes will be mentioned.

1.2.2.1 Chemical Diabetes

Various drugs and chemicals have been reported to cause an experimental situation somewhat similar to diabetes (Ingle, 1948, Bailey, 1949, Epand *et al.*,

1985, Bell and Hye, 1983, Lithell and Berne, 1991). Among these diabetogenic substances streptozotocin, (2 – deoxy – 2- (3 – methyl - 3 – nitrosourido) D-glycopyranose) and alloxan (ALL) are widely used inducers of diabetes mellitus in experimental animals, whereas others may exhibit only a weak and reversible diabetogenic activity, and their effects are not specific to the pancreatic β -cells (Lithell and Berne, 1991). Alloxan was the initial agent but has been replaced by STZ as the primary diabetogen for experimental DM. Both agents cause selective destruction of pancreatic β islet cells. Alloxan and STZ are thought to cause DNA strand breaks which activate the repair mechanism/nuclear poly (ADP-ribose) synthetase and deplete the cellular pool of NAD⁺, resulting in pancreatic β -cell damage (Gunnarson, *et al.*, 1974). It has been proposed that the basis for the increased pathogenicity of the diabetic state in streptozotocin (STZ)-induced diabetic rats may be due to oxidative stress (Baynes, 1991).

1.2.3 Mechanisms Involved in Diabetic Bone Loss

There are several theories on the pathogenesis of diabetic osteopenia (decreased bone mass) including hyperglycemia and insulin deficiency. They can be summarized as the following:

- Duodenal calcium malabsorption and a decrease in duodenal calbindin D-9K concentration (Schneider and Schedl, 1972, Wood, *et al.*, 1984, Verhaeghe *et al.*, 1988, Nyomba *et al.*, 1989).
- Abnormalities in calcium excretion. Hypercalciuria is frequent in both human and experimental diabetes (Raskin, *et al.*, 1978).
- Abnormalities in vitamin D metabolism. 25-Hydroxyvitamin D concentrations remained normal (Schneider, *et al.*, 1977, Nyomba *et al.*, 1989), but serum 1,25-dihydroxy vitamin D concentrations were usually depressed either in spontaneously diabetic BB rats, or in streptozotocin-induced diabetic rats. Less marked decreases have been observed in alloxan-diabetic rabbits, and human IDDM. (Schneider, *et al.*, 1977, Shires *et al.*, 1981, Hough *et al.*, 1981, Nyomba *et al.*, 1985, 1989).

- Decrease in Parathyroid hormone (PTH) concentration (Shires *et al.*, 1981, Hough *et al.*, 1981).
- In addition to abnormalities of calcium homeostasis, a decreased bone turnover plays a major role in diabetic bone disease. Less decreased bone resorption, which is judged from the number of osteoclasts, than bone formation is observed in diabetic animal models (Verhaeghe *et al.*, 1989, 1990). Therefore, impaired bone formation due to a deficit of osteoblasts has been recognized as one of the important factors in the development of diabetic osteopenia (Silberbera *et al.*, 1986, Rico *et al.*, 1989, Verhaeghe *et al.*, 1993, Krakauer *et al.*, 1995, Bouillon *et al.*, 1995, Terada *et al.*, 1998).
- Insulin has a stimulatory effect on osteoblasts (Canalis, 1983, Felsenfeld, 1992) and deficiency of insulin causes a reduction in the number of osteoblasts and, in turn lowered osteoid formation and cellular dysfunction (Shires *et al.*, 1981, Hough *et al.*, 1981, Goodman and Hori, 1984, Verhaeghe *et al.*, 1990).
- Since insulin dependent growth factor (IGF) 1 promotes osteoblast replication and function, the deficiency of IGF 1 in diabetics can also affect osteoblasts (Hock *et al.*, 1988, Raisz, 1988, Bouillon, 1992, Kissler *et al.*, 2000).
- Decreased total collagen content and defects in collagen cross-linking (Macey *et al.*, 1989, Hou, et al, 1993). Chronic hyperglycemia increases collagen glycation. Glucose exposure, either as non-enzymatic, *in vitro*, or in diabetic animals can cause changes in mechanical behaviors of collagenous tissues. These abnormalities in collagen metabolism can lead to brittleness of diabetic bones (Bouillon, 1991).
- Increased free radical generation in diabetic animals and in patients with type I and type II diabetes mellitus (Hiramatsu and Arimori, 1980, Mohan, and Das, 1997). Reactive oxygen species, ROS (or oxygen free radicals), such as hydrogen peroxide (H_2O_2), superoxide anions (O_2^-), singlet oxygen ($O\cdot$) and hydroxyl radicals ($OH\cdot$) can be formed in cells during ionizing radiation, and also during aerobic metabolism of either endogenous or exogenous substances. ROS play a specific role in sculpting or remodeling of bone (Silverton and Mesaros, 1975, Yang *et al.*, 1998). The role of ROS in bone metabolism is unique and dual considering their effect under physiological and pathological conditions (Karten *et*

al., 1994). Under physiological conditions, the production of ROS by osteoclasts assists in accelerating destruction of calcified tissue and hence assists in bone reported that an adequate intake of vitamin E and vitamin C was protective against the hip fracture risk in female smokers. However, Leveille *et al.* (1997) did not found protective effect of vitamin E or betacarotene in bone density of femoral neck of postmenapausal women. Age, sex, disease state and other factors can be effective in these conflicting results. In an animal study it was shown that a vitamin E-enriched diet promoted trabecular bone formation (Xu *et al.*, 1995). Similarly, palm vitamin E reduced bone resorption to a greater extent than bone formation in thyrotoxic rats (Ima-Nirvana *et al.*, 1999). In a later study, rats given red palm olein, that is rich in vitamin E and other antioxidants, exhibited increased endosteal bone mineral apposition rate and bone formation rate in tibia (Watkins *et al.*, 2001). Similar to vitamin E, one of the major physiological roles of Se is to function as a general antioxidant. It exerts its effect as being involved in the synthesis and enzymatic activity of Se-dependent glutathione peroxidase (Rotruck, 1973). In the following section basic structural and functional information about Se is presented.

1.3 Selenium

1.3.1 Basic Features of Selenium

Since the discovery of selenium (Se) in 1957 as an essential trace element in preventing liver necrosis in vitamin E deficient animals, interest in Se research has increased considerably (Schwarz and Foltz, 1957). In 1973, Rotruck, *et al.* identified Se to be an important component of antioxidant enzyme glutathione peroxidase, which is characterised as a tetrameric protein with four atoms of Se per molecule. This enzyme functions (in conjunction with vitamins A, C and E) as a cellular protector against oxidative damage, by catalyzing the breakdown of hydrogen peroxide and fatty acyl lipid peroxides to water and corresponding

alcohols in the presence of reduced glutathione (Duthie *et al.*, 1993). Se is not merely restricted its role in antioxidant activity but also involved in other multiple aspects of mammalian metabolism. It serves as an integral component of several enzymes, including 3 thyroidal and extrathyroidal iodothyronine 5'-deiodinases, thioredoxin reductase, selenoprotein P and W, formate dehydrogenase and plays role in the protection of membranes associated with blood filtration, equilibration of thyroid hormone metabolites and the reduction of cellular disulfides and ascorbate. (Köhrle, 1996, St Germain and Galton, 1997, May *et al.*, 1997, Foster and Sumar, 1997, Stapleton, 2000, Klein *et al.*, 2003).

1.3.2 Selenium Chemistry

Se is classified as a metalloid that lies between sulphur and tellerium in Group VIA and between arsenic and bromine in Period 4 of the periodic table. Se as selenol compounds ($\text{R}-\text{SeH}$) is readily dissociated at physiological pH. These compounds are important for their roles in catalytic reactions. Se can exist in the following oxidation states (Foster and Sumar, 1997, Tinggi, 2003):

- Selenate [+6] (SeO_3)
- Selenite [+4] (SeO_2)
- Elemental Se [0] (SeO),
- Selenide [-2] (H_2Se)
- Halides, oxohalides (SeF_4 , Se_2Cl_2 , Se_2Br_2 , SeOF_4 , SeOF_2 , SeOCl_2 , SeOBr_2)

Different oxidative states allow Se to form into several organic Se compounds (dimethylselenide, trimethylselenium) and into amino acids (selenomethionine, selenocysteine).

1.3.3 Selenium Deficiency and Toxicity in Human Population

The biological function of Se has a special characteristic that the Se content range between its essential and toxic concentrations is very narrow, and consequently daily dietary intake should be appropriately monitored in individuals.

Studies performed in vitro showed that the dose and form of selenium compounds are critical factors with regard to cellular responses. Inorganic (at doses equal to or greater than 10 μM) and organic selenium compounds (at doses equal to or greater than 10 μM) elicit distinctly different cellular responses (El-Bayoumy, 2001). The recommended daily allowance (RDA) is 50-70 μg Se per day for healthy adults with 40 μg Se as minimum requirement. Less than 11 μg Se will definitely put people at risk of deficiency that would be expected to cause genetic damage. Daily doses of 100-200 μg Se doses above the RDA are needed to inhibit genetic damage and cancer development in humans. About 400 μg Se per day is considered an upper limit (El-Bayoumy, 2001). According to the results of a large scale international study that was carried out in 1993, the RDAs of several countries did not meet those of the U.S. (Kumpulainen, 1993). Expressing as a percentage of the RDA in parentheses, the countries included in that study were Turkey (45%), Thailand (70%), Spain (85%), Italy (70%), Iran (85%) and Brazil (85%).

Selenium deficiency among human beings was reported to relate to a number of pathologies. The first reported cases of Se deficiency disease is Keshan's disease, which is a cardiomyopathy, seen in human population living in some areas of China where the soil is low in Se (Chen *et al.*, 1980). Another Se deficiency responsive disease, also reported in areas of China, is Kashin-Beck disease, which is an osteoarthropathy, a generative articular disease caused by oxidative damage to cartilage and bone cells that leads to deformation of bone structure (Sokoloff, 1985, Ge and Yang, 1993, Yang, *et al.*, 1993a, 1993b, Suetens, *et al.*, 2001). In animal model studies of this disease, evidence of over-modified lysine residues in collagen I of bone and in collagen II of cartilage, degeneration of the articular cartilage in the knee joints of the mice and irregular bone formation were reported (Yang, *et al.*, 1993a, 1993b). Similarly, the histological and biochemical studies carried out with bones and articular cartilages of rats fed with a low-Se diet showed a decrease in bone mineral density and in some biochemical parameters of

the blood depending upon the diet and the duration of feeding (Sasaki *et al.*, 1994). A decrease in the biomechanical strength of rabbit bones in a case of Se and vitamin E deficiency was also reported (Turan *et al.*, 1997a). In a later study, it was shown that combined deficiency of dietary Se and vitamin E and of sole Se excess induced a significant decrease in the biomechanical strength of rat long bones with respect to that of a control group (Turan *et al.*, 2000). In another study carried out with the second generation Se-deficient rats, some biochemical parameters related with bone metabolism and bone mineral densities of the femur and tibia were found to be lower with respect to the control groups (Reyes, *et al.*, 2001). In the same study, Se deficiency was also proposed as the main factor inducing impaired bone metabolism and osteopenia. Most of the pathologies associated with Se deficiency, appear to be directly attributable to increased free-radical damage in tissues (Hoekstra, 1975).

Experimental chronic Se toxicity in animals affects the major organs (Young *et al.*, 1981, Anundi *et al.*, 1982, Lin-Shiau, *et al.*, 1989, Turan *et al.*, 1996, 1997b, 1997c). Environmental toxicity of Se in humans is rare, however, the effects of Se toxicity have been reported to cause hypochromic anaemia and leucopenia and damaged nails to long-term workers employed in the manufacture of Se rectifiers (Rosenfeld and Beath, 1964). There have been a number of cases of reported acute and subacute Se poisoning in humans as a result of accidental ingestion of selenic acid (30 g/l) and vitamin tablets that contained high levels of Se (Tinggi, 2003). An ingestion of Se at high level is reported to cause gastrointestinal disturbances (vomiting, diarrhea), hair and nail changes and neurologic manifestations including acroparesthesias, weakness, convulsions and decreased cognitive function (Clark *et al.*, 1996; Gasmi *et al.*, 1997).

It has been suggested that Se toxicity may be due to the interaction of selenite with glutathione to form reactive selenotrisulfides to produce toxic superoxide and hydrogen peroxide (Spallohlz, 1994). However, the exact mechanisms of Se toxicity as well as deficiency are not clearly established yet. Although various

effects of Se excess or deficiency have been reported in animals and humans (Young *et al.*, 1981, Anundi *et al.*, 1982, Sokoloff, 1985, Lin-Shiau, *et al.*, 1989, Yang, *et al.*, 1993a, 1993b, Turan *et al.*, 1996, 1997a, 1997b, 1997c, 2000, Reyes, *et al.*, 2001), most of the studies give limited information about the status of vitamin E in Se deficiency. This point is of importance because vitamin E is known to decrease the threshold dietary Se needed to elicit Se deficiency symptoms in several species (Scott *et al.*, 1967; Hakkarainen, *et al.*, 1978; Ytrehus *et al.*, 1988).

1.3.4 Effects of Selenium on Glucose Metabolism and Diabetes

There is a close relationship between glucose metabolism and selenium. Souness *et al.* reported that, insulin - stimulated glucose oxidation was decreased in adipocytes from selenium-deficient rats (1983). In a later study it was reported that, glucose intolerance developed when Se deficiency was coupled with vitamin E deficiency (Asayama *et al.*, 1986). Ezaki showed for the first time the insulin-like effects of selenium in which the addition of sodium selenate to the incubation medium of adipocytes from normal rats stimulated glucose transport, cAMP phosphodiesterase activity and ribosomal S₆ protein phosphorylation (1990). In a later study it was reported that, frequent intra peritoneal administration of selenate to STZ induced diabetic rats for 7 weeks caused sustained decrease in their hyperglycaemia (McNeill *et al.*, 1991). Insulin mimetic effects of selenite have also been reported in STZ-induced diabetic mice, in which the selenite treatment was commenced prior to induction of diabetes (Ghosh, *et al.*, 1994). In another study, Becker *et al.* reported that oral selenate induced a sustained improvement of glucose homeostasis in STZ-diabetic rats by an insulin-like action, involving partial correction of altered pretranslational regulatory mechanisms in liver metabolism (1996). In a later study, Battell *et al.* showed that, sodium selenate corrected glucose tolerance and heart function in diabetic rats (1998). Similarly, renal hyperfiltration and increased renal lesions seen in the kidneys of STZ-induced diabetic rats were corrected by selenium supplementation (Douillet *et al.*, 1999, Reddi and Bollineni, 2001).

On the other hand, in a recent study an insulinomimetic role for selenate was also shown in type II diabetic dbdb mice, as indicated by enhanced glucose tolerance and changes in the activity of some major glycolytic and gluconeogenic marker enzymes (Mueller *et al.*, 2003). Decreased plasma glucose levels have also been observed in diabetic human beings treated with selenium (Wang *et al.*, 1995). The Se induces a sustained improvement of glucose homeostasis in diabetic individuals by an insulin-like action (Berg, 1995, Becker, 1996 and Kimura, 1996).

Selenate was demonstrated to evolve a direct insulinlike effect by stimulating tyrosyl phosphorylation reactions of the β -subunit of the insulin receptor and other downstream components of the insulin signaling pathway such as, insulin receptor substrates IRS 1 and IRS 2; pp 70 S6 kinase (plays a critical role in initiation of protein synthesis) and mitogen activated protein kinase (MAPK) (Ezaki, 1990, Stapleton *et al.*, 1997, Hei *et al.*, 1998). Consequently, Se, in modifying the phosphorylation state of insulin cascade proteins, appears to modify enzyme activities and glucose transport and thus participates in glucose homeostasis. On the other hand, like insulin, the observed increase in glucose transport activity by selenate is due to translocation of the glucose transporters GLUT-1 and GLUT-2 to the membrane surface (Stapleton, 2000).

In contrast to insulinlike effects of selenium in diabetic animals, there are some conflicting reports regarding the effects of selenium supplementation on plasma glucose levels of normal rats, such that no change or a rise, especially at high doses, has been observed (Rasekh *et al.*, 1991, Potmis *et al.*, 1993, Delilbaşı *et al.*, 2002). There is also controversy among the different clinical studies performed on the serum Se levels in diabetic patients. Some researchers found a significant decrease in patients with different types of diabetes mellitus (Schlienger *et al.*, 1988; Tawardska-Saucha *et al.*, 1994, Navarro *et al.*, 1999). Others observed that serum selenium levels were similar in patients and controls (Holecek *et al.*, 1995, Wang *et al.*, 1995, Armstrong *et al.*, 1996). Nevertheless, other

investigators even found a statistically-significant increase in Se concentrations in diabetic patients to those determined in the control group (Gebre-Medhin *et al.*, 1984, Cser *et al.*, 1993), which was interpreted as a possible protective mechanism of the vascular system against the aggressiveness of prooxidant agents and free radicals (Gebre-Medhin *et al.*, 1984).

1.4. Infrared Spectroscopy

1.4.1 The Basic Theory of Light Absorption by Molecules

For most purposes, it is convenient to treat a molecule as if it possesses several distinct reservoirs of energy. The total energy is given by:

$$E_{\text{total}} = E_{\text{transition}} + E_{\text{rotation}} + E_{\text{vibration}} + E_{\text{electronic}} + \\ E_{\text{electron spin orientation}} + E_{\text{nuclear spin orientation}}$$

Each E in the equation represents the appropriate energy as indicated by its subscript. In solution, a molecule can translate, rotate and vibrate. The energies associated with each of these are quantized (Campbell, 1984).

Light is an electromagnetic wave. The energy of the wave is given as:

$$E = h.c/\lambda = h.v$$

in which h is Planck's constant, c is the velocity of light, λ is the wavelength and v is the frequency. If an electromagnetic wave encounters a molecule, it can be scattered (i.e. its direction of propagation changes), absorbed (i.e. its energy is transferred to the molecule) or emitted (energy is released by the molecule). When the energy of the light is absorbed, the molecule is said to be *excited*. An excited

molecule can possess any one of a set of discrete amounts (quanta) of energy described by the laws of quantum mechanics. These amounts are called the *energy levels* of the molecule. The major energy levels are determined by the possible spatial distributions of the electrons and are called *electronic energy levels*, on these are superimposed vibrational levels which indicate the various modes of vibration of the molecule. All these energy levels are described by an *energy-level diagram* (Figure 6). The lowest electronic level is called the ground state and all others are excited states (Freifelder, 1982).

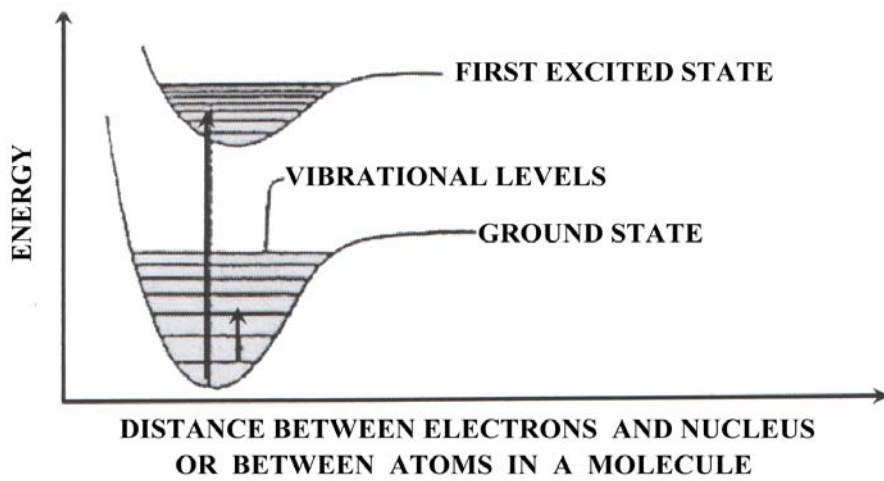


Figure 6 Typical energy-level diagram showing the ground state and the first excited state. Vibrational levels are shown as thin horizontal lines. A possible electronic transition between the ground state and the fourth vibrational level of the first excited state is indicated by the long arrow. A vibrational transition within the ground state is indicated by the short arrow (Freifelder, 1982).

1.4.2 Basis of Infrared Spectroscopy

Spectroscopy is defined as the study of interaction of electromagnetic radiation with matter. Electromagnetic wave consists of mutually perpendicular electric and magnetic fields, which, oscillate sinusoidally as they propagate through space. A change between energy levels is called a transition. Transitions between vibrational levels of the ground state of a molecule result from the absorption of light in infrared region of the electromagnetic spectrum, which extends from the red end of visible spectrum out to the microwave region. The region includes radiation at wavelengths between 0.7 and 500 μm or in wavenumbers between 14285 and 20 cm^{-1} . The infrared spectrum can be divided into three regions: the *far infrared* (400-20 cm^{-1}), the *mid infrared* (4000-400 cm^{-1}) and the *near infrared* (14285-4000 cm^{-1}). Most infrared applications employ the mid-infrared region, but the near and far infrared regions can also provide information about certain materials. The vibrational levels and hence, infrared spectra are generated by the characteristic twisting, bending, rotating and vibrational motions of atoms in a molecule. As shown in Figure 7 vibrations can involve either a change in bond length (*stretching*) or bond angle (*bending*).

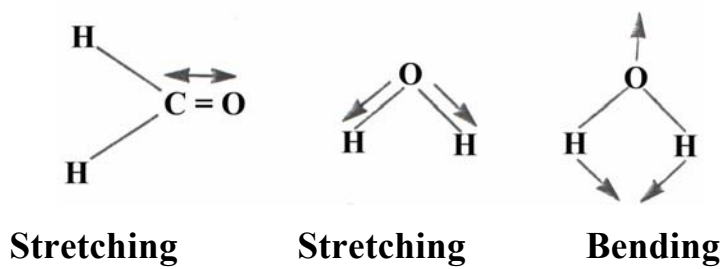


Figure 7. Stretching and bending vibrations (Stuart, 1997).

Some bonds can stretch in-phase (symmetric stretching) or out-of-phase (asymmetric stretching), as illustrated in Figure 8.

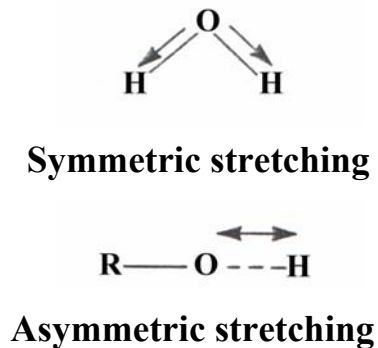


Figure 8. Symmetric and asymmetric stretching vibrations (Stuart, 1997).

Bending vibrations also contribute to infrared spectra and they are illustrated in Figure 9. It is best to consider the molecule as being cut by a plane through the hydrogen atoms and the carbon atom. The hydrogen can move in the same direction or in opposite directions in this plane.

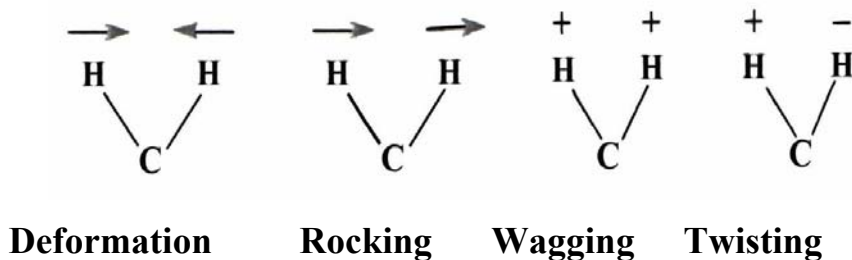
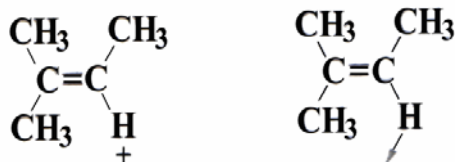


Figure 9. Types of bending vibrations (Stuart, 1997).

For more complex molecules hydrogen atoms can be considered in isolation since they are usually attached to more massive and rigid parts of the molecule. This results in *out-of-plane* and *in-plane* bending vibrations (Figure 10).



Out-of-plane bending In-plane bending

Figure 10. Out-of-plane bending and in-plane bending vibrations (Stuart, 1997).

Upon interaction with infrared radiation, portions of the incident radiation are absorbed at particular wavelengths. The multiplicity of vibrations occurring simultaneously produces a highly complex absorption spectrum, which is uniquely characteristic of the functional groups comprising the molecule and of the overall configuration of the atoms as well. The value of infrared spectral analysis comes from the fact that the modes of vibration of each group are very sensitive to the changes in chemical structure, conformation and environment.

The change in molecular vibrational energy after infrared absorption or emission is given by Bohr equation:

$$\Delta E = E_2 - E_1 = h \cdot v = h \cdot c \cdot \bar{v}$$

in which E_1 is the ground state of the molecule and E_2 is the excited state of the molecule, v is the vibrational frequency in sec^{-1} and \bar{v} is the wavenumber in cm^{-1} .

When vibrational transitions are considered, radiation is described with its wavenumber \bar{v} , rather than by its frequency, v . An infrared spectrum usually consists of a plot of the absorption of radiation as a function of wavenumber, which is sometimes referred to as frequency although its unit is the reciprocal of a wavelength (cm^{-1}) and is characterized only in terms of the positions of the maxima of each of the absorption bands v_{\max} (cm^{-1}).

1.4.3 Fourier Transform Infrared (FTIR) Spectroscopy

Fourier transform infrared (FTIR) spectroscopy has found increasing favor in laboratories since early eighties. This method is based on the idea of the interference of radiation between two beams to yield an *interferogram*, which is a signal produced as a function of the change of pathlength between the two beams.

The most important feature of an interferogram is that every individual data point of this signal contains information over the entire infrared region. This process is carried by an interferometer. It encodes the initial frequencies into a special form, which the detector can observe. For rapid-scanning interferometers liquid nitrogen cooled *mercury cadmium telluride (MCT)* detectors are used. For slower scanning types of interferometer, pyroelectric detectors (e.g. a *deuterated triglycine sulfate (DTGS)* detector element) can be used. In essence, the detector is always observing all frequencies at the same time (Griffiths and De Haseth, 1986). The two domains of distance and frequency are interconvertible by the mathematical method of Fourier transformation. Therefore, Fourier transformation is simply a mathematical means of sorting out the individual frequencies for the final representation of an infrared spectrum.

The basic components of an FTIR spectrometer are shown schematically in Figure 11. The radiation emerging from the source is passed through an interferometer to the sample before reaching a detector. Upon amplification of the signal, in which,

high frequency contributions have been eliminated by a filter, the data are converted to a digital form by an analog-to-digital converter and then transferred to the computer for Fourier transformation to be carried out.

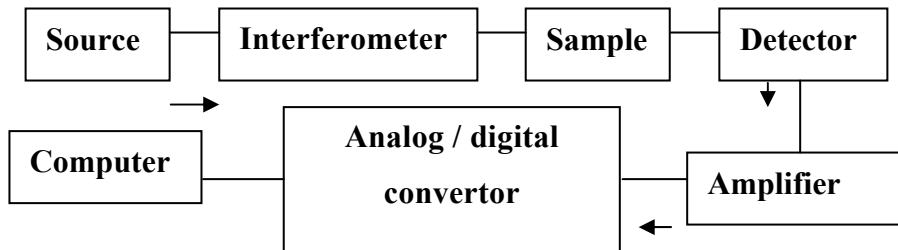


Figure 11. The components of an FTIR spectrometer.

1.4.4 Advantages of Fourier Transform Infrared Spectroscopy

- FTIR spectroscopy provides a precise measurement method, which requires no external calibration. It is a rapid and sensitive technique, which is easy to perform (Rigas *et al.*, 1990, Manoharan *et al.*, 1993, Ci *et al.*, 1999).
- The system can be applied to the analysis of any kind of material and that is not limited to the physical state of the sample. Samples may be solutions, viscous liquids, suspensions, inhomogeneous solids or powders (Colthup *et al.*, 1975).
- Digital subtraction (that is, point-by-point subtraction of the separate spectra by a computer) can be used to produce good difference spectra. This method has great advantages in obtaining infrared spectra in aqueous solutions (Campbell, 1984).

- Small sample quantities are sufficient to analyse and in vivo studies are possible (Mendelsohn and Mantsch, 1986).
- It is a non-destructive technique (Melin *et al.*, 2000, Severcan and Haris, 1999, Çakmak *et al.*, 2003).
- The instruments are relatively easy to use and data processing is simple with the computer softwares. Moreover, system permits permanent data storage, manipulation of data and quantitative calculations (Yono *et al.*, 1996, Ci *et al.*, 1999).
- Since a computer is already used to obtain the Fourier transform, it is easy to perform many scans to improve the signal-to-noise ratio (noise adds up as the square root of the number of scans, whereas signal adds linearly). It has dramatically improved signal to noise ratio by the averaging of numbers of scans per sample (Beaten *et al.*, 1998).
- Frequency and bandwidth values can be determined routinely with uncertainties of better than $\pm 0.05 \text{ cm}^{-1}$.

1.5 Scope and Aim of the Study

Mineral features such as crystallite size and perfection (crystallinity), phosphate content, carbonate content and mineral environment may be altered substantially as a function of tissue type, age and pathology. Several bone diseases such as *osteogenesis imperfecta*, *osteoporosis* and *osteoarthritis* are characterized by abnormal tissue mineral content, deposition and/ or turnover. It is thought that the microstructure of biological hydroxyapatite and collagen fibrils can affect the mechanical, chemical and biological properties of bone tissue (Nightingale and Lewis, 1971, Daculsi, *et al.*, 1997, Knott. and Bailey, 1998). In order to study structural properties of bone tissue at molecular level, several biophysical techniques such as x-ray diffraction, nuclear magnetic resonance, electron spin

resonance, Fourier transform infrared (FTIR) and in the last decade FTIR microspectroscopy (FTIRM) have been widely used.

In the last twenty years attention has been drawn to the hypothesis that oxidative stress is related to the complications to chronic diabetes. Diabetics and experimental animal models exhibit high oxidative stress due to persistent and chronic hyperglycemia, thereby deplete the activity of the antioxidative defense system and thus promote free radicals generation.

In the present study the aim is two fold. One of them is to gain information about mineral and organic matrix environment of diabetic bones and to investigate the possible therapeutic effects of Se on diabetic bone tissues. For this purpose femurs and tibias of control, STZ- induced diabetic, sodiumselenite treated STZ-induced diabetic and sodiumselenite treated control group rats were analyzed by using FTIR spectroscopy technique. This investigation was supported by light and transmission electron microscopy and x-ray diffraction techniques.

The second aim is to investigate the effects of combined deficiency of dietary selenium and vitamin E and/or of sole selenium excess on bone mineral and organic matrix of rat femurs and tibias at molecular level. This point is of importance because vitamin E is known to decrease the threshold dietary Se needed to elicit Se deficiency symptoms in several species. Previous studies mainly reported the histological and biomechanical properties of bones in the presence of Se deficiency or toxicity. In the present study detailed FTIR spectroscopic and light microscopic analysis will be reported on the effect of Se deficiency and toxicity on the rat bones. This will be the first study reporting the effect of both of Se and vitamin E deficiency or Se toxicity on rat bones at molecular level except that a previous paper of our group which reports very preliminary FTIR spectroscopy results (Turan *et al.*, 2000).

CHAPTER 2

MATERIALS AND METHODS

2.1. Reagents

Reagents used for the preparation of experimental animals:

- Streptozotocin (STZ), pentobarbital , α -tocopherol and sodium selenite were purchased from Sigma.

Reagents used for FTIR Analysis:

- Potassium Bromide (KBr) was purchased from Merck.
- Hydroxyapatite was purchased from Sigma.
- 99 % pure acetone was purchased from Sigma (It was used for cleaning process).

2.2 Preparation of Experimental Animals

2.2.1 Diabetes Induction and Selenium Treatment for Diabetes and Control Group Rats

Both sexes of weanling Wistar rats weighing 200-250 g (12-14 weeks) (Ankara University, Faculty of Medicine, Animal Care Facility) were selected randomly and housed in stainless-steel, wire bottomed cages, initially at a density of three per cage and as they grew, were then caged individually. They were maintained at an ambient air temperature of $22\pm1^{\circ}\text{C}$ and a 12-h light / dark cycle. All procedures used in the experiments were approved by the Ethics Committee of Ankara University, Faculty of Medicine. In this study, two diabetic and two control groups

were used. They were categorized as: 1: Control, 2: Streptozotocin (STZ)-induced diabetic, 3: Se treated STZ-induced diabetic. 4: Se treated control. Body weights and plasma glucose levels of the rats present in all these groups were measured at the beginning of the experimental period (just before the STZ injection) and then the first, the third and the fifth weeks following the STZ injection. Blood samples taken from tail vein was used for the measurement of blood glucose levels with MediSense Card Sensor.

2.2.1.1 Formation of Control Group

The Wistar rats were chosen randomly and Then, the rats were injected with 0.05 M citrate buffer (pH 4.5) intraperitonally (i.p.) as a single dose and also with comparable volume of saline solution. Then, they were fed without any restriction for five weeks. The animals were sacrificed under anesthesia (pentobarbital, 30 mg/kg). The femurs and tibias of the rats were taken, the surrounding soft tissue was removed and the bones were stored at –20 °C till experimental analysis.

2.2.1.2 Formation of Streptozotocin-Induced Diabetic Group

Streptozotocin (STZ) was dissolved in 0.05 M citrate buffer (pH 4.5) and injected i.p. as a single dose at a concentration of 50 mg/kg body weight (. One week after injection, blood glucose levels were measured and any STZ-treated rat having blood glucose level less than 2 times of the control value was excluded from further study. The rats with a blood glucose level of higher than 2 times of control value were accepted as diabetic and as being untreated diabetic group they were injected with saline solution everyday for four weeks. During this period they were fed without any restriction. At the end of the fifth week, the rats were sacrificed under anesthesia (pentobarbital, 30 mg/kg). The femurs and tibias of the rats were taken, the surrounding soft tissue was removed carefully and the bones were stored at –20 °C till experimental analysis.

2.2.1.3 Formation of Selenium Treated Diabetic Group

In order to induce diabetes, the rats were injected with STZ (dissolved in 0.05 M citrate buffer) i.p. as a single dose at a concentration of 50 mg/kg, as it was previously described. One week after STZ injection, blood glucose levels were measured as described before and the diabetic animals were injected with 5 µmole/kg/day sodium selenite i.p. everyday for four weeks (Ayaz *et al.*, 2004). At the end of the fifth week the animals were sacrificed under anesthesia (pentobarbital, 30 mg/kg). The femurs and tibias of the rats were taken, the surrounding soft tissue was removed and the bones were stored at -20 C till experimental analysis.

2.2.1.4 Formation of Selenium Treated Control Group

The randomly chosen Wistar rats were injected with 0.05 M citrate buffer (pH 4.5) intraperitoneally (i.p.) as a single dose and fed without any restriction. After one week, blood glucose levels were measured as described before and the animals were injected with 5 µmole/kg/day sodium selenite i.p. everyday, for four weeks. At the end of the fifth week the animals were sacrificed under anesthesia. The femurs and tibias of the rats were taken, the surrounding soft tissue was removed and the bones were stored at -20 C till experimental analysis.

2.2.2 Induction of Selenium Deficiency and Toxicity

Weanling Wistar rats of either sex were divided randomly into three equal groups ($n=5$ in each group) and housed in stainless-steel, wire-bottomed cages initially at a density of three rats per cage while growing up, then individually. They were maintained at an ambient air temperature of 22 ± 1 °C and a 12-h light/dark cycle.

2.2.2.1 Contents of Diets and Feeding Procedure of Animals

The rats were fed on either an adequate diet (control group), or a deficient diet (Se and vitamin E deficient group) or an excess diet (Se rich and vitamin E adequate group). The animals were permitted free access to the food and water for about 12 to 14 weeks. The deficient diet was obtained commercially (Sigma, USA). It contained 30 % torula yeast, 0.3 % D,L-methionine, 58.7 % sucrose, 2 % corn oil, 5 % Se deficient AIN-76 TM mineral mix, 1 % vitamin E deficient vitamin mix AIN-76 TM (Sigma, USA). Selenium and vitamin E were supplemented in the adequate and rich diets with sodium selenite and α -tocopherol acetate (Sigma, USA). The selenium content of the diets was determined by using a graphite furnace atomic absorption spectrometer (Varian Atomic Absorption Spectrometer AA-30/40, Australia). Based on analysis of random batches of diet, the Se concentration of the deficient diet was 9.8 μg Se/kg whilst the adequate and rich diets contained 225 μg Se/kg-diet and 4.2 mg Se/kg diet, respectively. Deionized water, which contained a small amount of Se (<1 $\mu\text{g}/\text{L}$), was given to the animals (Turan *et al.*, 1999). The deficiency and excess of selenium were verified by measuring selenium concentrations in the rats' plasma by using a Zeeman graphite furnace atomic absorption spectrometer (Varian Spectrophotometer AA-30/40) (Berly, Gillian, 1988). Plasma vitamin E concentrations were determined by high-performance liquid chromatography (HPLC) technique (McMurray and Blanchflower, 1979)

2.3. FTIR Spectroscopic Measurements

2.3.1. Preparation of Control, Diabetic and Se Treated Control and Diabetic Bone Samples

Small piece of bone sample taken from central region of diaphysis of the femurs and the tibias were ground in a liquid nitrogen-cooled colloid mill (Retsch MM200) at a constant frequency and period of time. In order to remove the water present in bone tissue, 1 mg of ground bone samples were placed in a vacuum freeze dryer

(Labconco) for 48 hours. KBr pellets for FTIR study were prepared by mixing the ground bone with KBr under vacuum as 1 mg sample per 100 mg KBr (KBr was dried in an oven at 68-70° C). FTIR spectra were recorded in the range of 4000-400 cm^{-1} on a Bomem MB157 spectrometer (Michelson Series; Bomem, Quebec, Canada) equipped with a deuterated triglycine sulfate (DTGS) detector. The spectrometer was left on continuously to minimize warm-up instability. It was also continuously purged with dry air to minimize contributions from water vapor in the spectral region of interest. Interferograms were averaged for four hundred scans at 4 cm^{-1} resolution. Background spectra were collected under identical conditions with the samples and automatically subtracted from spectra of samples.

In order to make comparison between the spectra of synthetic hydroxyapatite and bone tissue, synthetic hydroxyapatite present in solution form was dried at 90 °C and 1 mg dried hydroxyapatite mixed with 100 mg KBr and KBr pellet was prepared under vacuum with a hydrolic press. FTIR spectra were recorded as described above.

2.3.2. Preparation of Bone Samples from Selenium and Vitamin E Deficient and Selenium Excess Groups

Bone samples were ground in an agat mortar and were examined as KBr pellets (2.5 mg sample per 200 mg KBr). FTIR spectra were recorded in the range 4000-400 cm^{-1} on a Bomem MB157 spectrometer. Interferograms were averaged for one hundred scans at 2 cm^{-1} resolution.

2.4. Data Analysis

GRAMS/32 software (Galactic Industries, Salem, NH, USA) was used for all data manipulations. Firstly, the ν_1 , ν_3 phosphate (PO_4^{3-}) stretching (900-1200 cm^{-1}) and the Amide I (1595-1720 cm^{-1}) were baseline corrected (Camacho *et al.*, 1996, 1999, Boyar *et al.*, 2004). Then, mineral to matrix ratio was obtained by taking the ratio of

the integrated area under the peaks at ν_1 , ν_3 PO_4^{3-} stretching, and Amide I regions (Camacho *et al.*, 1996, 1999, Bohic *et al.*, 2000, Boyar *et al.*, 2004). The second derivative spectra were obtained in the ν_1 , ν_3 PO_4^{3-} stretching region (900-1200 cm^{-1}), which was resolved into six bands. The positions of these bands were used as initial parameters for curve-fitting analysis by choosing the band shape as Lorentzian-Gaussian (Pleshko *et al.*, 1991). For the curve-fitting analysis of this band and of the other spectral bands used in this study, a maximum of fifty iterated optimization algorithms were done in each fit routine. The iterations were performed until the correlation was better than 0.995.

In the ν_4 PO_4^{3-} bending domain (500-650 cm^{-1}), vibrations of acid phosphate (HPO_4^{2-}) ions and labile PO_4^{3-} ions gave rise to two main absorption bands at around 560 cm^{-1} and 600-610 cm^{-1} , respectively. In order to gain information about underlying sub-bands present in this domain, curve-fitting analysis was carried out. Upon the second derivative analysis, five bands were found which were taken into consideration in the curve-fitting analysis. After correction, a linear baseline was set and curve-fitting analysis was performed using Lorentzian peak-fit components (Bohic *et al.*, 2000). The bands located at 563, 575 and 604 cm^{-1} belong to PO_4^{3-} apatitic groups. The rest, belonging to nonapatitic HPO_4^{2-} and PO_4^{3-} , were located at ≈ 533 and 617 cm^{-1} , respectively (Bohic *et al.*, 2000; Miller *et al.*, 2001). The ratios of the areas under each of the peaks to the total area of the five peaks were calculated and compared.

Carbonate (CO_3^{2-}) is another substituent in the mineral phase. In order to calculate the relative carbonate content from the FTIR spectra, after baseline correction, the ratio of the integrated area of the ν_2 CO_3^{2-} band (850-890 cm^{-1}) to the ν_1 , ν_3 PO_4^{3-} stretching band (900-1200 cm^{-1}) was calculated (Paschalis *et al.*, 1996, Camacho *et al.*, 1996, 1999, Bohic *et al.*, 2000, Boyar *et al.*, 2003, 2004). The broad ν_2 CO_3^{2-} band is typically composed of three overlapping bands attributable to CO_3^{2-} substituted for OH^- , PO_4^{3-} and labile CO_3^{2-} positions in the apatite lattice. The bands

are found at 878 cm^{-1} , 871 cm^{-1} and 866 cm^{-1} , respectively (Rey *et al.*, 1989, 1990, Gadeleta *et al.*, 1996, Bohic *et al.*, 2000, Huang *et al.*, 2002). In this region curve-fitting analysis was used to obtain information about the changes in the relative ratios of different types of carbonate ions present in bone mineral. After baseline correction, curve-fitting was performed using Gaussian peak-fit components. The calculated area of each sub-band was reported as the partial area of the computed contour.

In the FTIR spectra, the amide I absorbance is mainly due to collagen I, since it constitutes around 90 % of protein present in bone tissue. For detailed spectral analysis of the amide I band, the ~ 1595 - 1720 cm^{-1} spectral region was taken into consideration, because the same region was also used for mineral / matrix ratio calculation (Camacho *et al.*, 1996, 1999). Before the curve-fitting analysis, baseline correction was carried out in this region. Then, the center positions for each sub-band were determined on the basis of previous assignments and confirmed by the second derivative analysis (Paschalis *et al.*, 2001, Miller and Tague, 2002). The shapes of the underlying three bands were chosen as Gaussian and the frequency of each sub-band was confined to $\pm 2\text{ cm}^{-1}$ (Paschalis *et al.*, 2001, Miller and Tague, 2002). The output of the analysis was expressed as peak position and relative percentage area. Then, the ratio of the relative percentage areas of the two spectral bands at $\sim 1660\text{ cm}^{-1}$ and $\sim 1690\text{ cm}^{-1}$ was calculated, which corresponds to relative ratio of collagen cross-links pyridinoline [Pyr] and dihydroxylysiononorleucine [DHLNL] (Paschalis *et al.*, 1998, 2001; Khan *et al.*, 2001, Miller and Tague, 2002, Atti *et al.*, 2002; Boskey *et al.*, 2003, Huang *et al.*, 2003, Boyar *et al.*, 2004).

The C-H stretching region (3000 - 2800 cm^{-1}) mainly reflects molecular changes of the lipid groups present in bone tissue. This region was baseline corrected for each spectrum. Fourier self-deconvolution (FSD) of the FTIR spectra increases the resolution of intrinsically overlapped bands by narrowing the bandwidth of the individual components. The FSD function was used to analyze the bands present in the C-H stretching region of FTIR spectra. For FSD calculations the gamma factor

was set as 0.7 for each of the spectra. After FSD application, in order to obtain relative lipid to protein ratio, the ratio of the intensities of the CH₂ symmetric and the CH₃ symmetric stretching bands was calculated.

In order to confirm the variations observed in intensity ratios, the curve-fitting analysis was carried out in the C-H stretching region. For this purpose, second derivative function was applied to determine the number and positions of the overlapping components. This information was used as initial parameters for curve-fitting analysis. Spectral region of interest was fitted with Gaussian components. Then, the fractional area ratio of the CH₂ symmetric and the CH₃ symmetric stretching sub-bands were taken in order to calculate the relative lipid to protein ratio.

2.5 X-ray Diffraction Analysis

The ground bone samples were placed into 0.5-1.0 mm capillary glass holder. Powder X-ray diffraction data were collected at room temperature with a Huber Guinier Imaging Plate Camera G670 diffractometer using a bent graphite monochromator. G670 improves the speed of the powder diffraction data collection without loosing the high accuracy and the resolution. The angular range was 5°-100° and it was scanned with a step width of 0.05° using CuK_{α1} radiation at 150mA and 50kV on a Rigaku rotating anode.

2.6 Light Microscopic Analysis

The femur and tibia specimens from all animals of each group under experiment were removed from freshly killed animals. For light microscopic evaluation, the removed tissues were fixed in phosphate buffered 10 % formaldehyde for 2 days, dehydrated in alcohols and embedded in paraffin. 4 to 6 micrometer thick sections were obtained by Leitz-1512 microtome, stained with haematoxylin and eosin and photographed by Zeiss Axioscope photomicroscope.

2.7 Electron Microscopic Analysis

For electron microscopic evaluations, the removed tissues were fixed in 2.5 % glutaraldehyde in a phosphate buffer for 24 hours and postfixed in 1 % osmiumtetroxide. The samples were then dehydrated in graded alcohols, embedded in Araldite CY 212 and sectioned with a Leica Ultracut R Ultratome. Thin sections were stained with uranyl acetate and lead citrate. The examinations were done with Leo 906 E transmission electron microscope.

2.8 Statistics

The results were expressed as mean \pm standard error of mean. The differences in the means of the experimental and control rats were compared by means of Mann-Whitney U test.

CHAPTER 3

RESULTS

3.1 General Findings Related with the Animals

3.1.1 Effects of Sodium Selenite Treatment on Body Weight and Blood Glucose Levels of Control and Experimental Group Rats

At the end of the fifth week the average body weight was lower for the diabetic and selenium treated diabetic rats as compared with the control rats (Figure 12, Table 1). Sodium selenite treatment led to an increase in the body weight of control group rats. (Figure 12, Table 1). The variations in blood glucose levels of control and experimental group rats within the experimental period are summarized in Figure 13 and Table 2. At the end of the fifth week, blood glucose levels of diabetic group rats were significantly higher as compared to control group. Sodium selenite treatment of the diabetic animals caused a decrease in blood glucose level as compared with untreated diabetic group. At the end of the fifth week, blood glucose levels of selenium treated control group rats were also slightly, but significantly higher than control group rats possibly due to pro-oxidant effect of selenium.

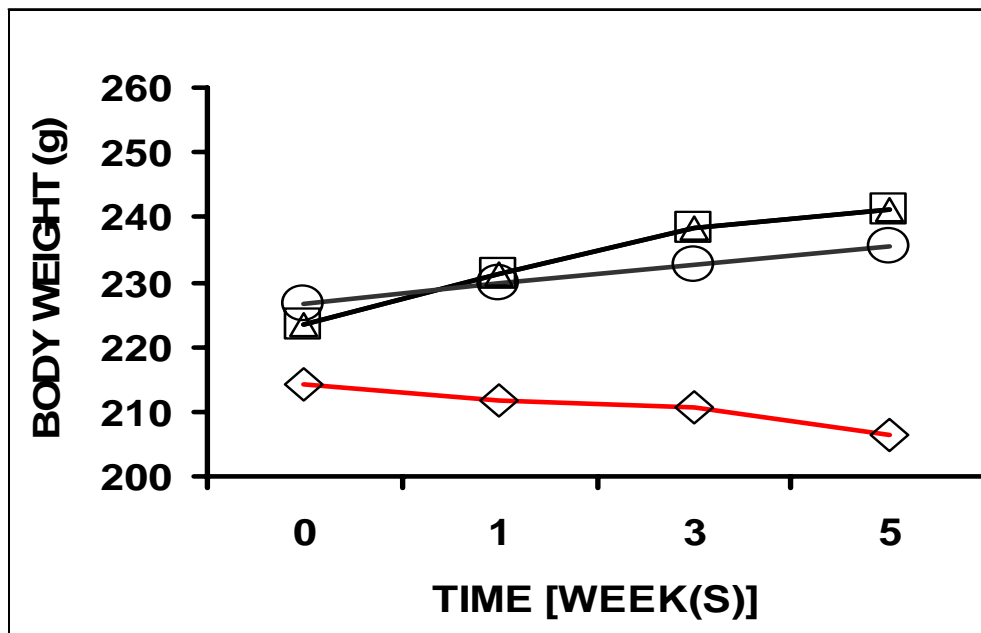


Figure 12. Variation of body weights within the experimental period. Body weights were given for control (■), diabetes (◇), diabetes + Se (△) and control + Se (○) groups.

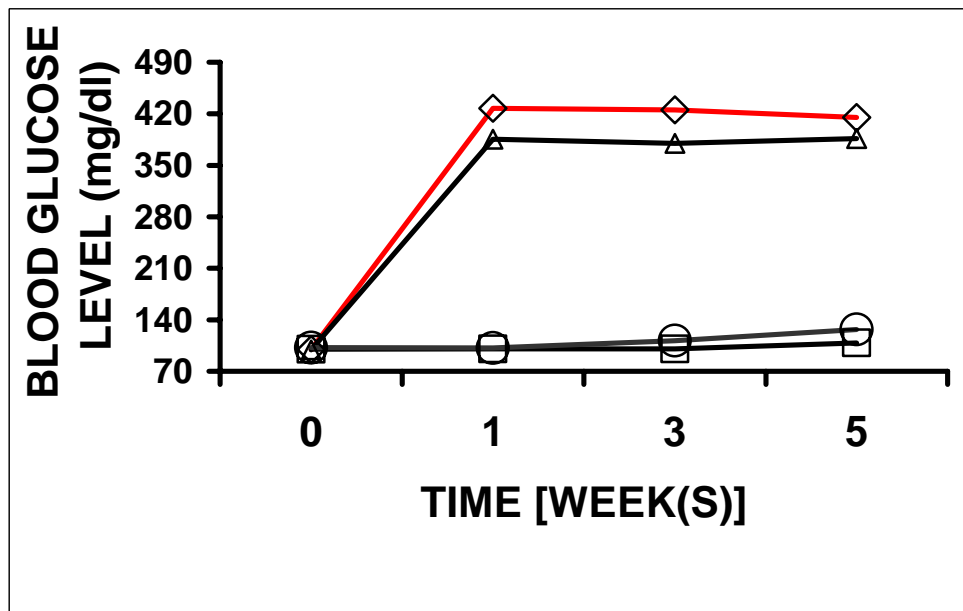


Figure 13. Variation of blood glucose levels within the experimental period. Body weights were given for control (■), diabetes (◇), diabetes + Se (△) and control + Se (○) groups.

Table 1. The body weights for control (C), diabetes (D), diabetes + Se (DS) and control + Se (CS) groups. Values are reported as mean \pm standart error of mean.

	BODY WEIGHT (g)			
TIME (week) GROUP	0	1st	3rd	5th
Control (n=9)	223.5 \pm 6.3	231.1 \pm 7.2	238.4 \pm 6.5	241.2 \pm 8.5
Diabetes (n=9)	195.6 \pm 6.3	194.5 \pm 6.8	192.0 \pm 9.9	189.6 \pm 8.6***
Diabetes + Se (n=8)	214.3 \pm 4.5	211.8 \pm 3.5	210.5 \pm 5.0	206.3 \pm 4.3***
Control + Se (10)	226.8 \pm 5.4	229.8 \pm 6.0	232.8 \pm 7.1	235.5 \pm 8.4

*** $p<0.001$ significantly different with respect to **control** group.

Table 2. The blood glucose levels (mg/dl) for control (C), diabetes (D), diabetes + Se (DS) and control + Se groups. Values are reported as mean \pm standart error of mean.

	BLOOD GLUCOSE LEVEL (mg/dl)			
TIME (week) GROUP	0	1st	3rd	5th
Control (n=9)	100.1 \pm 1.1	100.5 \pm 0.8	100.5 \pm 1.2	108.5 \pm 4.4
Diabetes (n=9)	99.4 \pm 0.5	427.6 \pm 29.5	425.5 \pm 26.7	415.0 \pm 19.5***
Diabetes + Se (n=8)	99.2 \pm 1.1	385.6 \pm 14.4	380.0 \pm 23.0	386.1 \pm 27.2***#
Control + Se (10)	102.3 \pm 1.1	101.7 \pm 0.8	111.5 \pm 2.7	127.0 \pm 4.2*

*** $p<0.001$ significantly different with respect to **control** group.

* $p<0.05$ significantly different with respect to **control** group.

$p<0.05$ significantly different with respect to **diabetes** group.

3.1.2 Effects of Antioxidant Deficiency and Excess on Some of the Physical and Biochemical Characteristics of Rats

In the second part of the present study bones taken from the rats, which were fed on either Se and vitamin E deficient or Se excess, vitamin E adequate diets, were used for FTIR spectroscopic and light microscopic analysis. Most of these experimental group animals showed hair loss in both cases. The body weights of the animals from these two experimental groups were significantly lower than those of the control group (Turan *et al.*, 1999) (Table 3). Selenium deficiency and selenium excess were verified by selenium concentration measured in plasma. Vitamin E level was also confirmed by vitamin E level measured in plasma. Both selenium and vitamin E levels in the deficient group were about 50 % of the corresponding levels of the control group. In the selenium rich group, the plasma selenium level was increased significantly (280 % of the control) while the vitamin E level was comparable to that of the control group (Turan *et al.*, 1999).

Table 3. The effects of dietary selenium and vitamin E on body weight and plasma selenium and vitamin E contents.

	Body Weight (g)	Plasma Se (nmol/ml)	Plasma Vit E (μg/ml)
CONTROL	233.6 ± 27.2	4.21 ± 1.16	7.2 ± 0.8
DEFICIENT	177.6 ± 14.4***	2.16 ± 1.13***	3.9 ± 0.2***
EXCESS	194.2 ± 25.8***	11.91 ± 1.08***	8.0 ± 1.3

*** *p* value less than or equal to **0.001** was accepted as statistically different with respect to **control** group.

3.2 FTIR Spectroscopic Investigation of Bone Samples

Bone tissue can be viewed as a dense packing of organic matrix, consisting principally of collagen fibers along with several different types of proteins, peptides and lipids, in which large amounts of solid mineral crystals are deposited (Walters *et al.*, 1990). The bone mineral is defined as a poorly crystalline, calcium deficient, carbonate (CO_3^{2-}) and acid phosphate (HPO_4^{2-}) containing analogue of calcium hydroxyapatite (HA), $[\text{Ca}_{10}(\text{PO}_4)_6(\text{OH})_2]$ (Posner, 1987). Organic matrix and mineral constituents in bone tissues produce intense, structure-sensitive infrared bands. In order to make spectral comparison between pure hydroxyapatite and bone tissue, FTIR spectra of pure hydroxyapatite and rat bone (control group femur) in the $4000\text{-}435\text{ cm}^{-1}$ region are displayed in Figure 14. There are several bands in the region between 4000 and 2800 cm^{-1} , and between $1800\text{-}435\text{ cm}^{-1}$ region. The latter one is called as finger print region. The bands of interest are labeled on the figure and their assignments are given in Table 4.

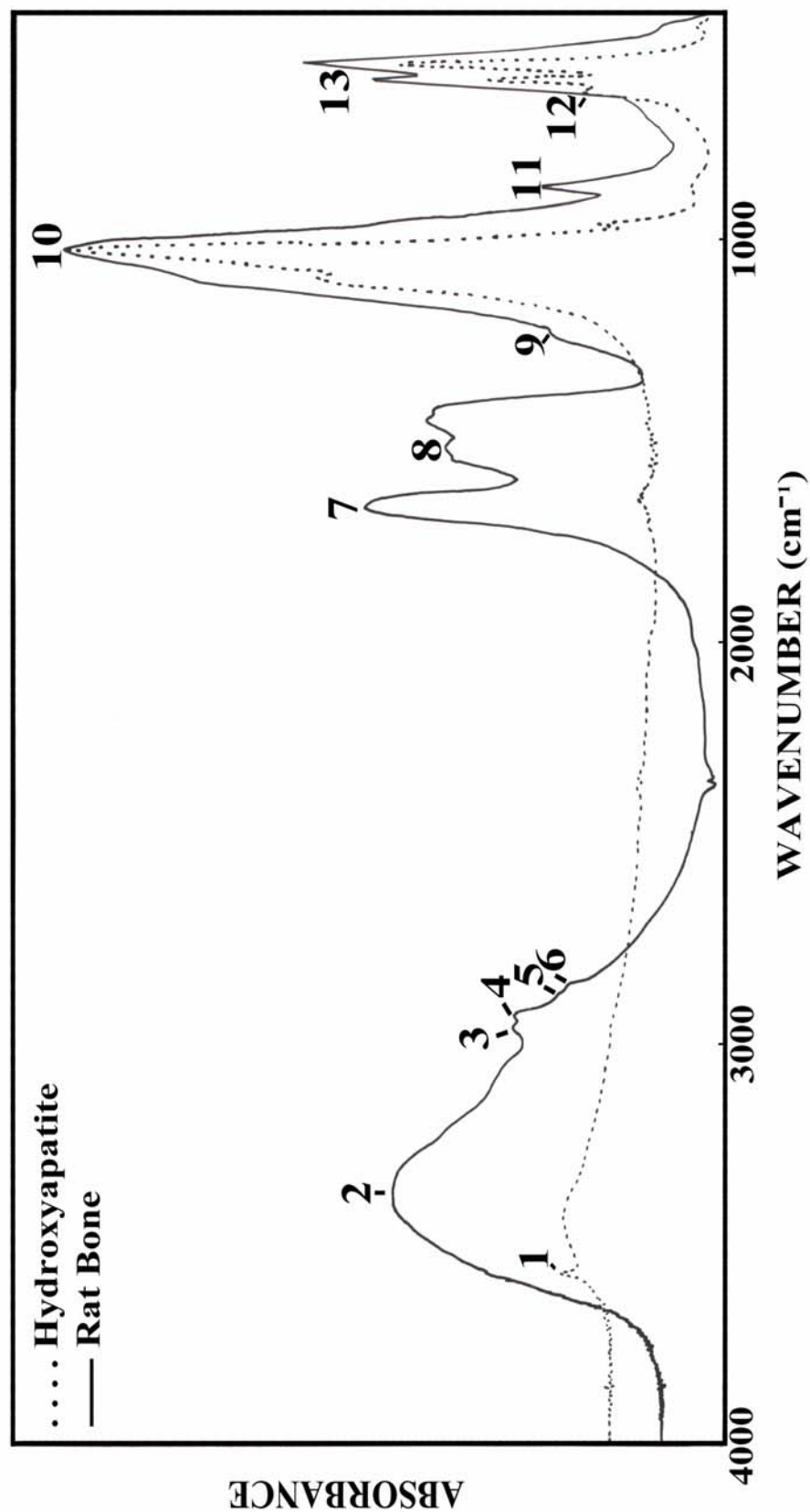


Figure 14. A typical FTIR spectrum of hydroxyapatite and of a normal rat femur in 4000 - 435 cm⁻¹ spectral region. The band assignments are given in Table 4.

Table 4. Major absorptions in the FTIR spectrum of synthetic highly crystalline hydroxyapatite and/or of rat bone tissue in the 4000-400 cm⁻¹ spectral region.

Band Number	Frequency (cm⁻¹)	Band Assignment
1	3570	OH stretching
2	3345	N-H group stretching vibration : polysaccharides, protein
3	2956	CH ₃ asymmetric stretching: mainly lipid with a small contribution from proteins, carbohydrates, nucleic acids.
4	2923	CH ₂ asymmetric stretching: mainly lipid with a small contribution from proteins, carbohydrates, nucleic acids.
5	2873	CH ₃ symmetric stretching: mainly proteins with a small contribution from, lipids, carbohydrates, nucleic acids.
6	2853	CH ₂ symmetric stretching: mainly lipid with a small contribution from proteins, carbohydrates, nucleic acids.
7	1651	Amide I (protein C=O stretch)
8	1550	Amide II (protein N-H bend, C-N stretch)
9	1238	Amide III (protein)
10	1200-900	ν_1, ν_3 PO ₄ ³⁻ stretching (mineral)
11	890-850	ν_2 CO ₃ ²⁻ (mineral)
12	633	OH libration
13	620-500	ν_4 PO ₄ ³⁻ bending (mineral)

In the spectrum of highly crystalline synthetic hydroxyapatite, the first peak at 3570 cm⁻¹ and the twelfth peak at 633 cm⁻¹ correspond to the stretching and the librational modes of hydroxyl (OH), respectively. In the spectrum of bone, these bands are not present at all, suggesting complete removal of OH groups.

The broad band in 3700-3100 cm⁻¹ region results from water, proteins and polysaccharides present in bone tissue (Figure 14). In the spectrum of highly crystalline hydroxyapatite the intensity of this band is very small. Hydroxyapatite in solution was dried in order to prepare KBr pellet for FTIR spectroscopic analysis. Therefore, in the FTIR spectrum of hydroxyapatite, the mentioned band is mainly due to intra molecular bond water. The bands located at 3000-2800 cm⁻¹ region are due to C-H stretching vibrations of mainly lipid groups present in bone matrix (Table 4). As it is expected, for inorganic synthetic hydroxyapatite there is no band in this spectral region (Figure 14). Similarly, the bands labeled as 7-9 (Amide I, II and III), which result from proteins present in the organic matrix, are absent in the spectrum of hydroxyapatite. As it can be noticed from this spectrum, there is some noise in this spectral region due to the presence of atmospheric water. In order to overcome this problem, smoothing process was applied for rat bone spectrum.

In order to see the differences in the finger print region clearly, the enlarged FTIR spectra is displayed in Figure 15. One of the differences between hydroxyapatite and bone tissue results from ~5-6 % carbonate substitution in bone tissue. Among the four vibration modes of the free carbonate (CO₃²⁻) ion, only two are of importance for infrared investigations in calcium-phosphates. These are denoted by ν_2 and ν_3 . The ν_1 mode is masked by the ν_3 phosphate band. The ν_4 mode gives very weak bands (757-670 cm⁻¹), which can be confused in the spectrum of bone with the baseline irregularities due to deformation vibrational modes of organic components (Rey *et al.*, 1989). The ν_3 mode (1400-1600 cm⁻¹), corresponding to the strongest infrared bands of the ion is obscured by several absorption bands of proteins (CH, Amide II, COO⁻) or glycosaminoglycans (NH) (Termine *et al.*, 1973).

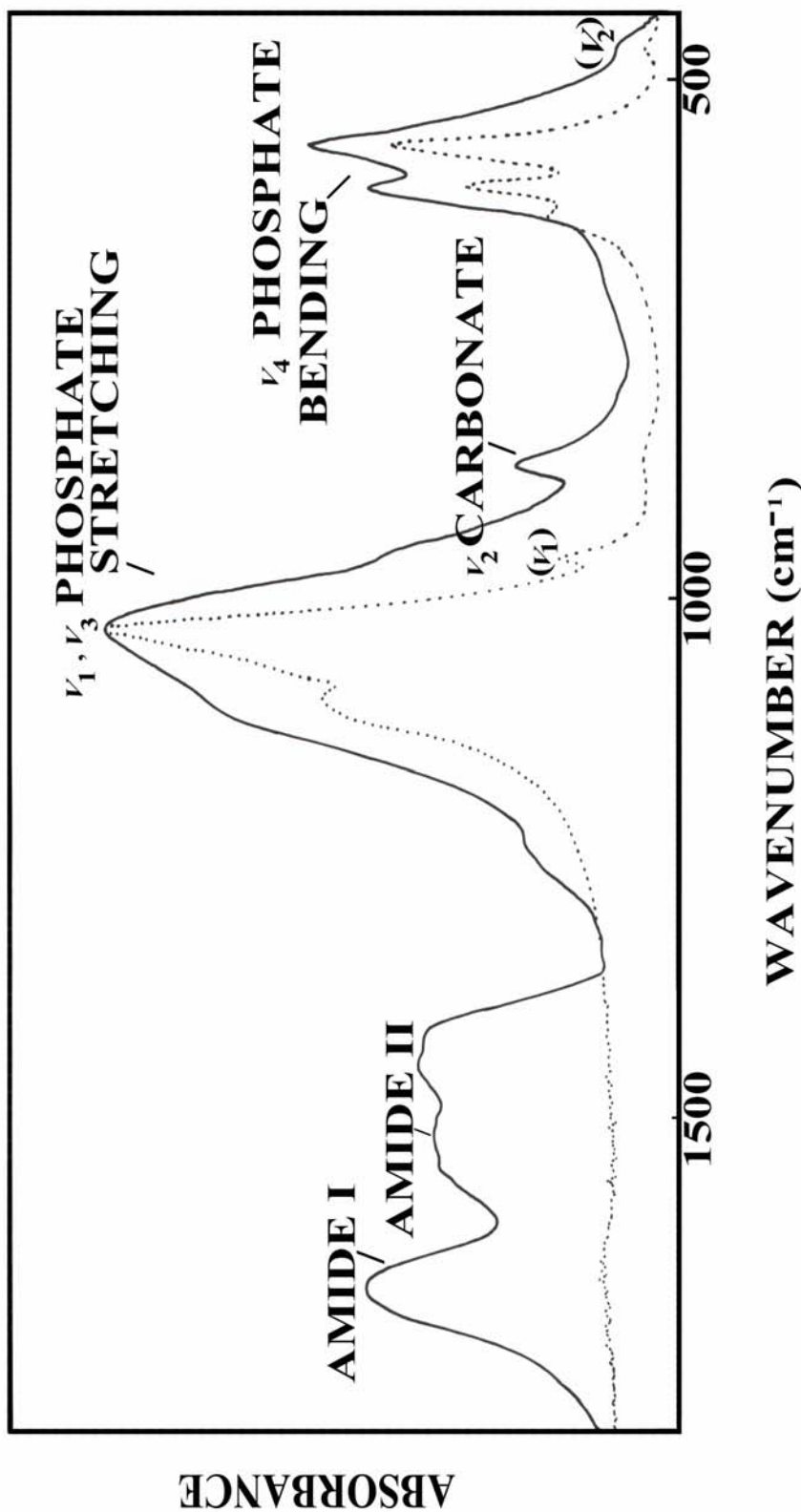


Figure 15. A typical FTIR spectrum of hydroxyapatite and of a normal rat femur in $1800 - 435 \text{ cm}^{-1}$ spectral region.
 HA: dashed line, bone (femur):solid line. The bands of interest are labeled on the figure. ν_1 and ν_2 given in parentheses correspond to weak phosphate bands.

The ν_2 vibrational domain of the carbonate ion is free of absorption by organic substituents and gives rise to a band in 880-850 cm⁻¹ region in the FTIR spectrum of rat bone tissue (peak 11 in Figure 14).

There are two inorganic orthophosphate ions in biological apatites present in mineralized tissue: phosphate (PO₄³⁻) and acid phosphate (HPO₄²⁻). The free PO₄³⁻ ion is tetrahedric and presents four vibrational modes. The ν_1 and ν_2 modes are normally inactive in infrared spectroscopy when the ion is in the regular tetrahedral symmetry, and only two bands due to the ν_3 and ν_4 modes can be observed (Rey *et al.*, 1990). The ν_2 mode produces faint bands at 470 cm⁻¹ (Figure 15) (Fowler *et al.*, 1966, Rey *et al.*, 1990). The ν_1 P-O symmetric stretching vibration is represented in apatites by a very narrow band (950-1000 cm⁻¹) which appears as a shoulder on the ν_3 P-O asymmetric stretching mode (900-1200 cm⁻¹) in a poorly crystalline apatite like bone mineral (Figure 15). The ν_4 asymmetric P-O bending mode appears as a sharp band in the 500-650 cm⁻¹ region. The stretching vibration of the P-OH band (ν_3 mode) appears at 870 cm⁻¹, where it is overlapped by the strong ν_2 CO₃²⁻ band in bone tissue. Therefore, the stretching vibration of the HPO₄²⁻ cannot be observed (Rey *et al.*, 1990).

It is thought that the microstructure of biological hydroxyapatite and collagen fibrils can affect the mechanical, chemical and biological properties of bone tissue (Nightingale *et al.*, 1971, Daculsi *et al.*, 1997, Knott and Bailey, 1998). Therefore, in the present study intense, structure sensitive infrared bands of mineral and organic matrix constituents were analysed for two different purposes, namely to determine the effects of selenium on diabetic rat bones and to determine the effects of selenium deficiency and vitamin E adequacy and selenium toxicity on rat bones. In the following section, the FTIR spectral analysis results will be presented for these two conditions, respectively.

3.2.1 FTIR Spectroscopic Analysis to Determine the Effects of Selenium on Diabetic Bone Samples

Mature bone consists of 60-70 % mineral and 30-40 % organic matrix. In order to gain information about the mineral environment of control, diabetes, diabetes + Se and control + Se group rat femurs and tibias, the ν_4 phosphate bending, ν_1 , ν_3 phosphate stretching and ν_2 carbonate regions of undeproteinized ground bone spectra were analyzed using second derivative and curve-fitting methods. Around 90 % of bone proteins consists of type I collagen. Therefore, the spectral changes seen in Amide I band directly reflect the changes seen in collagen micro-environment. Amide II band of proteins overlaps with intense ν_3 carbonate band. Therefore, this band is not suitable for FTIR spectroscopic analysis of bone proteins, without demineralizing the bone tissue. The information about lipid groups can be obtained from the C-H stretching region ($2800\text{-}3000\text{ cm}^{-1}$) of the FTIR spectrum of bone samples. For control and experimental groups, the results of spectral analysis of the mentioned bands are reported below.

3.2.1.1 ν_4 Phosphate Bending Region

In the ν_4 phosphate bending region, curve-fitting analysis was carried out to resolve the underlying bands. This band was decomposed into five bands. They are located around 533, 563, 575, 604 and 617 cm^{-1} (Figure 16). The peak labeled 1 in the figure is due to nonapatitic HPO_4^{2-} groups, which can be easily exchangeable with carbonate species. The peak labeled 5 results from nonapatitic PO_4^{3-} and indicates the presence of poorly crystalline apatites (Bohic *et al.*, 2000, Ou-Yang *et al.*, 2000). The other peaks are due to apatitic PO_4^{3-} ions (Rey *et al.*, 1990, Bohic *et al.*, 2000, Ou-Yang *et al.*, 2000).

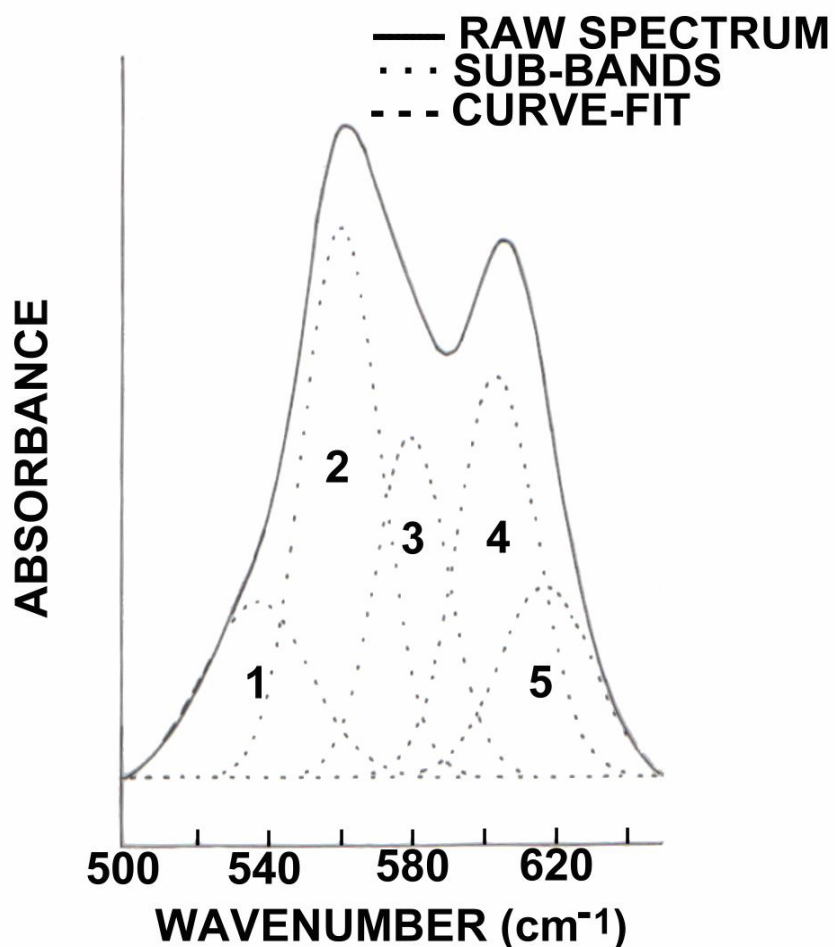


Figure 16. Curve-fitting analysis of the $\nu_4 \text{PO}_4^{3-}$ bending region. The sub-bands are assigned as a nonapatitic acid phosphate (band 1), apatitic phosphate (bands 2, 3 and 4) and nonapatitic phosphate (band 5).

In order to see the relative contribution of each of the underlying bands in the ν_4 phosphate bending region, the means of calculated partial peak areas are presented in Figure 17 A and B for the femur and tibia, respectively.

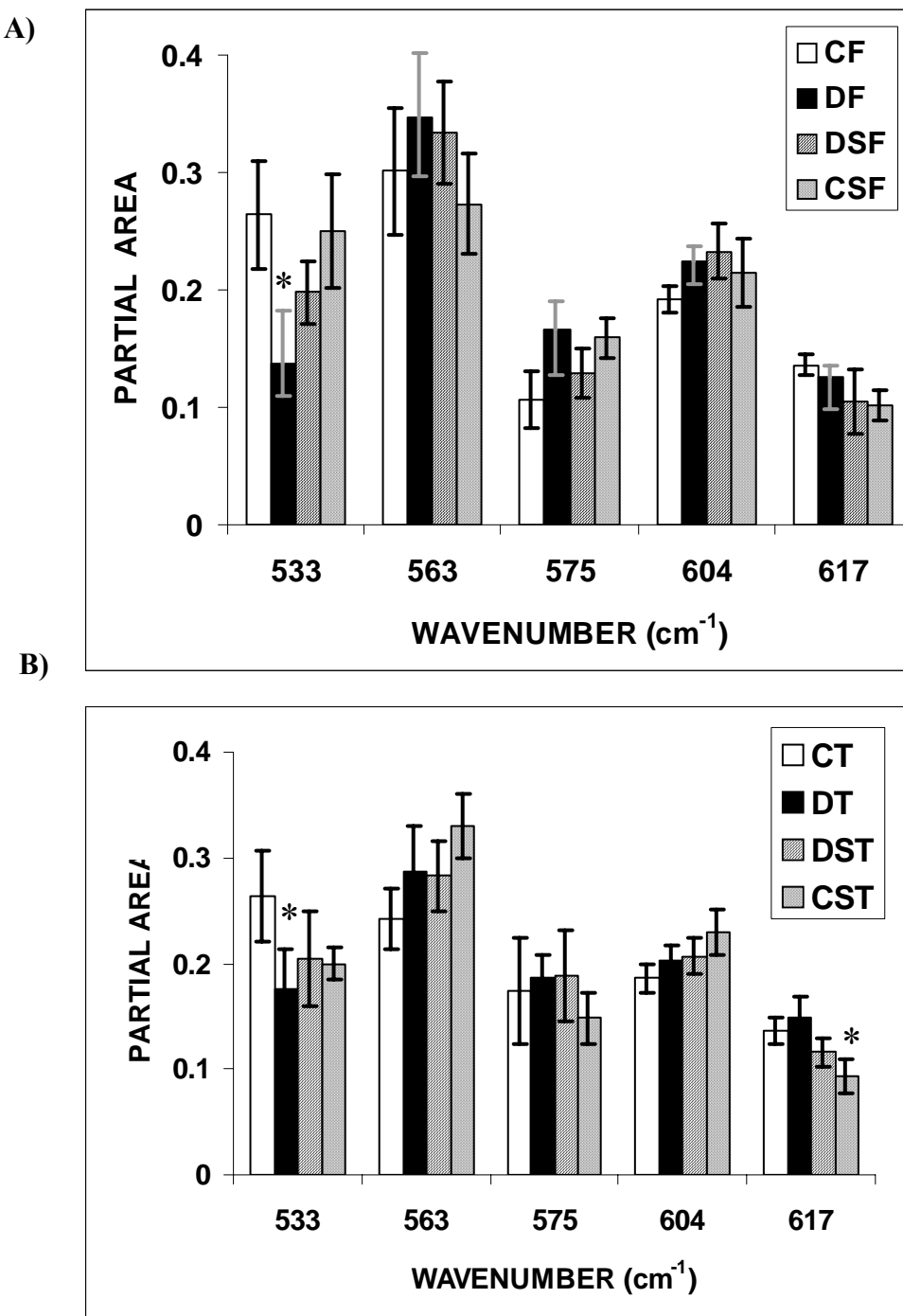


Figure 17. The means of partial peak areas obtained from curve-fitting analysis of the $\nu_4 \text{PO}_4^{3-}$ bending region for A) femurs (F) and B) tibias (T) of control (C), diabetes (D), diabetes + Se (DS) and control + Se group (CS) rats.

* p value equal to or less than **0.05** was accepted as significantly different with respect to **control** group.

In order to compare the results easily between the femurs and the tibias of control and experimental groups, the calculated mean values of partial peak areas in the ν_4 PO_4^{3-} bending region are summarized in Table 5.

Table 5. The partial peak areas of each of the five sub-bands calculated from the curve-fitting analysis results of the ν_4 PO_4^{3-} bending band (mean \pm standard error of mean (SEM) for A) femurs (F) and B) tibias (T) of control and experimental groups.

A)

	FEMUR				
	Nonapatitic HPO_4^{2-} 533 cm^{-1}	Apatitic PO_4^{3-} 563 cm^{-1}	Apatitic PO_4^{3-} 575 cm^{-1}	Apatitic PO_4^{3-} 604 cm^{-1}	Nonapatitic PO_4^{3-} 617 cm^{-1}
Control	0.264 \pm 0.046	0.301 \pm 0.054	0.107 \pm 0.024	0.192 \pm 0.012	0.136 \pm 0.009
Diabetes	0.137\pm0.027*	0.347 \pm 0.051	0.166 \pm 0.038	0.225 \pm 0.020	0.126 \pm 0.027
Diabetes+Se	0.198 \pm 0.027	0.334 \pm 0.043	0.129 \pm 0.021	0.233 \pm 0.024	0.105 \pm 0.028
Control+Se	0.250 \pm 0.049	0.273 \pm 0.043	0.159 \pm 0.017	0.215 \pm 0.029	0.102 \pm 0.013

B)

	TIBIA				
	Nonapatitic HPO_4^{2-} 533 cm^{-1}	Apatitic PO_4^{3-} 563 cm^{-1}	Apatitic PO_4^{3-} 575 cm^{-1}	Apatitic PO_4^{3-} 604 cm^{-1}	Nonapatitic PO_4^{3-} 617 cm^{-1}
Control	0.263 \pm 0.043	0.242 \pm 0.028	0.174 \pm 0.051	0.186 \pm 0.013	0.136 \pm 0.012
Diabetes	0.175\pm0.038*	0.287 \pm 0.043	0.187 \pm 0.021	0.203 \pm 0.014	0.149 \pm 0.019
Diabetes+Se	0.205 \pm 0.045	0.283 \pm 0.033	0.189 \pm 0.043	0.207 \pm 0.017	0.116 \pm 0.013
Control+Se	0.200 \pm 0.016	0.330 \pm 0.031	0.148 \pm 0.024	0.230 \pm 0.022	0.093\pm0.016*

* p value less than or equal to **0.05** was accepted as significantly different with respect to **control** group.

As seen from Figure 17 and Table 5, for the femurs and the tibias of the diabetic group rats, the relative ratio of nonapatitic HPO_4^{2-} significantly decreased, whereas relative apatitic PO_4^{3-} content increased. For Se treated diabetic rat bones the relative ratio of nonapatitic HPO_4^{2-} increased as compared with diabetic group and approached to control values. There were negligible changes in the relative apatitic PO_4^{3-} content of Se treated diabetic rat bones.

On the other hand, for Se treated control group tibias, the nonapatitic HPO_4^{2-} content decreased. Similarly, for both bones of the same group rats, the nonapatitic PO_4^{3-} content decreased significantly with respect to control group. A similar decrease with respect to control and diabetic group bones was also observed for nonapatitic PO_4^{3-} content of Se treated diabetic bones.

3.2.1.2 ν_1 , ν_3 Phosphate Stretching Region

A typical raw absorbance spectrum of the ν_1 , ν_3 phosphate stretching region ($900\text{-}1200\text{ cm}^{-1}$) is given in Figure 18A. This broad band consists of several narrow underlying bands. By using second derivative spectroscopy, this band was resolved into six bands locating at 957 cm^{-1} , 988 cm^{-1} , 1020 cm^{-1} , $\approx 1063\text{ cm}^{-1}$, 1112 cm^{-1} and $\approx 1145\text{ cm}^{-1}$, respectively (Figure 18B). The 957 cm^{-1} band was assigned to ν_1 symmetric stretching of phosphate ion (Fowler *et al.*, 1966, Pleshko *et al.*, 1991, Gadeleta *et al.*, 1996). The components of the ν_3 mode at 1020 cm^{-1} , 1060 cm^{-1} and 1112 cm^{-1} were assigned to phosphate in a poorly crystalline, nonstoichiometric apatite environment containing acid phosphate and/or carbonate (Rey *et al.*, 1991b, Camacho *et al.*, 1996, Gadeleta *et al.*, 1996, Boskey *et al.*, 1998). The other component of the ν_3 mode, which is located at 988 cm^{-1} was assigned to either PO_4^{2-} in nonapatitic / nonstoichiometric environment (Ou-Yang, *et al.*, 2000) or HPO_4^{2-} vibrations (Rey *et al.*, 1991b, Camacho *et al.*, 1996, Boskey *et al.*, 1998).

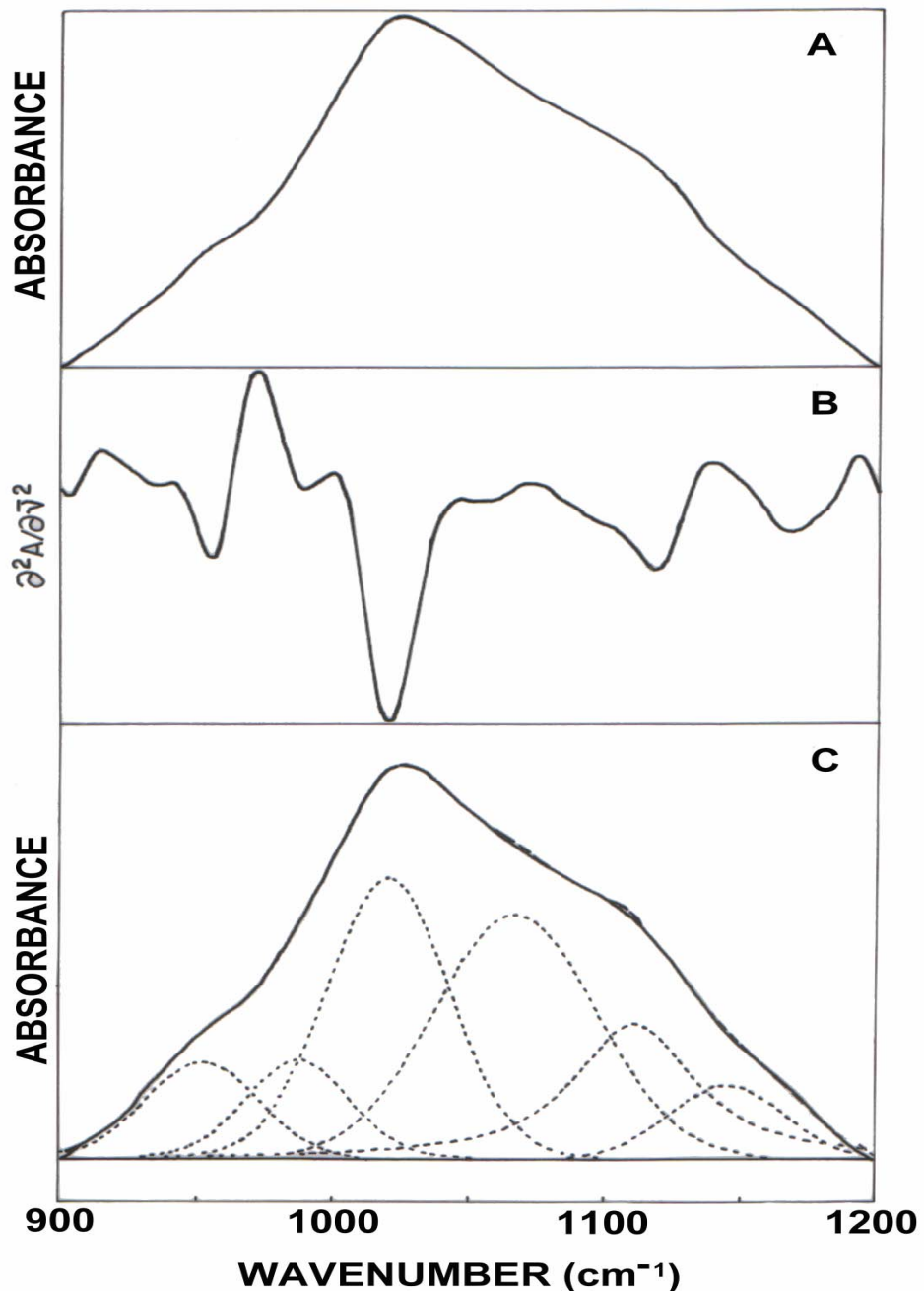


Figure 18 A) A typical FTIR spectrum of a rat femur in the ν_1 , ν_3 PO_4^{3-} stretching spectral region located at $900\text{-}1200\text{ }\text{cm}^{-1}$ B) its calculated second derivative C) the underlying six bands as deduced by curve-fitting analysis of the same region. Raw spectrum (solid line); calculated curve-fit (dashed line); sub-bands (dotted line).

Similarly, the band at $\approx 1145 \text{ cm}^{-1}$ was also assigned to HPO_4^{2-} vibrations (Rey *et al.*, 1991b, Camacho *et al.*, 1996, Boskey *et al.*, 1998, Ou-Yang, *et al.*, 2000).

It was previously stated that in the ν_1 , ν_3 phosphate stretching spectral region, at least six components are necessary and sufficient for a proper curve-fitting analysis of poorly crystalline apatites (Pleshko *et al.*, 1991). Considering this fact and the second derivative analysis results obtained in the present study, the curve-fitting analysis was carried out by placing six sub-bands in this spectral region. Figure 18C shows a typical curve-fitting analysis of the ν_1 , ν_3 phosphate stretching region. As can be noticed from the figure, the calculated curve-fit is almost completely overlapped with the raw spectrum. The results of the curve-fitting analysis are expressed as mean of peak areas for each of the six sub-bands and are given in Table 6 for the femurs and the tibias of control and experimental groups, respectively.

Table 6. Peak areas of sub-bands (mean \pm SEM) obtained from curve-fitting analysis of the ν_1 , ν_3 phosphate stretching region of the FTIR spectra for the femurs and the tibias of control and experimental groups.

Mean of partial areas of the sub-bands obtained from curve-fitting analysis of the ν_1 , ν_3 phosphate stretching region ($900\text{-}1200\text{ cm}^{-1}$) of the FTIR spectra.

	Sub-band ₁ 957 cm⁻¹	Sub-band ₂ 988 cm⁻¹	Sub-band ₃ 1020 cm⁻¹	Sub-band ₄ 1063 cm⁻¹	Sub-band ₅ 1112 cm⁻¹	Sub-band ₆ 1145 cm⁻¹
FEMUR (F)						
Control (C)	7.02 \pm 0.81	15.44 \pm 2.28	33.39 \pm 1.91	35.77 \pm 3.04	16.72 \pm 4.25	7.86 \pm 1.99
Diabetes (D)	7.43 \pm 1.81	7.50 \pm 2.49	36.75 \pm 7.68	17.49\pm6.13*	27.85 \pm 7.55	4.57 \pm 1.01
Diabetes+Se (DS)	8.77 \pm 0.96	12.01 \pm 2.69	30.60 \pm 3.80	37.04\pm3.22#	21.47 \pm 2.35	7.20 \pm 0.90
Control+Se (CS)	7.20 \pm 1.87	6.26 \pm 2.78	26.70 \pm 5.44	27.47 \pm 6.33	17.47 \pm 5.38	6.25 \pm 1.49
TIBIA (T)						
Control (C)	8.66 \pm 2.12	11.02 \pm 2.80	25.99 \pm 4.93	31.80 \pm 4.20	20.35 \pm 4.30	6.28 \pm 1.15
Diabetes (D)	10.87 \pm 1.77	8.58 \pm 3.60	39.45 \pm 7.77	18.64 \pm 5.48	31.40 \pm 6.64	5.26 \pm 0.74
Diabetes+Se (DS)	6.66 \pm 1.58	8.39 \pm 4.05	20.33 \pm 5.79	28.96 \pm 7.16	13.10 \pm 4.05	5.51 \pm 1.27
Control+Se (CS)	6.28 \pm 0.94	5.71 \pm 2.07	40.89 \pm 5.58	38.39\pm2.70#	22.51 \pm 1.96	6.17 \pm 0.68

* p value equal to or less than **0.05** was accepted as statistically significant with respect to **control** group.

p value equal to or less than **0.05** was accepted as statistically significant with respect to **diabetes** group.

Because of the presence of HPO_4^{2-} , CO_3^{2-} and some other ions, bone tissue is defined as nonstoichiometric, poorly crystalline hydroxyapatite. As stated above, the variations in the sixth band (1145 cm^{-1}) are due to HPO_4^{2-} and in literature it was stated that the contour of this band positively correlates with the nonapatitic HPO_4^{2-} component of the $v_4 \text{ PO}_4^{3-}$ bending band (Ou-Yang *et al.*, 2000). As seen from Table 6, though the changes are not significant for this band, the trends of the variations with respect to control groups are similar to those seen in the nonapatitic HPO_4^{2-} sub-band of the $v_4 \text{ PO}_4^{3-}$ bending band (Table 5).

The alterations in mean peak area of other sub-bands as compared with those of control group demonstrate the presence of some alterations in the local environment of the mineral phase in experimental groups. For diabetic group, the highest changes in the mean peak area of the control groups are seen in the fourth band locating at 1063 cm^{-1} . The percent area of this sub-band is correlated with the crystal size of minerals present in calcified tissues according to the following equation (Pleshko *et al.*, 1991, 1992):

$$Y = aX^b + c \quad (3.1)$$

Where Y is the crystal size (\AA), X is the percent area of the fourth component and a, b and c are constants, determined by least squares regression analysis ($r= 0.84$) as - 30.70, 0.284 and 227.8, respectively.

Ground rat bone samples were used in the studies cited above for FTIR spectroscopic analysis. Therefore, in the present study the same equation was used to see the variations in crystal size of control and experimental group rat bones. In Figure 19 the results are summarized as bar diagram and in Table 7 calculated crystal sizes are given for control and experimental groups. As seen from the results of statistical analysis, the crystal size of diabetic femurs increased significantly. For diabetic tibias the increase in the crystal size with respect to control group was also

high. For Se treated diabetic group the crystal size led to reversal of crystal sizes to normal values. This was more pronounced in Se treated diabetic femurs as compared with the tibias of the same group. On the other hand, although the changes are not statistically significant, Se treatment led to increase in the crystal size of control group femurs as compared with untreated control group femurs. An opposite change was observed for the tibias of the Se treated control group rats. Considering the alterations in the mean peak area of the fourth band given in Table 6, it can be briefly concluded that, as the mean peak area of the fourth band decreases the mineral crystal size increases. However, equation 3.1 is valid for the mineral crystal sizes between 135-190 Å.

Another way of taking information about the crystal size of the mineral components present in bone tissue is to analyze the peak position of the third band in the ν_1 , ν_3 PO_4^{3-} stretching domain. It was previously reported that a component at $\approx 1020 \text{ cm}^{-1}$ is indicative of nonstoichiometric apatites containing HPO_4^{2-} and / or CO_3^{2-} whereas, the one at $\approx 1030 \text{ cm}^{-1}$ is indicative of stoichiometric apatites (Rey *et al.*, 1991b, Gadeleta *et al.*, 1996, Boskey *et al.*, 1998). This difference can be clearly seen from Figure 18, which illustrates the spectra of control and experimental group femurs comparatively with highly crystalline synthetic hydroxyapatite in 1200-900 cm^{-1} ν_1 , ν_3 phosphate stretching region. In the present study the peak of this broad band is observed between 1020-1027 cm^{-1} for control and experimental groups which is indicative of the presence of nonstoichiometric poorly crystalline mineral structure, whilst the peak of the spectrum of highly crystalline synthetic hydroxyapatite is located at $\approx 1030 \text{ cm}^{-1}$ (Figure 20).

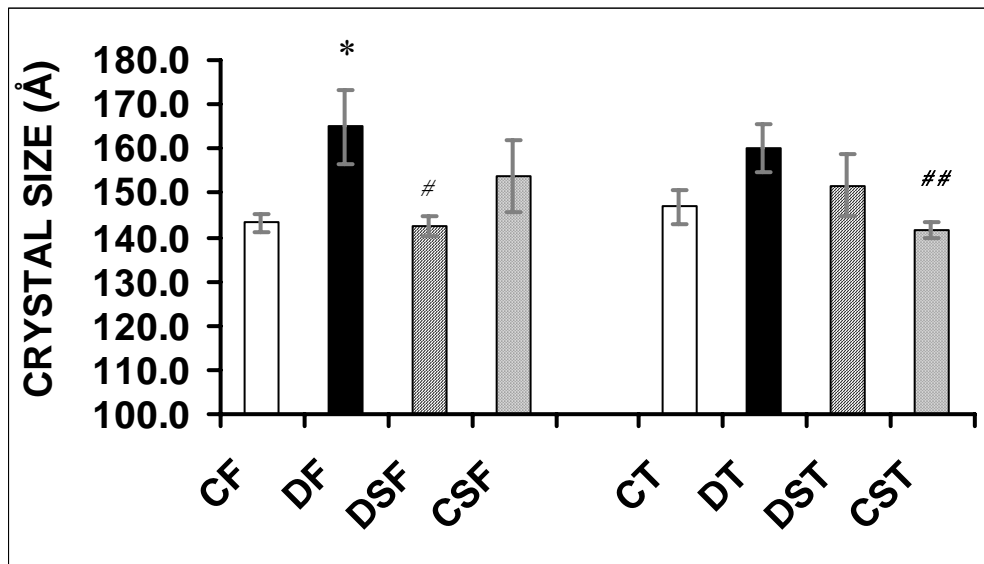


Figure 19. Bar diagram illustrating the mean of crystal sizes of control (C), diabetes (D), diabetes + Se (DS) and control + Se (CS) group femurs (F) and tibias (T).

p* value less than or equal to **0.05 was accepted as significantly different with respect to **control** group.

#*p* value less than or equal to **0.05** was accepted as significantly different with respect to **diabetes** group.

##*p* value less than or equal to **0.01** was accepted as significantly different with respect to **diabetes** group.

Table 7. Crystal sizes of control (C), diabetes (D), diabetes + Se (DS) and control + Se (CS) group femurs (F) and tibias (T).

Crystal Size (Å)		
GROUP	FEMUR	TIBIA
Control (C)	143.3±2.1	146.8±3.8
Diabetes (D)	164.9±8.4*	160.2±5.5
Diabetes + Se (DS)	142.5±2.1#	151.7±7.2
Control + Se (CS)	153.7±8.3	141.5±1.9##

p* value less than or equal to **0.05 was accepted as significantly different with respect to **control** group.

#*p* value less than or equal to **0.05** was accepted as significantly different with respect to **diabetes** group.

##*p* value less than or equal to **0.01** was accepted as significantly different with respect to **diabetes** group.

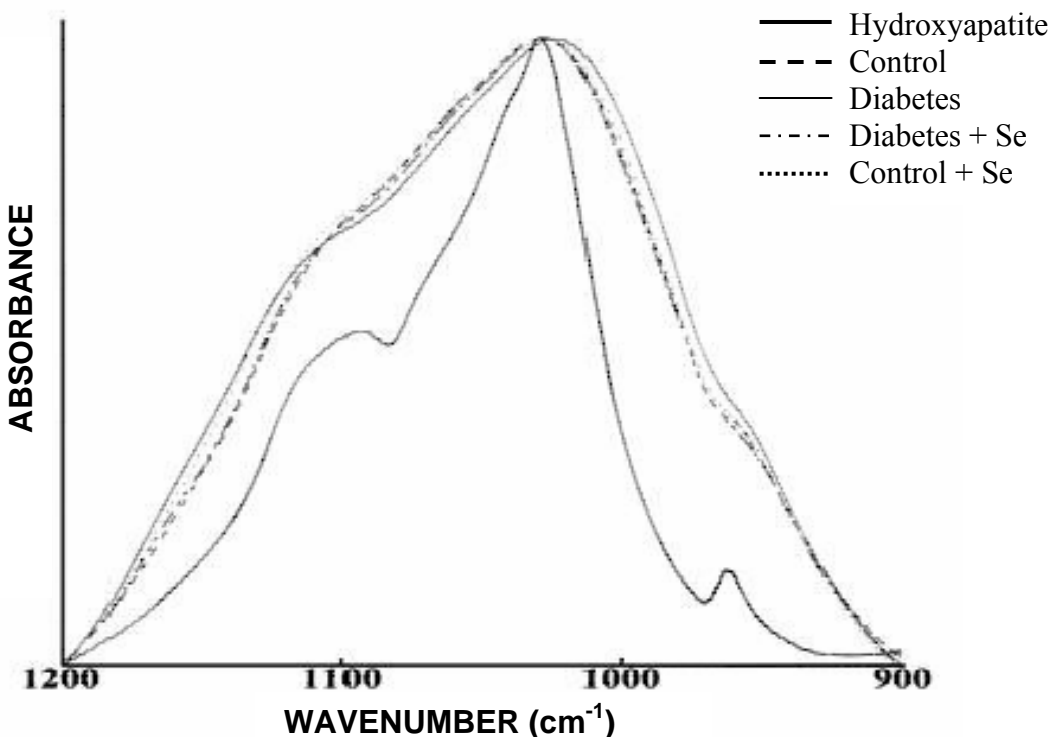


Figure 20. Comparison of the spectra of poorly crystalline control and experimental group femurs, with highly crystalline synthetic hydroxyapatite in the ν_1 , ν_3 phosphate stretching region ($1200\text{-}900\text{ cm}^{-1}$).

3.2.1.3 ν_2 Carbonate (CO_3^{2-}) Region

Carbonate present in the apatite mineral phase of bone plays a significant role in bone resorption. In the $\nu_2 \text{CO}_3^{2-}$ domain, the curve-fitting analysis was carried out and this band was decomposed into three sub-bands. A component at 871 cm^{-1} is due to the carbonate ions occupying the trivalent anionic (PO_4^{3-}) sites (type B carbonate). A band at 878 cm^{-1} is due to the carbonate ions substituting for monovalent anionic (OH^-) sites (type A carbonate) and a band at 866 cm^{-1} corresponds to a labile carbonate environment locating in perturbed regions of the mineral crystals (Rey *et al.*, 1989, 1991a, 1991c, Bohic *et al.*, 2000).

Figure 21 shows the curve-fitting analysis of the $\nu_2 \text{CO}_3^{2-}$ region for the determination of apatitic and nonapatitic environments of bone samples. The ratios of the area of each of the underlying bands to total area in the $\nu_2 \text{CO}_3^{2-}$ domain are given in Table 8 for femurs and tibias of control and experimental groups, respectively. As can be seen from the table, type B carbonate is the major constituent and type A and labile type carbonate ions are present at a lower extend. This implies that the carbonate ions mainly substitute for phosphate groups rather than hydroxyl ions.

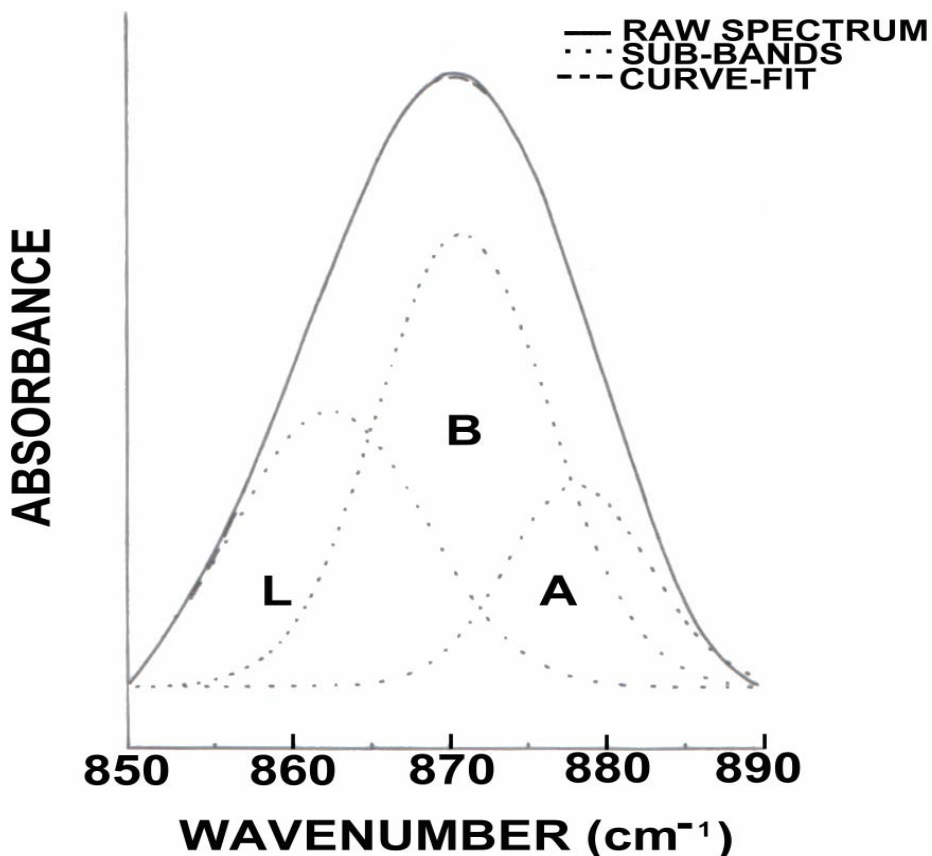


Figure 21. Curve-fitting analysis of the $\nu_2 \text{CO}_3^{2-}$ region ($850\text{-}890 \text{ cm}^{-1}$). The sub-bands are assigned as non-apatitic labile carbonate (866 cm^{-1}) (band L), Type B carbonate (871 cm^{-1}) (band B) and Type A carbonate (878 cm^{-1}) (band A).

Table 8. ν_2 CO_3^{2-} spectral region curve-fitting analysis results.

GROUP	Nonapatitic labile	Apatitic Type B	Apatitic Type A
	CO_3^{2-}	CO_3^{2-}	CO_3^{2-}
	Partial Area ₁ (866 cm ⁻¹)	Partial Area ₂ (871 cm ⁻¹)	Partial Area ₃ (878 cm ⁻¹)
FEMUR			
Control	0.306±0.019	0.562±0.026	0.132±0.003
Diabetes	0.194±0.015	0.669±0.009*	0.138±0.009
Diabetes + Se	0.372±0.016	0.427±0.021	0.201±0.023
Control + Se	0.346±0.020	0.389±0.010	0.266±0.015*
TIBIA			
Control	0.180±0.037	0.625±0.023	0.195±0.019
Diabetes	0.120±0.053	0.629±0.020	0.251±0.015
Diabetes +Se	0.338±0.020*	0.414±0.021**	0.248±0.005
Control + Se	0.373±0.009*	0.423±0.015**	0.204±0.009

* $p<0.05$ was accepted as significantly different with respect to **control** group.

** $p<0.01$ was accepted as significantly different with respect to **control** group.

Diabetes caused a decrease in labile carbonate content and significant increase in type B carbonate content of femurs. Similarly for diabetic tibia the relative amount of labile carbonate decreased. Selenium treatment led to reversal of labile type carbonate content in diabetic femurs. For selenium treated control femur, type A carbonate content increased significantly.

For tibias of both of the selenium treated groups, the relative amount of labile type carbonate increased significantly whereas, the relative amount of type B carbonate decreased significantly as compared with the control group tibias. Therefore, the changes in type L and type B carbonate contents are parallel for the femurs and the tibias in experimental groups as compared with the control groups of femurs and tibias. But, the selenium treatment in tibias caused more significant changes in relative amounts of labile and type B carbonates as compared with femurs.

3.2.1.4 Amide I Region

The curve-fitting analysis of the Amide I region revealed three sub-bands locating at 1690 cm^{-1} , 1660 cm^{-1} and 1633 cm^{-1} as can be seen in Figure 20. The band at 1633 cm^{-1} represents one of collagen's secondary structural elements (Lazarev *et al.* 1985, Miller and Tague, 2002). The bands at $\sim 1660\text{ cm}^{-1}$ and $\sim 1690\text{ cm}^{-1}$ were assigned to non-reducible pyridinoline [Pyr] and reducible dihydroxylysinoornithine [DHLNL] cross-links present in collagen I of the bone tissue, respectively (Paschalis *et al.*, 1998, 2001, Atti *et al.*, 2002, Huang *et al.*, 2003).

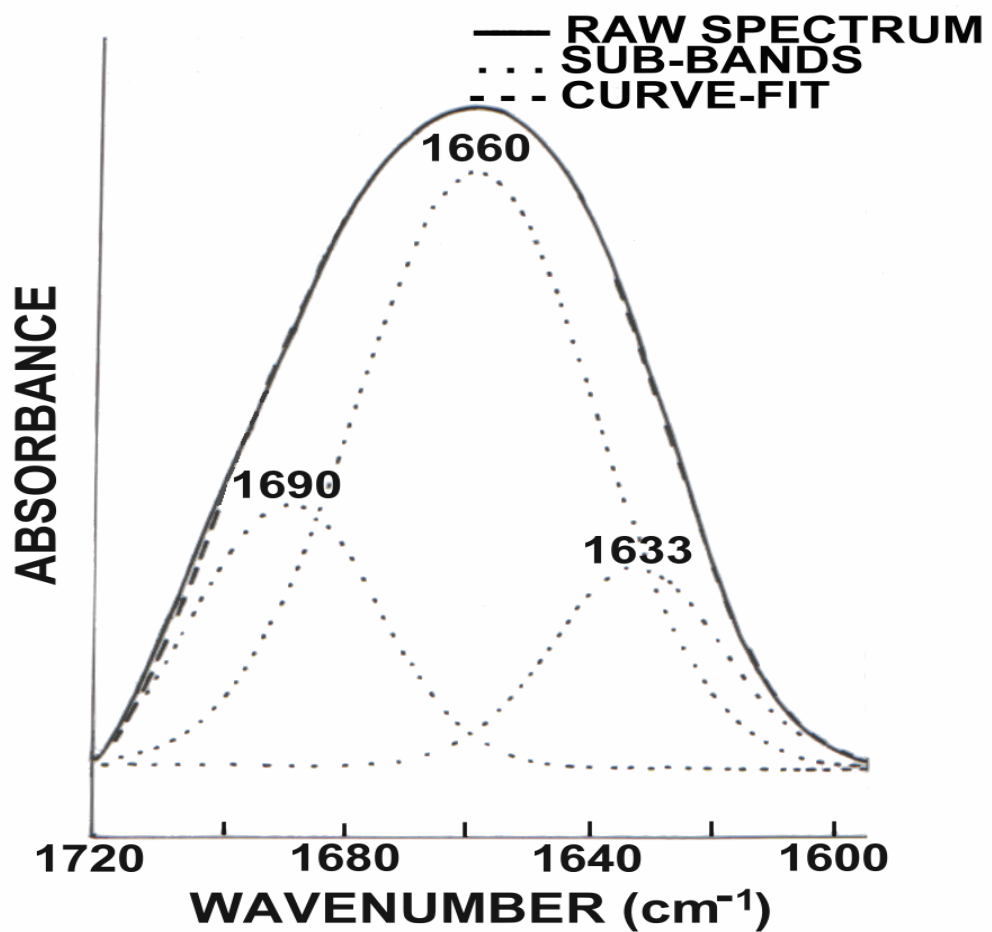


Figure 22. A typical FTIR spectrum of ground rat femur in the Amide I region and its underlying sub-bands obtained from curve-fitting analysis.

In order to evaluate the variations in the relative ratio of non-reducible cross-links to reducible cross-links, the ratio of the areas under the 1660 cm⁻¹ and 1690 cm⁻¹ sub-bands was calculated and the results are summarized in Figure 23 and Table 9.

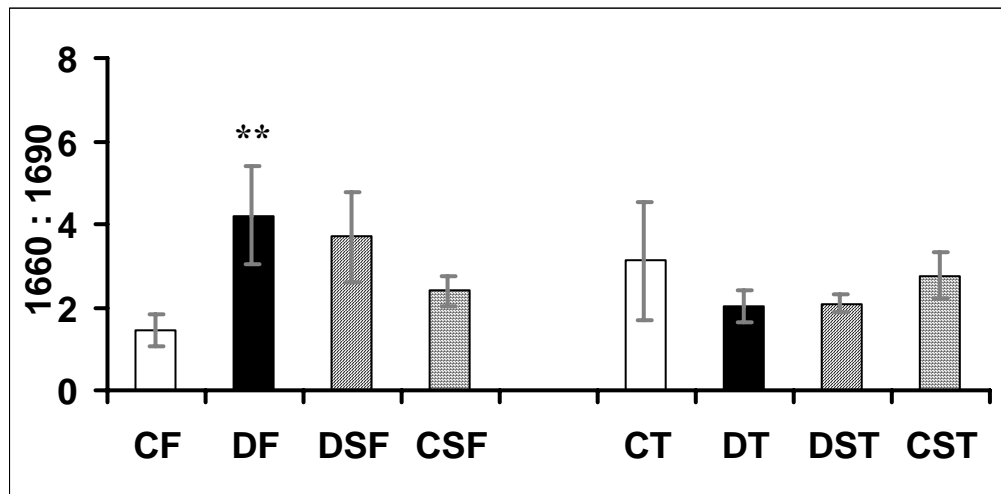


Figure 23. Comparison of the 1660 to 1690 cm⁻¹ peak area ratio for the femurs (F) and tibias (T) of control (C), diabetes (D), diabetes + Se (DS) and control + Se (CS) group rats.

p* value less than or equal to **0.05 was accepted as significantly different with respect to **control** group.

** *p* value less than or equal to **0.01** was accepted as significantly different with respect to **control** group.

Table 9. 1660 : 1690 ratio calculated from curve-fit spectra of control (C), diabetes (D), diabetes + Se (DS) and control + Se (CS) group femurs (F) and tibias (T).

1660 : 1690		
GROUP	FEMUR	TIBIA
Control (C)	1.455±0.381	3.127±1.822
Diabetes (D)	4.197±1.177**	2.019±0.373
Diabetes + Se (DS)	3.693±1.097	2.094±0.224
Control + Se (CS)	2.399±0.352	2.756±0.546

p* value less than or equal to **0.05 was accepted as significantly different with respect to **control** group.

** *p* value less than or equal to **0.01** was accepted as significantly different with respect to **control** group.

For diabetic group femurs the relative ratio of non-reducible cross-links to reducible cross-links increased significantly. Se treatment led to restoring effect in diabetic femurs. For femurs of Se treated control group the $1660 : 1690\text{ cm}^{-1}$ ratio was higher than control group femurs. Whilst, the $1660 : 1690\text{ cm}^{-1}$ ratios for all of the experimental group tibias were less than the same ratio for control group tibias. But the changes with respect to control group were not significant.

3.2.1.5 Mineral to Matrix and Carbonate to Phosphate Ratios

Table 10 shows the mineral to matrix ratios calculated for the femurs and tibias of control and experimental groups and Table 11 shows the carbonate to phosphate ratios calculated for the femurs and tibias of control and experimental groups. As seen from Tables 10 and 11, femur specimens taken from diabetic group rats had significantly higher mineral to matrix (phosphate to amide I) ratio and a lower carbonate to phosphate ratio compared with control group rats. For tibia specimens taken from the same group rats though the changes in these ratios were not significant, the trends were similar to those for diabetic femurs.

Table 10. Mineral to matrix ratios calculated for the femurs (F) and tibias (T) of control (C), diabetes (D), diabetes + Se (DS) and control + Se (CS) groups

Mineral : matrix (phosphate : amide I)		
GROUP	FEMUR	TIBIA
Control (C)	3.371 ± 0.285	4.255 ± 0.389
Diabetes (D)	$4.324 \pm 0.314^*$	4.616 ± 0.494
Diabetes + Se (DS)	3.904 ± 0.264	$3.482 \pm 0.185^\#$
Control + Se (CS)	3.702 ± 0.136	3.452 ± 0.286

* p value less than or equal to **0.05** was accepted as significantly different with respect to **control** group.

p value less than or equal to **0.05** was accepted as significantly different with respect to **diabetes** group.

Table 11. Carbonate to phosphate ratios calculated for the femurs (F) and tibias (T) of control (C), diabetes (D), diabetes + Se (DS) and control + Se (CS) groups.

Carbonate : phosphate		
GROUP	FEMUR	TIBIA
Control (C)	0.0503 ± 0.0048	0.0340 ± 0.0025
Diabetes (D)	0.0340 ± 0.0031*	0.0300 ± 0.0044
Diabetes + Se (DS)	0.0415 ± 0.0043	0.0350 ± 0.0036
Control + Se (CS)	0.0401 ± 0.0042	0.0316 ± 0.0026

p* value less than or equal to **0.05 was accepted as significantly different with respect to **control** group.

Se treated diabetic and control group femurs had higher mineral to matrix ratio with respect to control group whereas, opposite changes were valid for tibias of the same groups.(Table 10). As seen from Table 11, Se treatment led to some restoring effect in the carbonate to phosphate ratio for diabetic femurs. For Se treated control group femurs the relative carbonate to phosphate ratio decreased with respect to control group as well. For the tibias of the experimental groups, the trends of the alterations in this ratio with respect to control group were parallel to those seen in experimental group femurs but none of the changes was significant.

3.2.1.6 C-H Stretching Region

In biological systems the CH₂ bending (or scissoring) mode gives rise to bands around 1470 cm⁻¹ and their exact frequency is dependent on acyl chain packing and conformation of lipids. However, in the FTIR spectrum of a bone tissue this band is obscured by several absorbtion bands of carbonate ions (Mendelsohn and Mantsch, 1986, Rey *et al.*, 1989). Therefore, in order to investigate the effects of selenium, as an antioxidant, on mainly lipid components of diabetic and normal rat long bone

tissues the C-H stretching region is taken into consideration. The C-H stretching vibrations of the fatty acyl chains of all cellular lipids as well as protein groups lead to bands in the 3050-2800 cm^{-1} spectral region. The changes in olefinic =CH band (3012 cm^{-1}) can be used as an index of relative concentration of double bonds in the lipid structure from unsaturated fatty acyl chains. In the FTIR spectra of control and experimental group bone tissues, this band is not observable (Figure 24). Therefore, it may be concluded that predominant constituents of the membranes of bone cells are saturated phospholipids. The bands centered at 2956 cm^{-1} and 2923 cm^{-1} , correspond to the stretching mode of asymmetric CH_3 and CH_2 vibrations, and the bands centered at 2873 cm^{-1} and 2853 cm^{-1} correspond to CH_3 and CH_2 symmetric stretching vibrations, respectively (Mendelsohn and Mantsch, 1986, Melin, *et al.*, 2000).

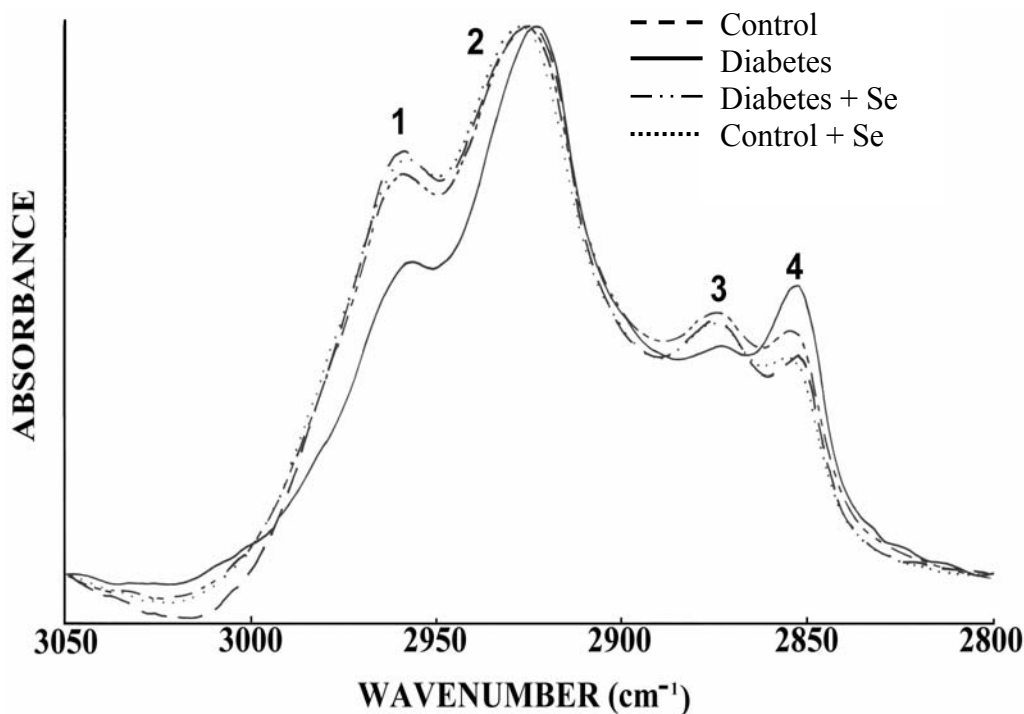


Figure 24. FTIR spectra in $3050\text{-}2800 \text{ cm}^{-1}$ spectral region for control and experimental group rat femurs. Spectra were normalized with respect to CH_2 antisymmetric stretching band. Band assignments: 1- CH_3 asymmetric stretching, 2- CH_2 asymmetric stretching, 3- CH_3 symmetric stretching 4- CH_2 symmetric stretching.

The frequencies of the CH₂ stretching bands, which contain contributions mainly from the acyl chains of the phospholipids, depend on the degree of conformational disorder and hence can be used to monitor the average trans/gauche isomerisation in the systems (Umemura *et al.*, 1980, Casal and Mantsch, 1984, Boyar and Severcan, 1997). In the present study, the CH₂ antisymmetric and symmetric stretching peaks for diabetic group femurs slightly shifted to lower values whereas, for femurs of the Se treated groups, they shifted to higher values (Figure 24). For the tibias similar changes were observed. The shifts to higher wavenumbers are associated with an increase in the number of gauche conformers along the lipid hydrocarbon chains. Therefore, application of selenium may lead to some compositional changes in lipid components of bone tissue.

For control group rat tibias, the average absorbtion spectrum in the C-H stretching region and its Fourier self deconvoluted spectrum, are given in Figure 25 A and B, respectively.

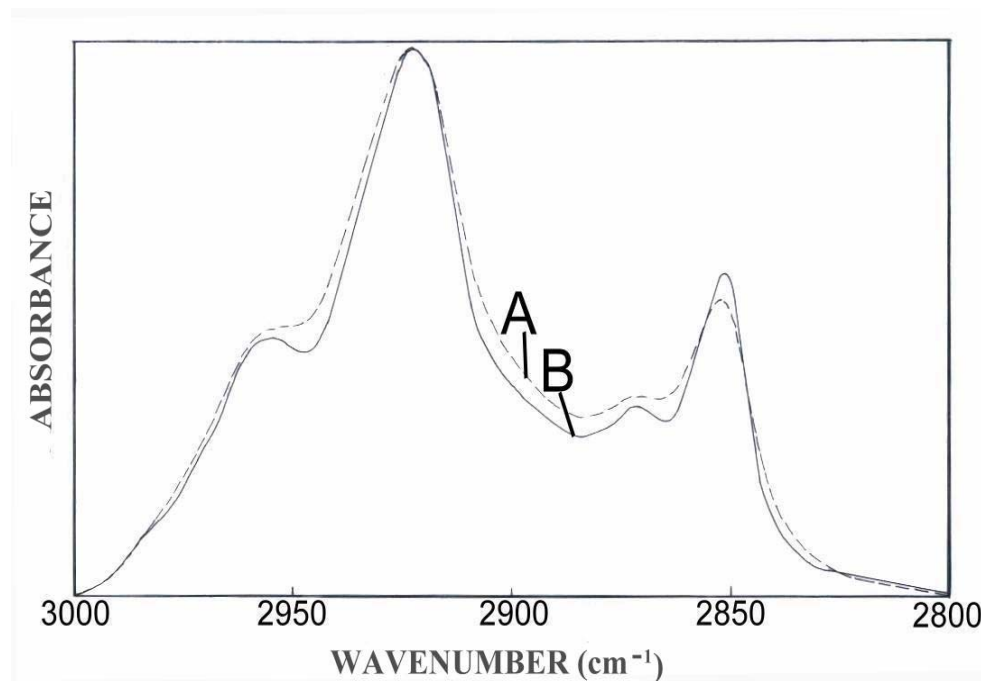


Figure 25 For control group rat tibias the average FTIR spectra in the C-H stretching region: A) raw spectrum B) Fourier self deconvoluted spectrum.

As seen from figure 25B, the CH_3 symmetric stretching band becomes more apparent after Fourier self deconvolution. In this spectral region, the CH_3 symmetric stretching vibrations are mainly due to protein groups and the other bands mainly result from stretching vibrations of lipid groups. Thus, the ratio of the intensities of CH_2 symmetric and CH_3 symmetric bands corresponds to the relative lipid to protein ratio (Melin *et al.* 2000, Severcan *et al.*, 2000). After the application of Fourier self deconvolution, the ratio of the intensities of these bands are used to calculate the relative lipid to protein ratios for control and experimental group bones. The results are summarized in Figure 26.

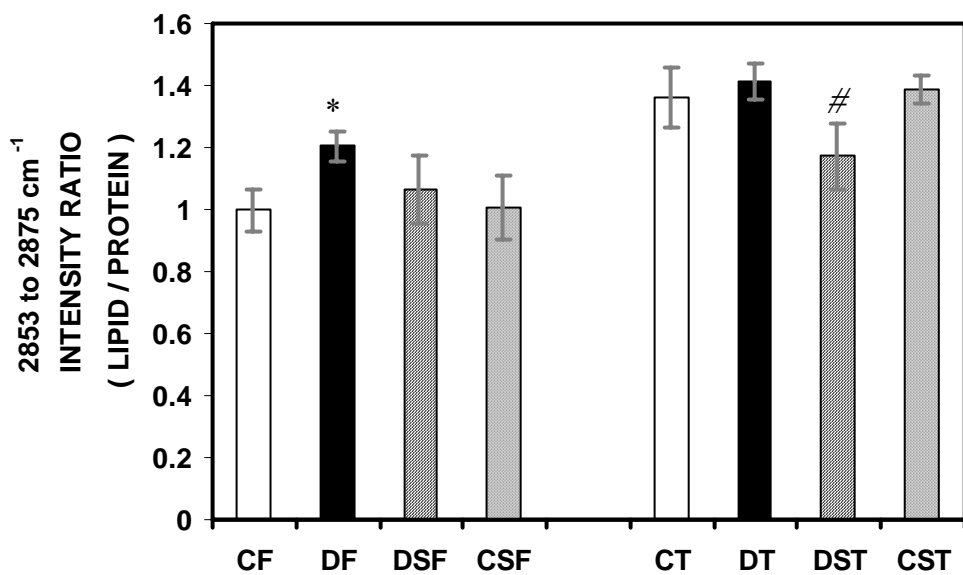


Figure 26. Comparison of the lipid to protein (CH_2 symmetric stretching to CH_3 symmetric stretching) ratio for the femurs (F) and tibias (T) of control (C), diabetes (D), diabetes + Se (DS) and control + Se (CS) group rats.

* p value less than or equal to **0.05** was accepted as significantly different with respect to **control** group.

p value less than or equal to **0.05** was accepted as significantly different with respect to **diabetes** group.

Table 12. Lipid to protein ratios calculated for the femurs (F) and tibias (T) of control (C), diabetes (D), diabetes + Se (DS) and control + Se (CS) groups.

Lipid to protein intensity ratio		
GROUP	FEMUR	TIBIA
Control (C)	0.997±0.068	1.361±0.099
Diabetes (D)	1.204±0.051*	1.414±0.059
Diabetes + Se (DS)	1.066±0.109	1.171±0.108[#]
Control + Se (CS)	1.006±0.102	1.388±0.047

[#] *p* value less than or equal to **0.05** was accepted as significantly different with respect to **diabetes** group.

As seen from Figure 26, the relative lipid to protein ratio is higher for diabetic group bones as compared with control group bones. As can be noticed from the same figure, for selenium (Se) treated diabetic and control group bones (femurs and tibias) it is closer to control group values.

In FTIR spectroscopic and microspectroscopic investigation of biological samples, the curve-fitting analysis was rarely used in the C-H stretching region (Lin *et al.*, 1998, Szalontai *et al.*, 2000). In these studies 4-7 sub-bands were used for the curve-fitting analysis. In the present study in order to be sure about the number of sub-bands present in the C-H stretching region, second derivative analysis was applied. For control, diabetes, diabetes + selenium and control + selenium groups, the second derivative spectra of the same spectral region are given in Figure 27.

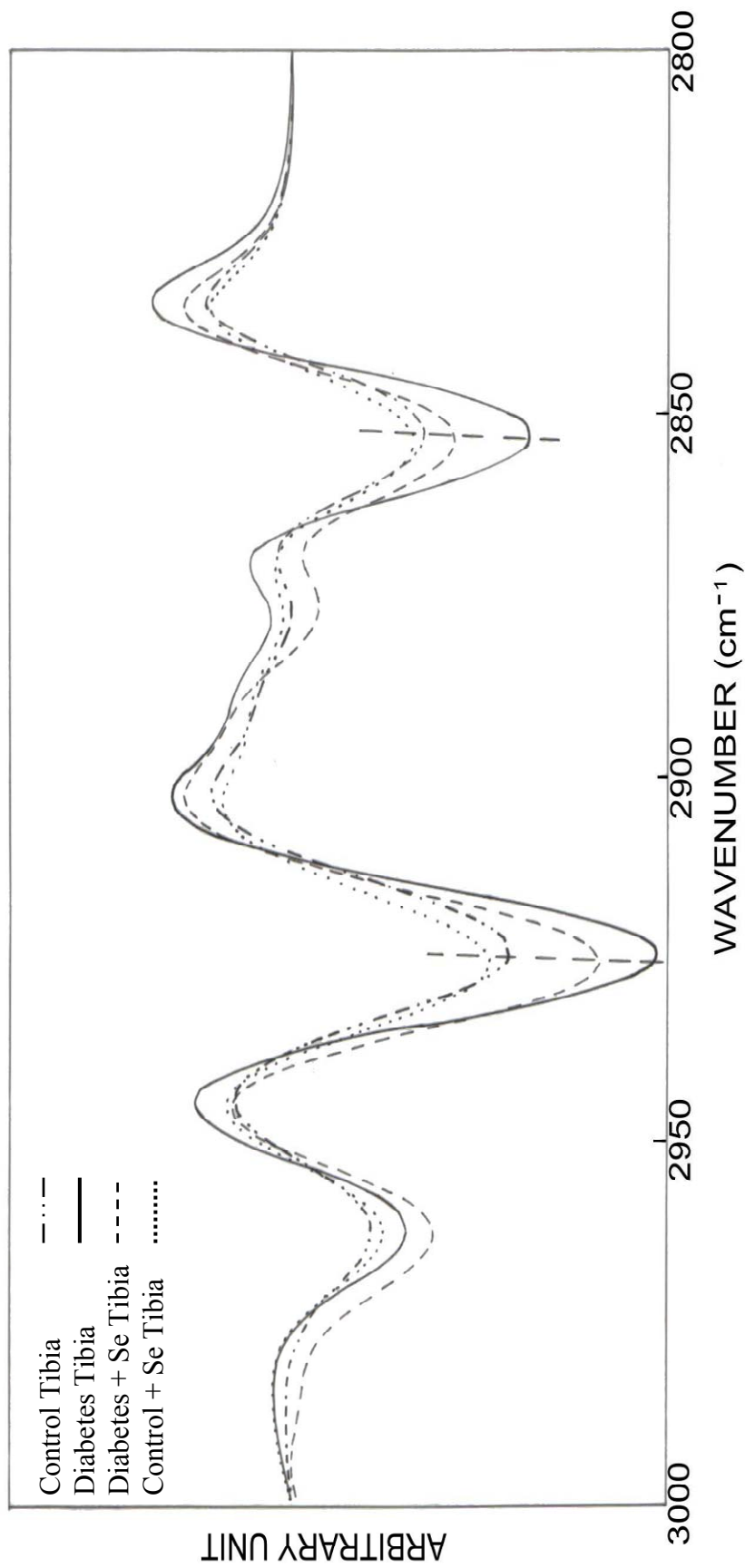


Figure 27. The average second derivative spectra for the tibias of control and experimental groups in the C-H stretching region.

As seen from the figure, there are four sub-bands in this spectral region. The information about the position and number of components obtained from second derivative analysis was used as initial parameters for curve-fitting analysis of the C-H stretching region. The curve-fitted FTIR spectrum of a control group rat femur is given in Figure 28.

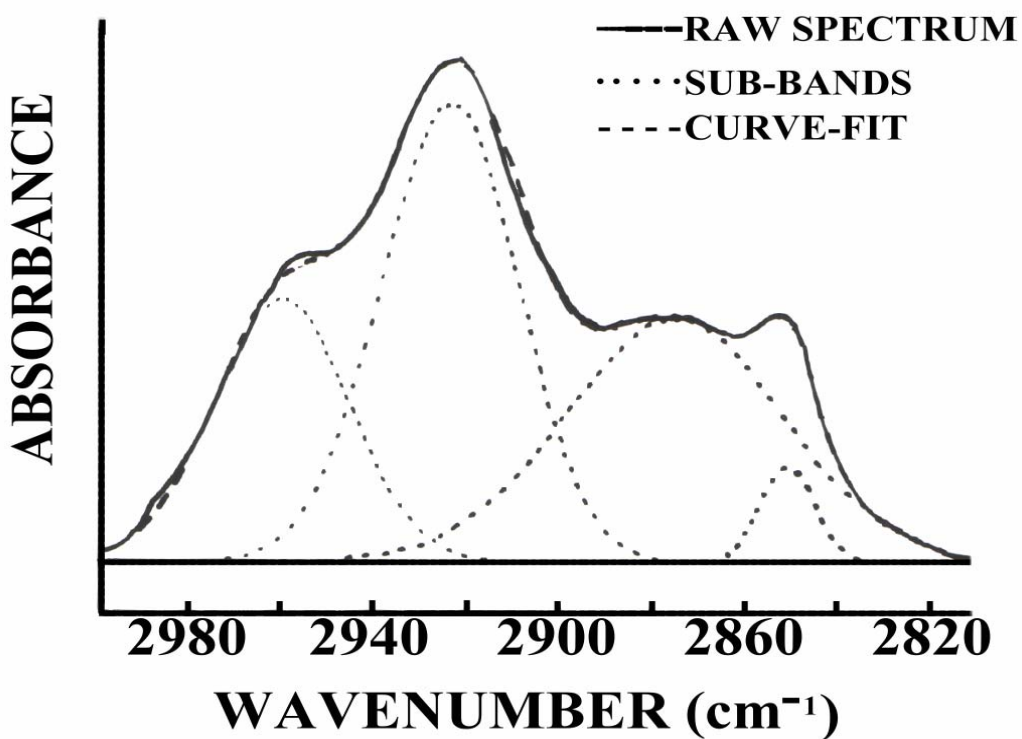


Figure 28 A typical curve-fit spectrum and the best fitted individual component bands of the control group rat femur in $3000\text{-}2810\text{ cm}^{-1}$ C-H stretching region.

The ratio of partial areas of the sub-bands at 2853 cm^{-1} and 2875 cm^{-1} are calculated and the results are summarized in Figure 29 and Table 13. The changes observed in this graph are parallel to the variations in the intensity ratios calculated for control and experimental groups (Figure 26, Table 12). Therefore, both of intensity ratio and curve-fitting analysis of FTIR spectra revealed that diabetes led to increase in the relative lipid content and Se application caused reversal to normal values.

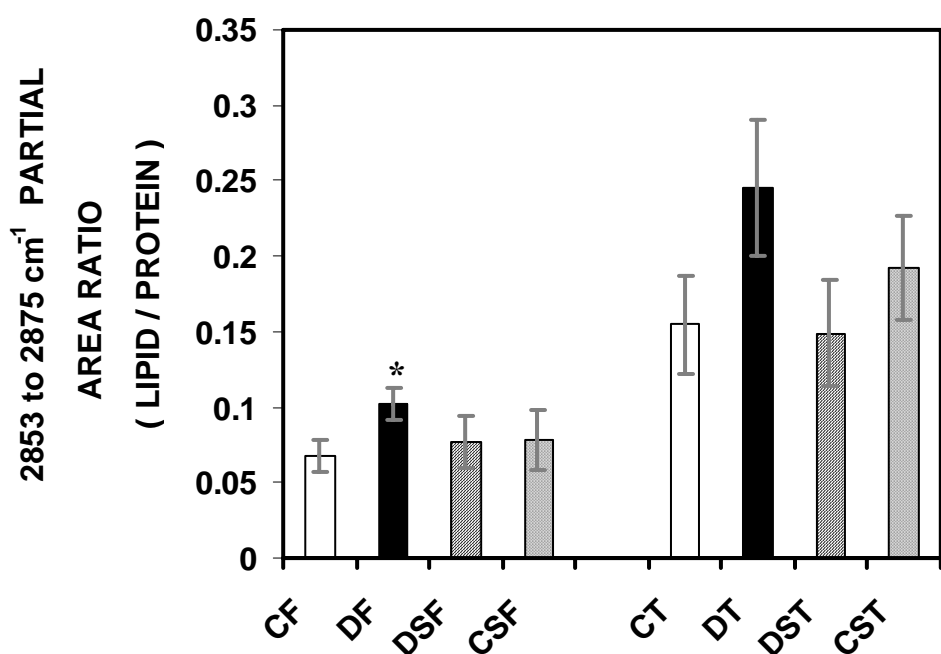


Figure 29. For control (C), diabetes (D), diabetes + Se (DS) and control + Se (CS) group femurs (F) and tibias (T), the relative lipid to protein ratio calculated by taking the ratios of the partial areas of the CH_2 symmetric stretching and the CH_3 symmetric stretching sub-bands obtained from curve-fitting analysis of the FTIR spectra in the C-H stretching region.

* p value less than or equal to **0.05** was accepted as significantly different with respect to **control** group.

Table 13. Lipid to protein ratios calculated from the curve-fitting analysis of the FTIR spectra of the femurs (F) and tibias (T) of control (C), diabetes (D), diabetes + Se (DS) and control + Se (CS) groups.

Lipid : protein		
GROUP	FEMUR	TIBIA
Control (C)	0.067±0.011	0.155±0.032
Diabetes (D)	0.102±0.011*	0.246±0.045
Diabetes + Se (DS)	0.077±0.017	0.149±0.035
Control + Se (CS)	0.077±0.020	0.193±0.034

p* value less than or equal to **0.05 was accepted as significantly different with respect to **control** group.

3.3 FTIR Spectroscopic Investigation of Bone Samples Taken From Selenium and Vitamin E Deficient or Selenium Excess and Vitamin E Adequate Group Rats

Since the preliminary results about the carbonyl groups of the FTIR spectra for the analysis of Se deficiency and toxicity on rat bones were reported by our group previously, the analysis of the C-H stretching region was not included in the present study. The results for the FTIR spectroscopic analysis of the other bands under consideration are given in the following sections.

3.3.1 ν_4 Phosphate Bending Region

The results of curve-fitting analysis of the FTIR spectra in the ν_4 phosphate bending region ($500\text{-}650\text{ cm}^{-1}$) for the femurs and the tibias taken from control, Se and vit E deficient and Se excess, vitamin E adequate group rats are summarized as a bar diagram in Figure 30 and statistical analysis results are given in Table 14. As can be noticed from the Figure 30 and Table 14, for both the femurs and the tibias of the

antioxidant *deficient* group, the relative ratio of nonapatitic HPO_4^{2-} and PO_4^{3-} groups slightly decreased, whereas an increase was observed for apatitic PO_4^{3-} groups. For the Se excess-vitamin E adequate group, or briefly *excess* group, opposite results were observed however, the changes in the relative apatitic PO_4^{3-} content were negligible for both types of bones.

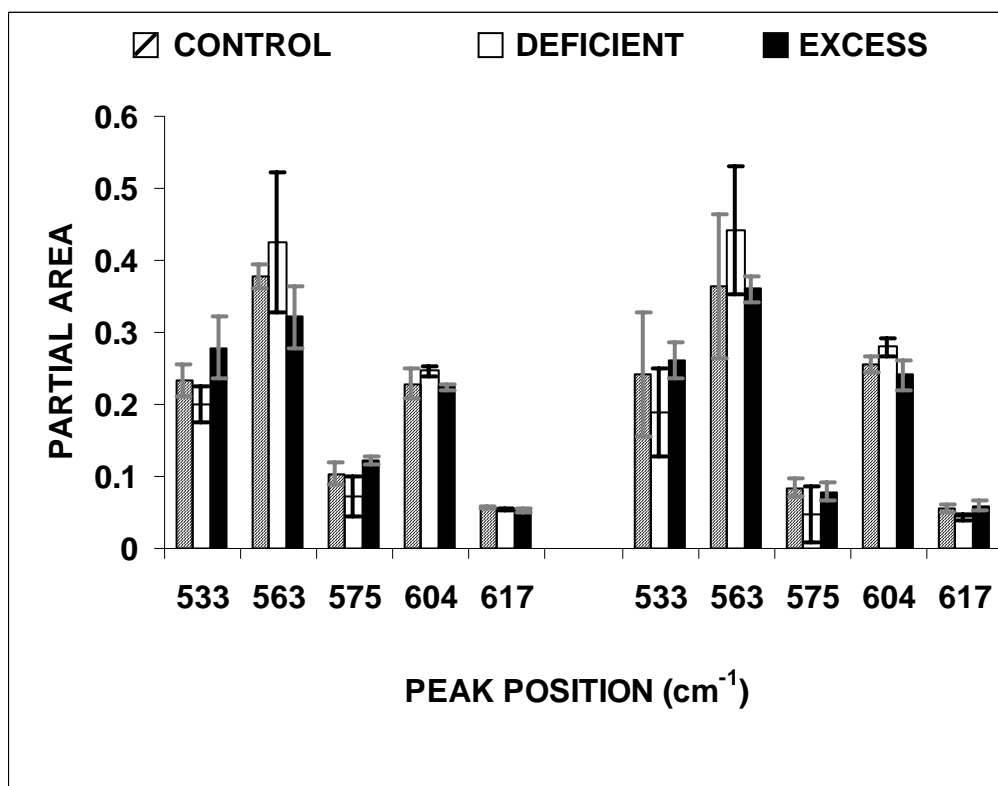


Figure 30. The results of curve-fitting analysis of the FTIR spectra in the ν_4 phosphate bending region for the femurs and the tibias taken from control, Se and vitamin E deficient and Se excess, vitamin E adequate group rats. Partial areas for each of the sub-bands are given as mean of curve-fitting analysis results for FTIR spectra of five bone samples taken from control and experimental group rats.

Table 14. The mean partial peak areas obtained from curve-fitting analysis of the ν_4 PO_4^{3-} bending region of the FTIR spectra of femurs and tibias of control, Se and vitamin E deficient (DEFICIENT) and Se excess, vitamin E adequate (EXCESS) group rats.

FEMUR	Nonapatitic HPO_4^{2-} 533 cm^{-1}	Apatitic PO_4^3 563 cm^{-1}	Apatitic PO_4^3 575 cm^{-1}	Apatitic PO_4^3 604 cm^{-1}	Nonapatitic PO_4^3 617 cm^{-1}
CONTROL	0.233±0.021	0.378±0.017	0.104±0.01	0.228±0.021	0.056±0.001
DEFICIENT	0.200±0.026	0.426±0.090	0.073±0.028	0.246±0.008	0.055±0.002
EXCESS	0.279±0.044	0.321±0.044	0.122±0.005	0.224±0.004	0.053±0.003
TIBIA					
CONTROL	0.241±0.086	0.365±0.100	0.084±0.013	0.255±0.011	0.055±0.005
DEFICIENT	0.188±0.061	0.441±0.089	0.047±0.040	0.280±0.012	0.044±0.005
EXCESS	0.260±0.025	0.361±0.018	0.079±0.012	0.241±0.021	0.059±0.007

3.3.2 ν_1, ν_3 Phosphate Stretching Region

In the ν_1, ν_3 phosphate stretching region ($900\text{-}1200 \text{ cm}^{-1}$) the curve-fitting analysis was also used to gain information about mineral environment and crystal size of the control and experimental group bones. In this spectral region the curve-fitting analysis results revealed that the variations in local mineral environment of experimental group bones were not significantly different with respect to control group bones. Therefore, only the variations in the fourth sub-band were taken into consideration and the equation given in section 3.2.1.2 was used to calculate the crystal size for control, deficient and excess group femurs and tibias. The results are summarized in Table 15 for both the femurs and the tibias of the control and experimental groups. As can be noticed from the table, the crystal size increased significantly for the femurs of the deficient and excess groups. Although a similar trend was obtained for the tibias, the increase was not significant in Se excess group.

Table 15. The mean crystal size (\AA) values obtained from the curve-fitting analysis of the v_1 , v_3 PO_4^{3-} stretching ($900\text{-}1200 \text{ cm}^{-1}$) region.

GROUP	Crystal size (\AA)	
	FEMUR	TIBIA
CONTROL	136.8 ± 0.1	135.7 ± 0.4
DEFICIENT	$154.6\pm1.1^*$	$146.0\pm5.9^*$
EXCESS	$148.6\pm0.1^*$	141.9 ± 0.7

* p value less than or equal to **0.05** was accepted as statistically different with respect to **control** group.

3.3.3 v_2 Carbonate (CO_3^{2-}) Region

The curve-fitting analysis was applied for FTIR spectra of control, deficient and excess group femurs and tibias in $850\text{-}890 \text{ cm}^{-1}$ v_2 carbonate region and the results are summarized in Figure 31 and Table 16.

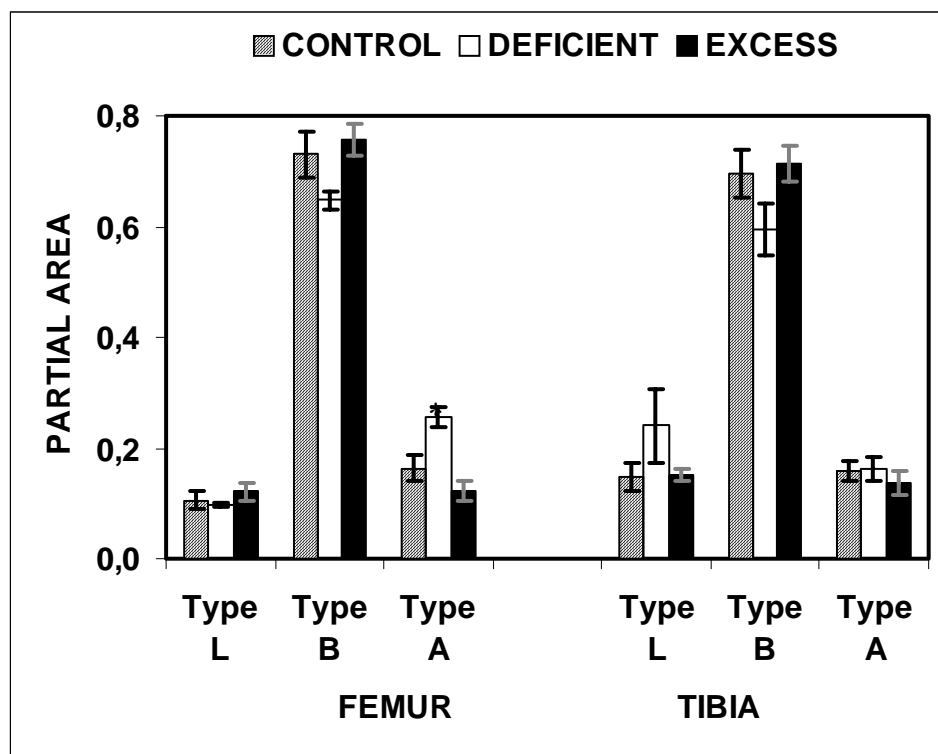


Figure 31. ν_2 carbonate region curve-fitting analysis results for control, deficient and excess group rat bones.

Table 16. For control (CON), deficient (DEF) and excess (EXC) groups, the partial areas obtained from curve-fitting analysis of the FTIR spectra in the ν_2 carbonate region.

	FEMUR			TIBIA		
	Type L 866 cm^{-1}	Type B 871 cm^{-1}	Type A 878 cm^{-1}	Type L 866 cm^{-1}	Type B 871 cm^{-1}	Type A 878 cm^{-1}
CON	0.106 \pm 0.024	0.730 \pm 0.057	0.163 \pm 0.034	0.148 \pm 0.036	0.694 \pm 0.061	0.159 \pm 0.025
DEF	0.097 \pm 0.005	0.647 \pm 0.022	0.256 \pm 0.026*	0.241 \pm 0.095	0.596 \pm 0.067	0.163 \pm 0.031
EXC	0.121 \pm 0.021	0.757 \pm 0.040	0.121 \pm 0.025	0.150 \pm 0.015	0.714 \pm 0.045	0.136 \pm 0.031

* p value less than or equal to **0.05** was accepted as statistically different with respect to **control** group.

For Se and vitamin E deficient femurs, the relative amount of type B carbonates substituting for phosphate ions and nonapatitic-labile type carbonates slightly decreased whereas the relative amount of type A carbonates substituting for hydroxyl ions was found to increase significantly. However, this increase was not significant for the tibias. For the same bones of the deficient group, the relative amount of type B carbonate decreased whereas that of labile carbonate increased.

In contrast to the deficient group, the relative amount of type A carbonate decreased and the relative amount of type B carbonate and labile type carbonate slightly increased for the femurs of the Se excess group. The alterations in these ratios for the tibias of the excess group were negligible.

3.3.4 Amide I Region

In order to gain information about maturity of type I collagen in the case of Se deficiency or toxicity, curve-fitting analysis was carried out in the Amide I band of the FTIR spectra of control and experimental group bones. 1660 cm^{-1} to 1690 cm^{-1} mean peak area ratio was calculated for control and experimental groups and the results are summarized in Figure 32 and Table 17. For the deficient group this ratio increased for the femurs and decreased for the tibias significantly. Similar, but slight alterations were determined for both bones of the excess group.

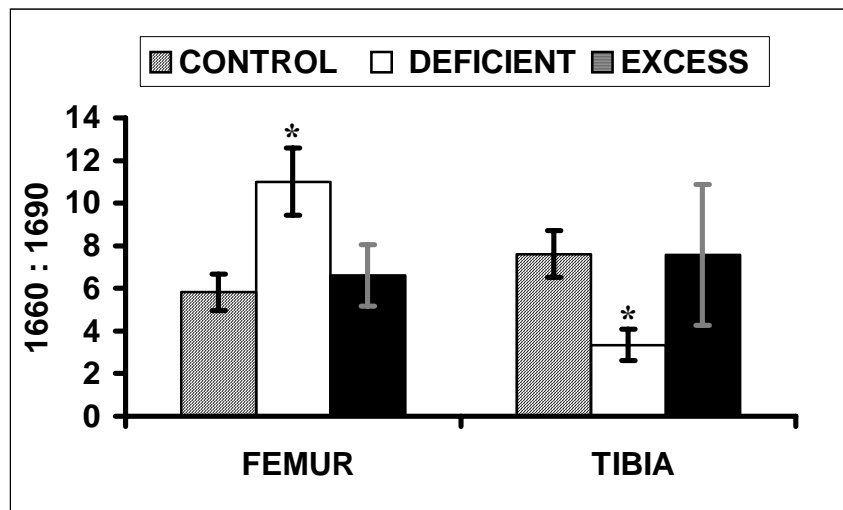


Figure 32. Comparison of the 1660 : 1690 ratio for the femurs and tibias of control, deficient and excess group rats.

p* value less than or equal to **0.05 was accepted as statistically different with respect to **control** group.

Table 17. The variations in 1660 : 1690 ratios for the femurs and tibias of control, deficient and excess group rats.

1660 : 1690		
GROUP	FEMUR	TIBIA
CONTROL	5.819±0.861	7.611±1.095
DEFICIENT	11.007±1.584*	3.349±0.740*
EXCESS	6.616±1.439	7.573±3.312

p* value less than or equal to **0.05 was accepted as statistically different with respect to **control** group.

3.3.5 Mineral to Matrix and Carbonate to Phosphate Ratios

According to semi-quantitative analysis of FTIR spectra, the relative mineral to matrix ratio slightly decreased, whereas the carbonate to phosphate ratio increased for the femurs of both experimental groups (Table 18). The mineral to matrix and the carbonate to phosphate ratios increased for both of the experimental groups in the tibias (Table 18).

Table 18. Mineral : matrix and carbonate : phosphate ratios for the femurs and the tibias of the control, Se and vitamin E deficient (DEFICIENT), Se excess, vitamine E adequate (EXCESS) group rats.

	Mineral : matrix ($v_1, v_3 \text{PO}_4^{3-}$: Amide I)	Carbonate : phosphate ($v_2 \text{CO}_3^{2-}$: $v_1, v_3 \text{PO}_4^{3-}$)
FEMUR CONTROL	5.124±0.062	0.0245±0.002
DEFICIENT	4.827±0.065	0.0311±0.009
EXCESS	4.458±0.057	0.0251±0.001
TIBIA CONTROL	4.874±0.686	0.0254±0.002
DEFICIENT	5.853±0.219	0.0270±0.001
EXCESS	6.691±0.435*	0.0281±0.002

* p value less than or equal to **0.05** was accepted as statistically different with respect to **control** group.

3.4 Powder X-Ray Diffraction Analysis of Normal, Diabetic and Selenium Treated Normal and Diabetic Rat Bone Samples.

In order to gain information about apatite crystal size of bone tissue, powder x-ray diffraction analysis was carried out. Powder x-ray diffraction pattern of highly

crystalline synthetic hydroxyapatite was used as a reference (Figure 33). The region of highest intensity between $30\text{--}35^\circ$ 2θ consists of four sub-peaks. The peak between $24.5\text{--}27^\circ$ 2θ is assigned as 002 reflection and the peak between $37.5\text{--}42^\circ$ 2θ is assigned as 310 reflection.

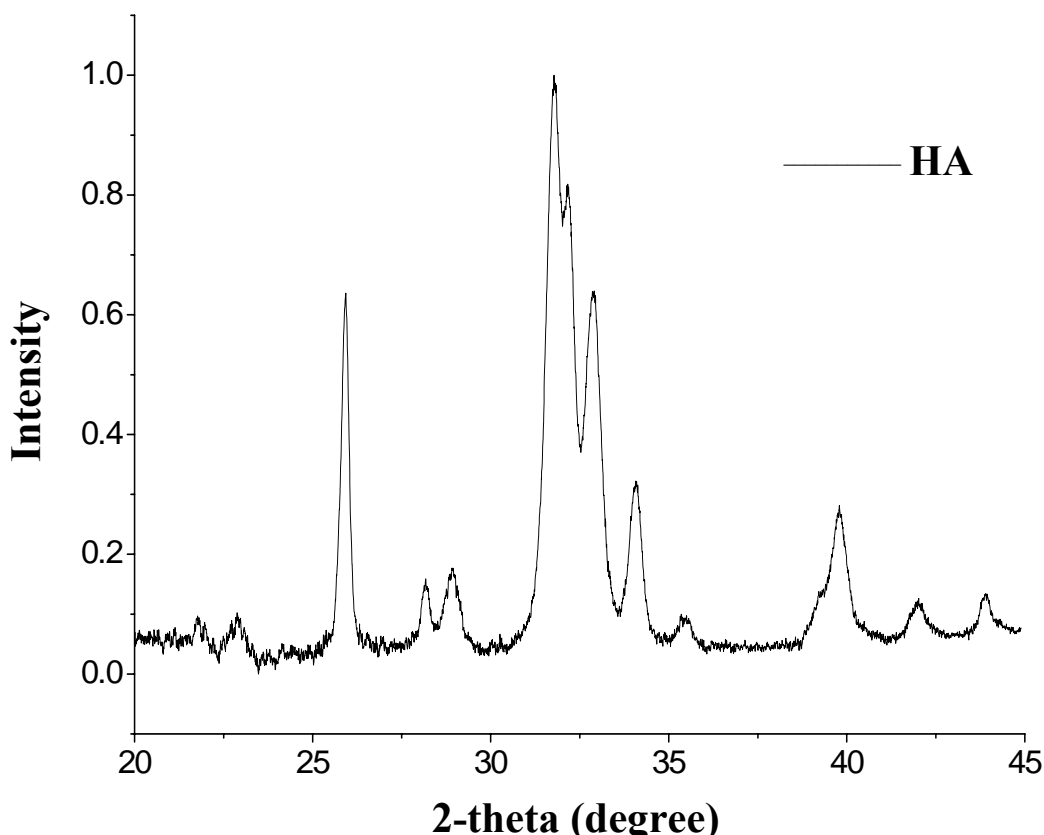


Figure 33. Powder x-ray diffraction pattern of highly crystalline synthetic hydroxyapatite (HA). Its intensity was normalized to one.

The line broadening of the 310 and 002 reflections are used to evaluate the mean crystal sizes. D_{hkl} values, which are related to the crystal size in length (002) and width/thickness (310) of the apatite crystals can be calculated from the width at half maximum intensity ($\beta_{1/2}$) using the Scherrer equation (Alexander, 1969):

$$D_{hkl} = 57.3K\lambda / \beta_{1/2} \cdot \cos\theta \quad (\text{Equation 3.2})$$

where 57.3 is a conversion factor from degrees to radians, λ is the x-ray wavelength and θ is the diffraction angle. K is a constant varying with crystal habit and for hydroxyapatite it is chosen as 0.9, reflecting the elongated crystals of bone.

Figure 34 shows powder x-ray diffraction pattern of a poorly crystalline control group rat femur. As seen from this figure the region of the highest intensity consists of unresolved peaks with unmeasurable overlapping breadths. Therefore, this peak is less suitable for the analysis of the bone tissues.

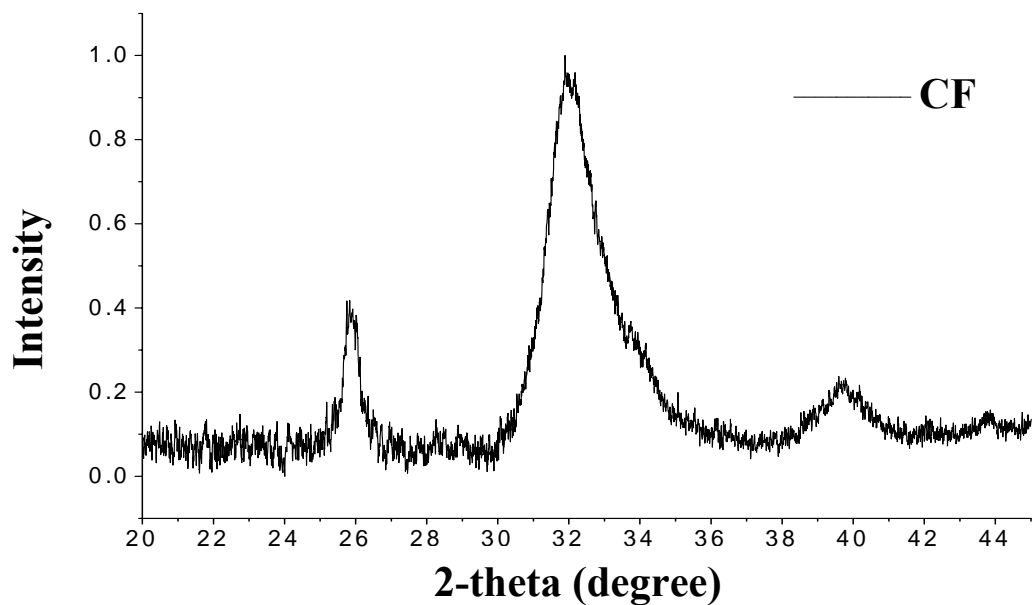


Figure 34. Powder x-ray diffraction pattern of poorly crystalline control group rat femur. The maximum intensity was normalized to one.

In figure 35 powder x-ray diffraction patterns of highly crystalline synthetic hydroxyapatite and poorly crystalline control group rat femur are given as overlaid on the same scale. As seen from the figure the intensities of both of 002 and 310 reflections are lower as compared with those of synthetic hydroxyapatite. The 310 reflection between 37.5 - 42 $^{\circ}$ 2θ is highly broadened for bone tissue. Thus, in the present study only 002 peak locating between 24.5 - 27 $^{\circ}$ 2θ is taken into consideration.

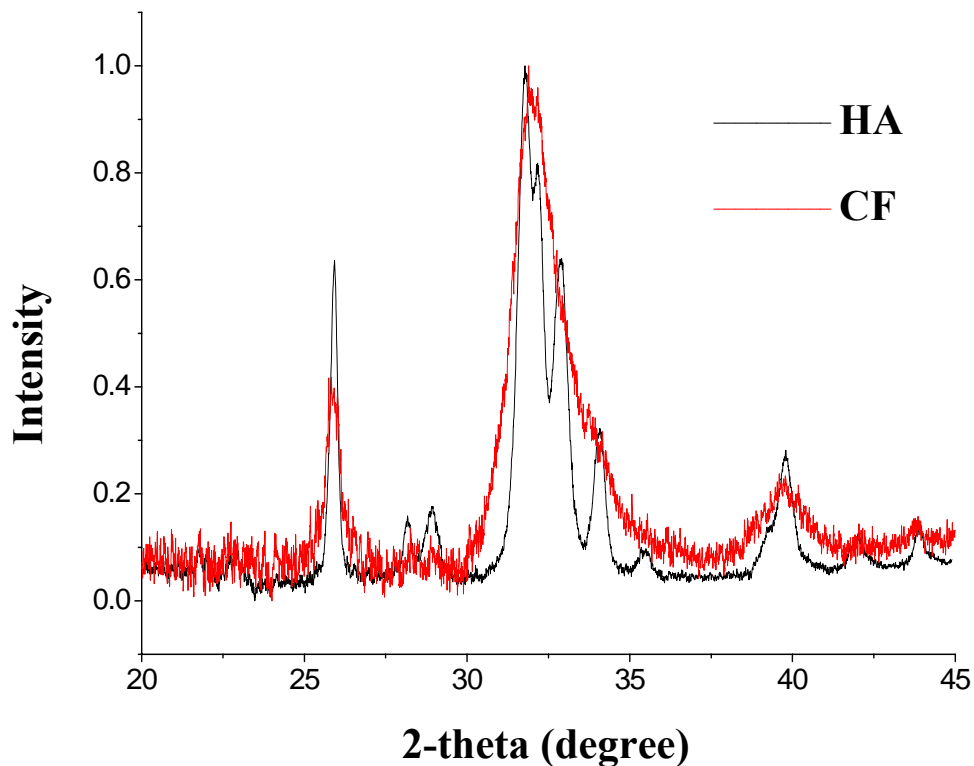


Figure 35. Comparison of powder x-ray diffraction patterns for highly crystalline synthetic hydroxyapatite (HA) and for poorly crystalline control group rat femur (CF). The maximum intensity was normalized to one.

Figure 36 illustrates the 002 reflection patterns for highly crystalline synthetic hydroxyapatite and for poorly crystalline control and diabetes group rat femurs. As seen from the figure the peaks for bone samples are highly broadened with respect to peak of highly crystalline hydroxyapatite. The peak broadening is inversely related to both crystal size and internal lattice perfection (i.e., the broader the peak, the smaller and/or more strained the crystals). Therefore, poor crystallinity of bone samples is clearly seen.

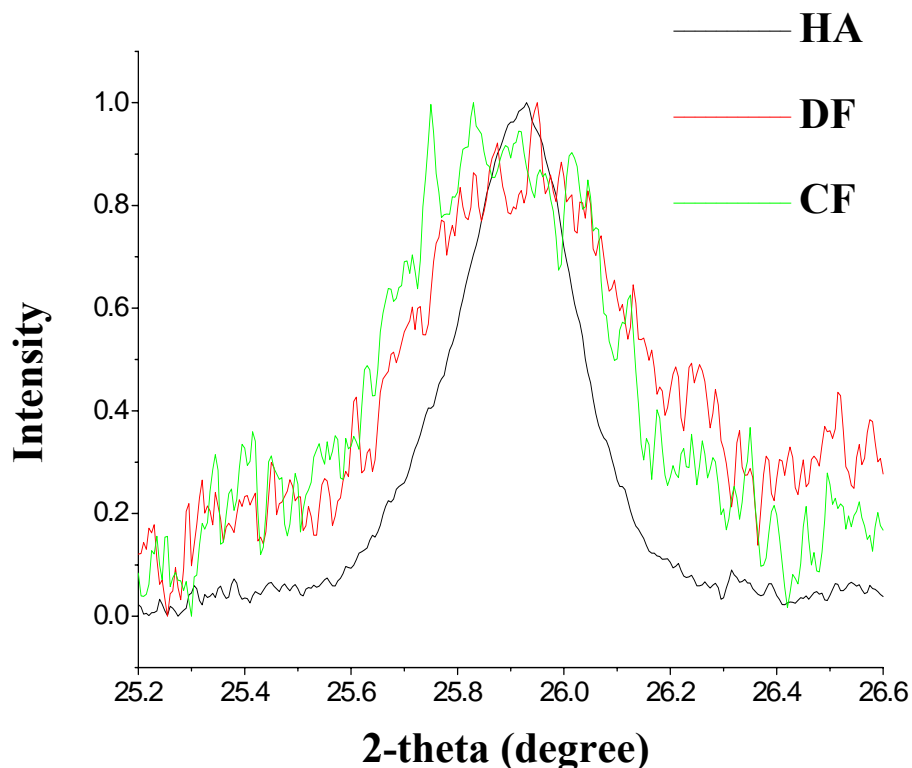


Figure 36. Comparison of powder x-ray diffraction patterns in the 002 reflection for highly crystalline synthetic hydroxyapatite (HA) and for poorly crystalline control (C) and diabetes (D) group rat femurs (F). The maximum intensity was normalized to one.

The crystal sizes for control and experimental group femurs and tibias calculated by using Sherrer equation are given in Table 19. As seen from the table there are not significant variations between groups.

For FTIR spectroscopic analysis a small piece of bone sample was always taken from the center of diaphysis. However, for powder x-ray diffraction analysis, as 3-4 grams of bone powder was necessary whole of the diaphysis was ground. Therefore, the bone powder used for x-ray diffraction analysis was more heterogenous as compared with that used for FTIR spectroscopic analysis. The difference in the variations of crystal sizes obtained by two different biophysical techniques can be due to the level of heterogeneity.

Table 19. Mineral crystal sizes calculated by using Scherrer equation for the femurs (F) and tibias (T) of control (C), diabetes (D), diabetes + Se (DS) and control + Se (CS) groups. The values are reported as mean \pm standart error of mean.

Mineral Crystal Size (\AA)		
GROUP	FEMUR	TIBIA
Control (C)	179.54 \pm 4.65	196.95 \pm 10.02
Diabetes (D)	175.07 \pm 7.81	189.59 \pm 2.65
Diabetes + Se (DS)	167.44 \pm 25.13	181.69 \pm 6.24
Control + Se (CS)	178.63 \pm 4.92	165.79 \pm 6.19

3.5 Light and Electron Microscopic Investigation of Control, Diabetic and Selenium Treated Control and Diabetic Group Rat Bone Ultra-structures

3.5.1 Light Microscopic Investigations

In light microscopy examinations, the long bones from the control group are seen in usual appearance. The tissue samples have a characteristic trabecular formation with osteoblasts in the periphery of trabeculae and osteocytes within the lacunae. The bone marrow cells are also in normal structure (Figure 37).

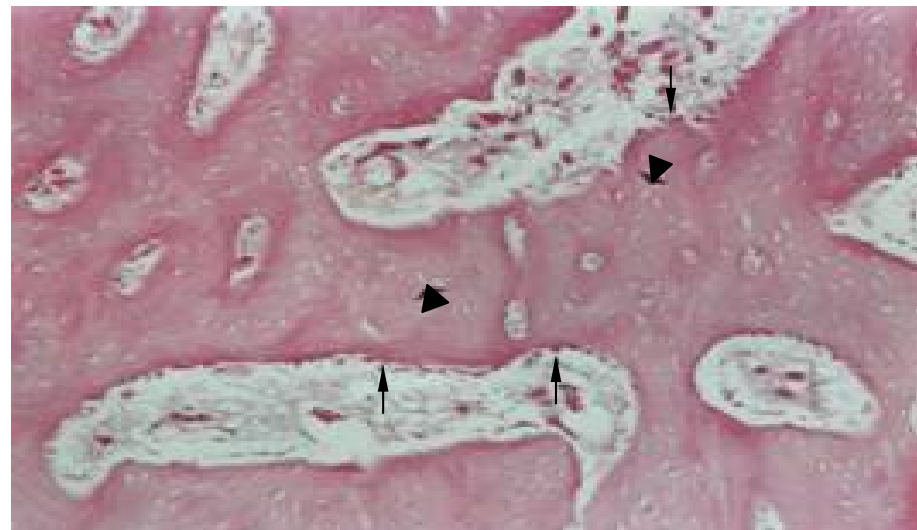


Figure 37. Light micrograph of a section from control group bone. Arrows are showing osteoblasts and arrowheads are representing osteocytes. Haematoxyline Eosin x40.

Histopathologically, the observed changes in the bone of diabetic group rats can be summarized mainly as increased amount of osteocytes placed in trabeculae and heterogeneous appearance of mineralized matrix (Figure 38).

In light micrograph of sodium selenite treated diabetic group bone, newly formed trabeculae with different shapes and sizes are seen under the proliferation cartilage (PC). The calcification is not complete in trabecular matrix and it is still continuing (Figure 39).

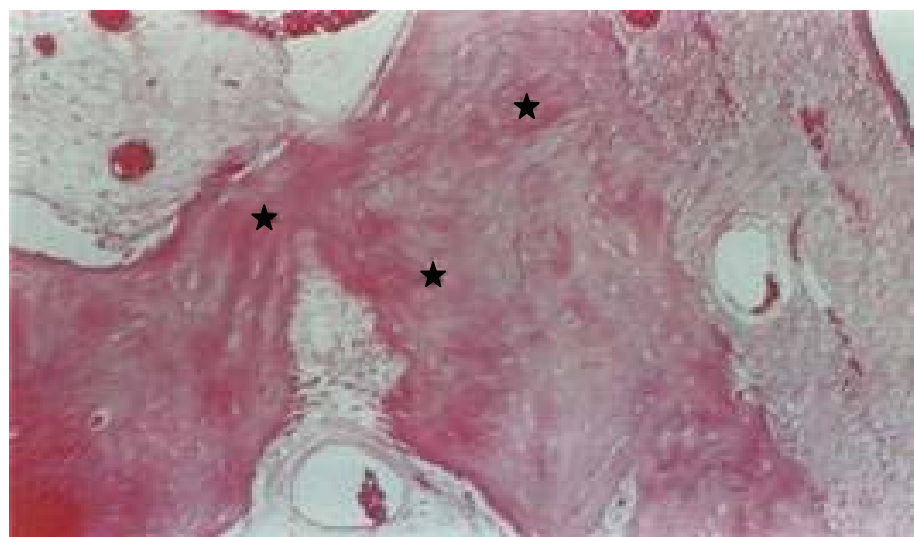


Figure 38. Light micrograph of a bone section taken from diabetic group rats. Osteocytes are increased in bone trabeculae. Appearance of the matrix (star) is heterogeneous. Heamotoxyline Eosin x40.

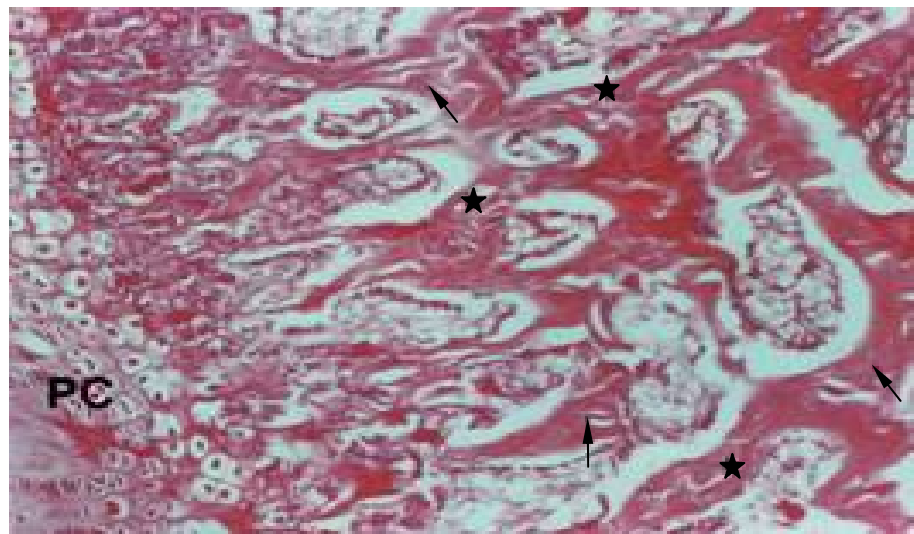


Figure 39. Light micrograph of a section from sodium selenite treated diabetic group. Epiphyseal plate showing zone of proliferation cartilage (PC), newly formed bone trabeculae (star) and osteocytes are seen (arrows). Heamotoxyline Eosin x40.

On the other hand, the light microscopic investigation shows that treatment of the normal rats with sodium selenite does not affect the structure of the long bones significantly. It can be observed that together with an increase in the trabecular formations, both unmineralized matrix and mineralized matrix are enlarged (Figure 40).

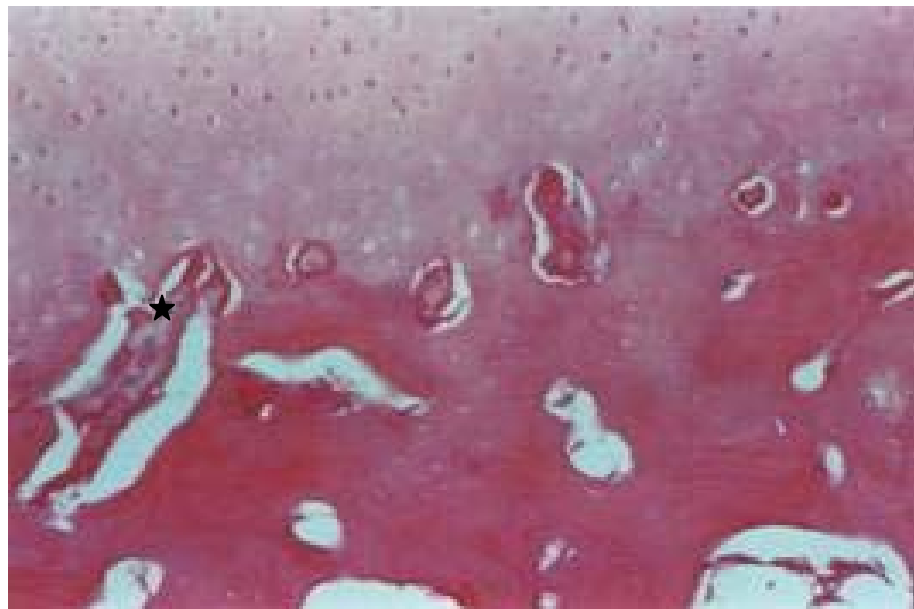


Figure 40. Light micrograph of a bone section taken from sodium selenite injected control group. Enlarged unmineralized matrix (star) and newly formed trabeculae are seen. Heamotoxylin Eosin x40.

3.5.2 Electron Microscopic Investigations

As seen from the electronmicrograph of a bone section taken from control group bones, osteoblasts are seen in their active formation with their eucromatin nucleus and rich cytoplasmic organelles. Newly synthesized collagen fibers are also seen clearly besides the osteoblasts (Figure 41).

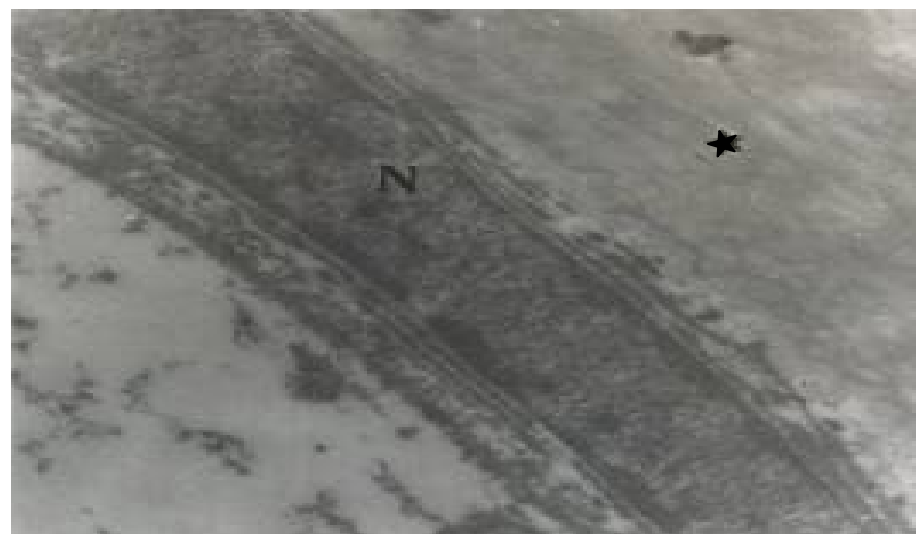


Figure 41. Electronmicrograph of a bone section taken from control group. Bone formation by osteoblasts is seen. Nucleus of osteoblast (N) and unmineralized matrix (star) are also labeled. Uranyl acetate-lead citrate x16700.

The most prominent effect induced by diabetes can be observed in osteocytic cells. The extension of canaliculus towards the cytoplasm seems to be shortened. Diabetes also seems to affect the normal cytoplasmic processes in a negative manner. Together with the heterochromatin material seen in the periphery of the nucleus, vacuolar formations are present in the cytoplasm. The unmineralized matrix is highly enlarged and there are crowded haemopoietic cells and adipocytes (Figure 42).

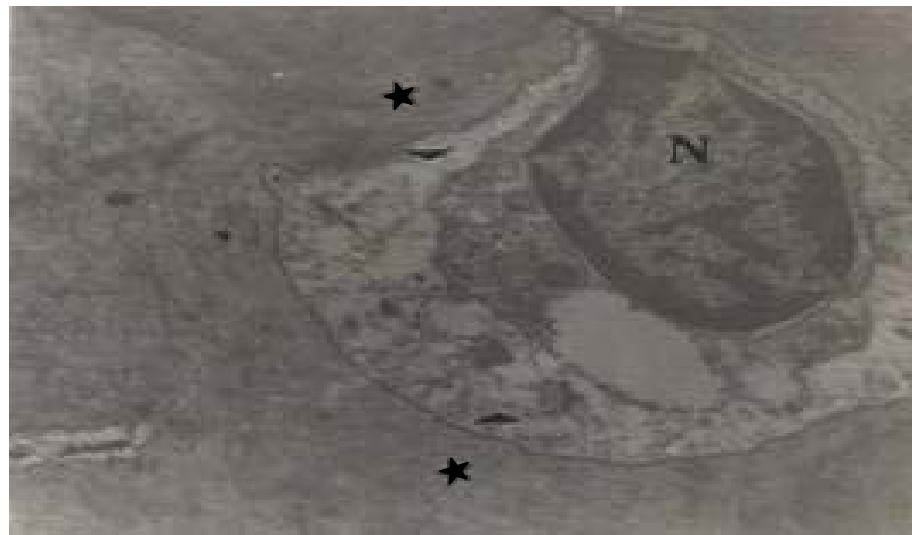


Figure 42. Electronmicrograph of a bone section taken from diabetic group rats. The nucleus of an osteocyte is in its lacunae (N), unmineralized matrix (arrow head) and mineralized matrix (star) can be seen. Uranyl acetate-lead citrate x10000.

In the electronmicrograph of sodium selenite treated diabetic group bone, active osteoblasts around the trabecules are observed. It shows that the density of the osteoblasts increased. Contrary to the diabetic groups, the extensions of canaliculars towards the cytoplasm seemed much more clear and active. These findings can imply that the structural changes induced by diabetes are prevented and/or restored by sodium selenite treatment (Figure 43).

As seen from the electronmicrograph of a bone section taken from sodium selenite injected control group, the osteocytes are normal compared with the age matched untreated control group (Figure 44).

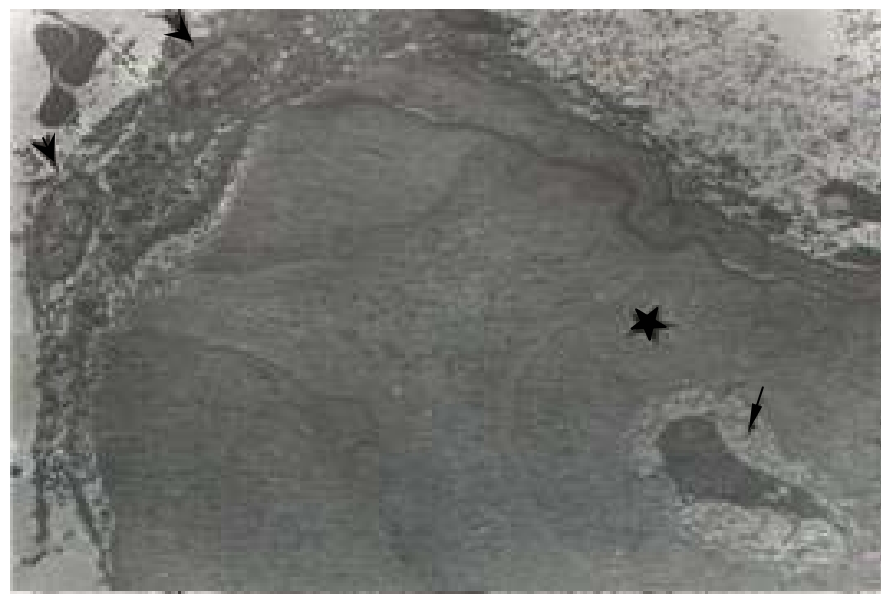


Figure 43. Electronmicrograph of a bone section taken from sodium selenite treated diabetic group. Active osteoblasts (arrowhead) are seen as surrounding the bone trabeculae. An osteocyte (arrow) is placed in unmineralized matrix. Mineralized matrix (star) is also observable. Uranyl acetate-lead citrate x2156.

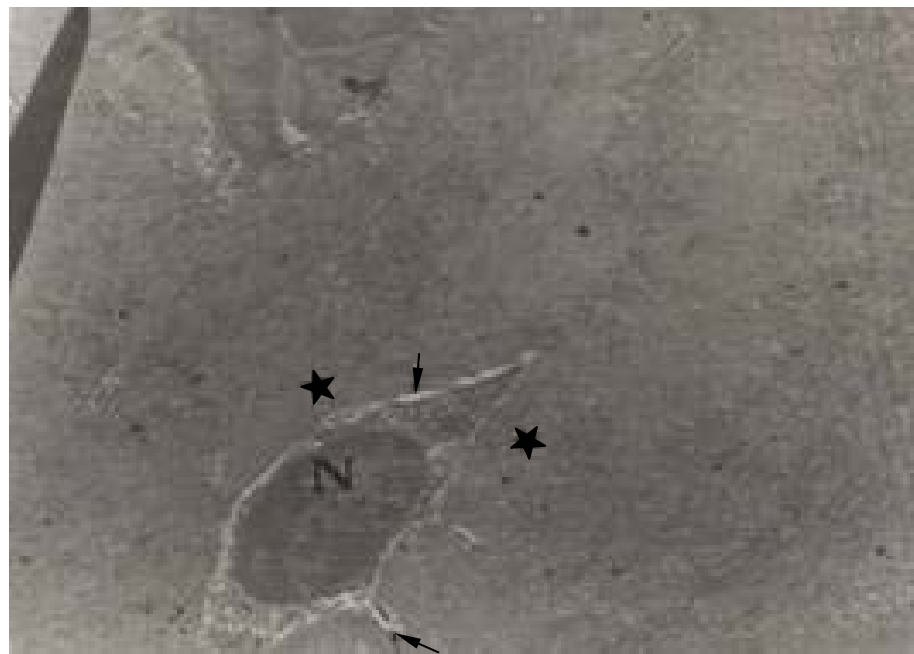


Figure 44. Electronmicrograph of a bone section taken from sodium selenite treated control group. An osteocyte in its lacunae is seen. Nucleus of an osteocyte (N), unmineralized (arrow) and mineralized (star) matrix are also observable. Uranyl acetate-lead citrate x4646.

3.6 Light Microscopic Investigation of Rat Bones Fed on Antioxidant Deficient and Excess Diet

Compact bone structure, lamellar structure of osteons and interstitial structure, and oblique Volkmann's canals are present in the femurs and tibias of the control group (Figures 45 A and B, respectively). In femurs of the deficient group, newly formed bone is observed and this woven bone is seen to contain more bone cells and intercellular substance in which collagen fibrils are disposed in an irregular arrangement (Figure 45 C). In tibia of the same group, destruction and resorption in bone matrix and formation of new bone matrix are observed (Figure 45 D). In the femurs and tibias of the Se-excess group, although cortex and trabeculae are observed to be thinner and reduced in number with respect to the control, they are not well mineralized. In addition, osteoblasts and osteoclasts are seen to be simultaneously present in the samples (Figure 45 E and F).

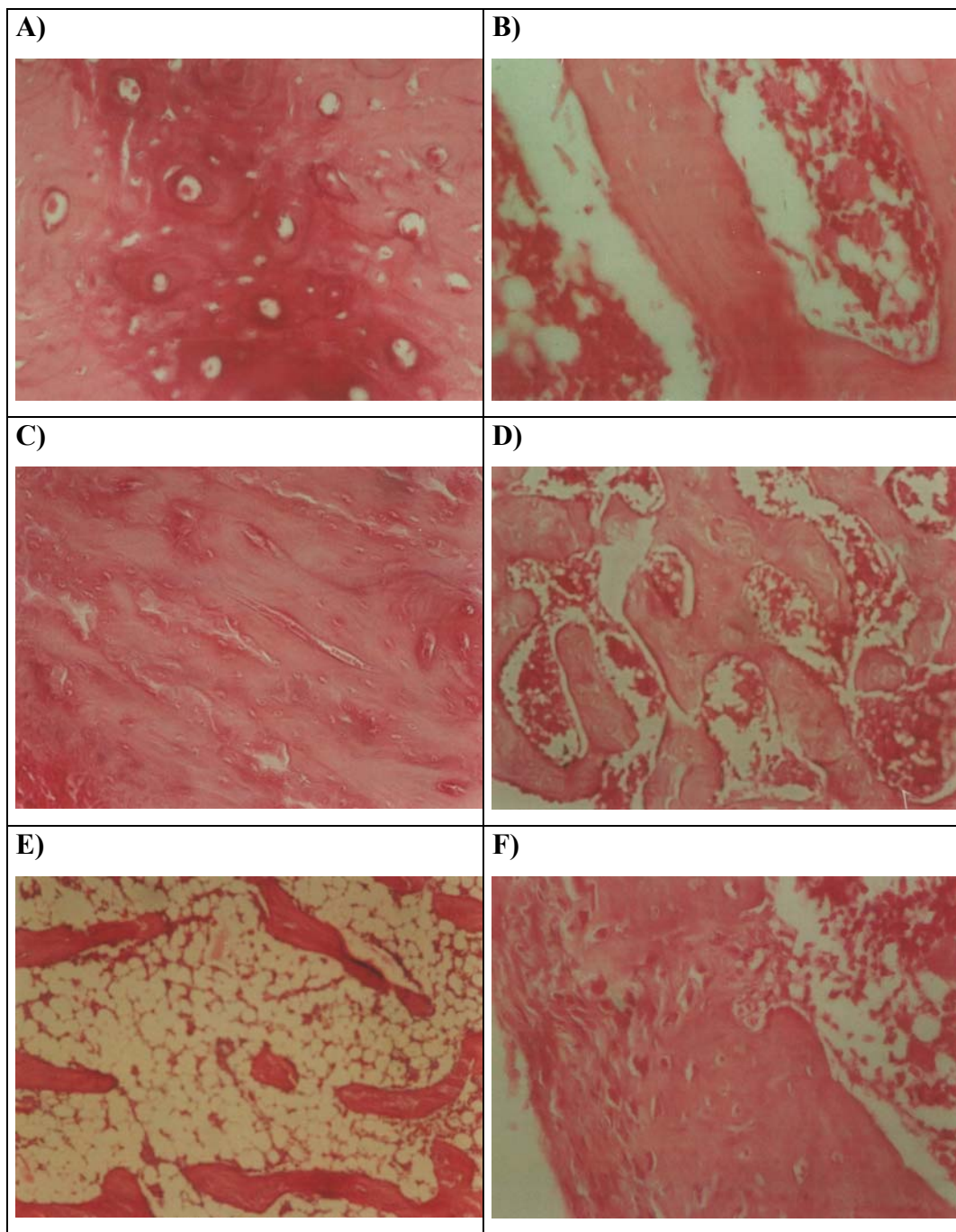


Figure 45. Light microscopy of: **(A)** femur (X100) and **(B)** tibia of the CONTROL group (X200); **(C)** femur (X100) and **(D)** tibia of the DEFICIENT group (X200); **(E)** femur (X100) **(F)** and tibia of the EXCESS group (X200).

CHAPTER 4

DISCUSSION

It is known that estrogen deficiency in post menopausal women can lead to osteoporosis. On the other hand, obesity, oxidative stress, hypertension and diabetes mellitus have been shown as risk factors of low bone mineral density (McFarlane *et al.*, 2004). Actually, diabetes mellitus is associated with an extensive list of complications involving nearly every tissue in the body. Diabetes mellitus is known as one of the major causes of low turnover osteopenia (Okuna *et al.*, 1991). It has been shown both clinically and experimentally to affect the properties of intact bone and bone with a healed fracture. Clinically it is often associated with reduced bone mass (Heap *et al.*, 2004) and delayed fracture healing in humans (Cozen, 1972, Levin *et al.*, 1976, Loder, 1988). Experimentally, diabetes adversely affects the properties of intact bone and impairs fracture healing in rats (Herbsman *et al.*, 1968, Einhorn *et al.*, 1988, Macey *et al.*, 1989, Hou *et al.*, 1993, Funk *et al.*, 2000). Most studies indicate that it is a complication for children and adolescents with insulin-dependent diabetes mellitus (IDDM, or, Type I). (Silberberg, 1986, Piepkorn *et al.*, 1997), especially for those with poor metabolic control and in the first few years from the time of diagnosis (McNair *et al.*, 1979a,b, McNair, 1988). However, there are some confictions. For example, in a recent study Ingberg et al stated that patients with long-standing Type I diabetes with onset in childhood and adolescence seem to show no difference in bone mineral density compared with closely matched healthy controls (2004). There are also conflicting findings for patients with non-insulin dependent diabetes mellitus (NIDDM, or, Type II) who showed evidence of decreased, normal or increased skeletal mass (Levin *et al.*, 1976, Meema and Meema, 1967, Deleeuw and Abs, 1977, El Miedany *et al.*, 1999).

The ovariectomized animal models, similar to patients with osteoporosis, tend to show reduced mechanical strength (Kasra and Grynpas, 1994; Newman *et al.*, 1995). Similarly, animal models that mimic human diabetic condition have been used to elucidate diabetes-induced alterations in bone tissues. Dixit and Ekstrom reported that the biomechanical behavior of bone showed a decrease in the breaking strength of the femoral shaft of diabetic rats (1980). Other biomechanical tests investigating the characteristics of bones of STZ-induced diabetic rats revealed that bones are stiffer (Einhorn *et al.*, 1988, Funk *et al.*, 2000, Reddy *et al.*, 2001), weaker, highly fragile and brittle as compared with those of normal control rats (Reddy *et al.*, 2001). The mechanical properties of bone tissue depend both on the mineral and the matrix (primarily type I collagen fibrils) constituents (Reilly and Burstein, 1974, Currey, 1984, Martin and Ishida, 1989, Keaveny *et al.*, 1994, Camacho *et al.*, 1995, Shah *et al.*, 1995). Although, the pathogenesis of osteopenia in diabetes is a poorly understood phenomenon, diminished bone formation, mineralization and resorption appears to be related to the inferior biomechanical properties of bone tissue in diabetes (Reddy *et al.*, 2001). On the other hand, decreased total collagen content and defects in collagen cross-linking have been noted in the fracture callus of rats with STZ-induced experimental diabetes compared with those in the controls (Einhorn *et al.*, 1988, Macey *et al.*, 1989).

During normal osteogenesis, following formation of calcifiable matrix and initial mineral deposition, remodeling permits alteration of the initial matrix and perfection of the mineral (Boskey and Marks, 1985). Biological apatites from different normal and pathological calcified tissues, at different degrees of calcification, exhibit different chemical composition, crystallinity and stability (Rey *et al.*, 1990). The mineral, protein and lipid constituents of calcified tissues produce intense, structure sensitive infrared bands. Therefore, in the present study structural information about the mineral and matrix environment of control, diabetic, Se treated diabetic and control group rat femurs and tibias was gained by detailed analysis of inorganic mineral and organic matrix bands of the FTIR spectra .

As mentioned in the introduction part, other ultrastructural analyses together with FTIR spectroscopy studies have determined the bone mineral to be a poorly crystalline, carbonate and acidic phosphate containing analog of hydroxyapatite (HA) $[\text{Ca}_{10}(\text{PO}_4)_6(\text{OH})_2]$. However, there is still some controversy and uncertainty as to whether bone crystals contain OH groups, and if they do, whether the failure to detect such groups by infrared spectroscopy. Rey et al suggested that instrumental factors may be ruled out, since the presence of the OH group in synthetic apatite crystals can be detected easily by FTIR spectroscopy (1995), as in the case of the present study and other previous studies (Baddiel and Berry, 1966, Fowler *et al.*, 1966, El Feki *et al.*, 1991). Moreover, studies carried out with magic angle spinning, proton nuclear magnetic resonance spectroscopy (Rey *et al.*, 1995) and inelastic neutron-scattering spectroscopy (Loong *et al.*, 2000) confirmed that bone apatite crystals do not contain detectable amounts of hydroxyl ions. However, in contrast to the findings of Loong *et al.*, Taylor *et al.* reported the presence of hydroxyl groups in bone tissue by using the same technique (2000). Therefore, further studies are necessary to clarify this point.

In skeletal tissues the crystal size appears as a key factor in the mineralization process. Because, the knowledge of the hydroxyapatite crystal size, its association with the organic matrix and neighboring crystals provide a basis for the nature of the deposition and remodeling events that occur in normal and pathological processes and it can influence the stoichiometry and the solubility properties of biological apatites (Arsenault and Grynpas, 1988, Ou-Yang *et al.*, 2000).

It was previously shown that the percent area of 1060 cm^{-1} sub-band, obtained from the curve-fitting analysis of the $\nu_1, \nu_3 \text{ PO}_4^{3-}$ stretching region, is inversely related to the crystal size (Pleshko *et al.*, 1991, 1992, Boskey *et al.*, 1998). We found out that (Boyar *et al.*, 2003) the mineral crystal sizes increased for diabetic femurs and tibias. In order to reach that result, the $\nu_1, \nu_3 \text{ PO}_4^{3-}$ stretching region of the FTIR spectra was analyzed. As can be deduced from the curve-fitting analysis of this spectral region, there is a significant decrease in the percent mean peak area of the

fourth (1060 cm^{-1}) sub-band in the diabetic group (Table 9). This means an increase in the crystal size of diabetic rat femurs and tibias. In the continuing part of this study, the same spectral analysis was carried out to see the effects of Se treatment on diabetic and control group rat bones. The mean peak areas of the fourth band for Se treated diabetic and control groups were larger than those of diabetic femurs and tibias. This means a smaller crystal size with respect to diabetic group.

Previously it was reported that trabecular bone from ovariectomized monkeys contained larger apatite crystals (increased crystallinity) (Gadeleta *et al.*, 2000). Similarly, different parts of bone tissue from postmenopausal osteoporotic human subjects exhibited increased crystallinity (Baud *et al.*, 1976, Rai and Behar, 1986, Paschalis *et al.*, 1997, Gadeleta *et al.*, 2000; Mendelsohn *et al.*, 2000). Therefore, in the present study the results regarding the crystal size of the minerals seem to be in agreement with these studies and may reflect the presence of pathology in diabetic rat bone tissues. Because, in establishing the biomechanical properties of skeletal and dental tissues, the texture of the apatite crystals (i.e. the size, shape and arrangement) that comprise the mineral phase acts as a major determinant (Wagner, and Weiner, 1992, Landis, 1995). However, in one study it was reported that osteoporotic bone mineral consisted of smaller and less perfect crystals (Grynpas and Holymard, 1988). Thus, it is better to analyze the other features of the mineral phase present in the diabetic rat bones.

On the other hand, although the changes are not statistically significant, Se treatment led to the increase in the crystal size of control group femurs as compared with untreated control group femurs. An opposite change was observed for the tibias of the Se treated control group rats. Differences in the crystallite size has been linked to collagen fibrils, to the location of crystals within collagen, and the differences between inter and intrafibrillar crystals. Therefore, this result will be discussed later.

The presence of carbonate and acid phosphate ions and their relative amounts in bone and other calcified tissues are determining factors of several of the physical

and chemical properties of natural apatites and the crystallinity and solubility of apatites are affected by these ions. For the diabetic group rat bones, the relative ratio of nonapatitic HPO_4^{2-} significantly decreased, whereas relative apatitic PO_4^{3-} content increased (Figure 17 and Table 7). This means that there was less newly formed mineral crystals in diabetic bone tissues (Huang *et al.*, 2002). This finding supports the presence of larger crystals in diabetic rat bones. For Se treated diabetic rat bones there was negligible changes in the relative apatitic PO_4^{3-} content and the relative ratio of nonapatitic HPO_4^{2-} increased as compared with diabetic group and approached to control values. This can be an indication of the presence of new bone formation. On the other hand, for Se treated control group tibias, the nonapatitic HPO_4^{2-} content decreased. However, the crystal size of these bones was closer to that of control group. Then, there can be other factors that played role in the determination of the crystal size. Similarly, for both bones of the Se treated control group rats, the nonapatitic PO_4^{3-} content decreased significantly with respect to control group. A similar decrease with respect to control and diabetic group bones was also observed for nonapatitic PO_4^{3-} content of Se treated diabetic bones. This may indicate the presence of more stable environment in selenium treated bones.

Carbonate ions are known to destabilize the apatite structure by decreasing the crystallinity, causing structural disorder (Apfelbaum *et al.*, 1990) and by inducing proliferative growth of new crystals (Eanes and Hailer, 2000). In the current study, a significant decrease in the relative carbonate / phosphate ratio was observed for diabetic rat femur. A similar decrease was also present for the diabetic tibia but at a less extend (Boyar *et al.*, 2003). Considering above properties of carbonate ions, it can be concluded that the increase in the crystal size of the minerals present in diabetic bones can be affected from the decrease in the relative amount of carbonate ions. On the other hand, the relative carbonate content of Se treated diabetic and control group rat bones was closer to that of control group bones and in turn, the crystal sizes of the same groups were also closer to that of control group bones.

In a previous study carried out with ovariectomized rats, it was shown that the total

carbonate content decreased in trabecular rat bone (Bohic *et al.*, 2000). The carbonate contents of bone apatites of osteoporotic Eskimos were also determined to be lower as compared with normal bone (Thompson, *et al.*, 1983). Similarly, in another study it was reported that the relative amount of carbonate decreased in the subchondral and cortical bone regions of proximal tibias of ovariectomized cynomolgus monkeys as compared with sham controls (Huang, *et al.*, 2002). These studies are in agreement with our present findings. In contrast, in a Fourier transform infrared microscopy (FTIRM) study of lumbar vertebrae from ovariectomized cynomolgus monkeys, the carbonate/phosphate ratio was shown to be higher as compared with the sham controls (Gadeleta *et al.*, 2000). This may be due to functional and structural differences in bone tissues taken from different anatomical regions of the same species.

On the other hand, the presence of carbonate, which usually occupy B sites in biological apatites, can also reduce the destabilizing effect of some ions, such as magnesium on HA structure (Baravelli *et al.*, 1984). Phosphate, carbonate, and pH can influence the location of the carbonate ions during the formation and maturation of apatitic crystals. The curve-fitting analysis of the ν_2 carbonate domain revealed that diabetes caused a decrease in labile carbonate content and significant increase in type B carbonate content of femurs. Similarly for diabetic tibia the relative amount of labile carbonate decreased. This can indicate a low bone turnover rate in diabetic group bones. Selenium treatment led to reversal of labile type carbonate content in diabetic femurs. This can be due to formation of new crystals. For selenium treated control femur, type A carbonate content increased significantly.

For tibias of both of the selenium treated groups, the relative amount of labile type carbonate increased significantly whereas, the relative amount of type B carbonate decreased significantly as compared with the control group tibias. Therefore, the changes in type L and type B carbonate contents are parallel for the femurs and the tibias in the experimental groups as compared with the control groups of femurs and tibias and indicative of the presence of newly formed crystals. But, the selenium

treatment in tibias caused more significant changes in relative amounts of labile and type B carbonates as compared with femurs. This may show higher bone turnover rate for tibias than for femurs of Se treated control and diabetic groups.

Since the mechanical properties of bone tissue depend both on the mineral and the matrix constituents, the curve-fitting analysis was carried out in the Amide I region, which primarily results from type I collagen fibrils. Although, decreased osteoblastic collagen synthesis (Tamayo *et al.*, 1981), decreased total collagen content and defects in collagen cross-linking have been noted in the fracture callus of STZ-induced experimental diabetes compared with those in the controls (Einhorn *et al.*, 1988, Macey *et al.*, 1989), the effect of Se treatment on the distribution of reducible and non-reducible cross-links of collagen I has not been reported yet. According to the curve-fitting analysis of the Amide I region, the bands at \sim 1660 cm^{-1} and \sim 1690 cm^{-1} were assigned to non-reducible pyridinoline [Pyr] and reducible dihydroxylysinonorleucine [DHLNL] cross-links present in collagen I of the bone tissue, respectively (Paschalis *et al.*, 1998, 2001, Khan *et al.*, 2001, Miller *et al.*, 2002, Atti *et al.*, 2002, Huang *et al.*, 2003, Boskey *et al.*, 2003, Boyar *et al.*, 2004). As the bone tissue matures, divalent DHLNL is converted to the trivalent hydroxylysyl / lysylpyridinolines and pyrroles. Therefore, the alterations in the ratio of these two sub-bands give information about the maturity of collagen I present in bone tissue.

For diabetic group femurs the relative ratio of non-reducible cross-links to reducible cross-links increased significantly. This increase in the 1660 to 1690 ratio can be an indication of a decrease in immature DHLNL cross-links and the disturbances in collagen maturation can also affect mineralization and functional properties of the bone tissue. (Paschalis *et al.*, 2001, Khan *et al.*, 2001). Therefore, it can be concluded that there was less bone turnover for diabetic group bones. Regarding this ratio, Se treatment led to restoring effect for diabetic femurs.

For femurs of Se treated control group the 1660 : 1690 cm^{-1} ratio was higher than

control group femurs. Therefore, for Se treated femurs the rate of bone turnover could be lower and as mentioned before, this in turn causes an increase in the crystal size of control group femurs. Whilst, the $1660 : 1690\text{ cm}^{-1}$ ratios for all of the experimental group tibias were less than the same ratio for control group tibias. But the changes with respect to control group were not significant. Thus, the differences in the crystallite size are not only attributable to variations in the collagen fibrils, but also to the location of crystals within collagen and to the differences between inter and intrafibrillar crystals. The variations in different types of carbonates also has to be taken into consideration. For selenium treated control femur, type A carbonate content increased significantly. This may also play role in the presence of greater crystals in selenium treated control group femurs.

Although, with our recent knowledge the changes in relative pyrrole content could not be determined from FTIR spectra, the contribution of pyrrole to FTIR bands must be taken into consideration as well. Cross-link analysis of collagen molecule is generally carried out by high-performance liquid chromatography to determine collagen maturity. This technique requires some complicated procedures such as homogenization, hydrolysis with acid/alkali (Eyre *et al.*, 1984, Knott and Bailey, 1998). However, with the aid of FTIR spectroscopy, information about collagen cross-links can be provided easily.

In the formation of osteoporosis oxidative stress plays an important role. Oxidative stress in an organism occurs when the production of oxidants exceeds antioxidant capacity. The free radicals resulting from oxidative stress can damage tissues by reacting with cellular proteins, nucleic acids and lipids. Considering this fact, in the present study the variations in the lipid band of the FTIR spectra of control and experimental groups were also analyzed. Several studies demonstrated that free radical generation is increased in diabetic animals and in patients with Type I and Type II diabetes mellitus (Hiramatsu. and Arimori, 1980). In the present study we determined that the relative ratio of lipids in diabetic bone tissues increased with respect to control group bones. Therefore, the possibility of free radical production

is high. This point has an importance for bone physiology, because free radicals are inhibitors of osteoblasts (bone forming cells) (Moreau *et al.*, 1998), but activate osteoclasts and result in decreased bone formation (Hosoya *et al.*, 1998) and increased bone resorption (Garrett *et al.*, 1990, Suzuki *et al.*, 1997).

On the other hand, it is known that bone marrow stromal cells (also known as mesenchymal stem cells) are capable of differentiating into several different cell types including osteoblasts and fat forming adipocytes (Grigoriadis *et al.*, 1988, Bennett *et al.*, 1991). In osteoporosis and age related osteopenia the bone volume decreases substantially. According to previous histomorphometric observations, it was suggested that a change in bone marrow stromal cell dynamics can cause osteoporosis by replacing the functional bone-forming cell population of the marrow with adipose tissue (Meunier *et al.*, 1971, Burkhardt *et al.*, 1987). Later, it was shown that an increase in the number of adipocytes occurs at the expense of osteoblasts and human trabecular bone cells are able to express both osteoblastic and adipocytic phenotypes (Beresford *et al.*, 1992, Nuttall *et al.*, 1998). In an other study it was demonstrated that, the cells expressing an osteoblastic phenotype can be changed in vitro to adipocytic by addition of rabbit serum, rich in fatty acids (Diascro *et al.*, 1998). Therefore, in the present study similar to bone marrow, the increased ratio of lipids with respect to proteins in diabetic rat bone tissue may be an indication of presence of impairments in the distribution of bone forming osteoblasts and in turn, possible increase in the formation of osteoporotic pathologies. Actually as mentioned before, the mineral crystal sizes increased and carbonate content decreased for diabetic rat femurs and tibias [Figure 19, Tables 9 and 12], indicative of the presence of pathology in bone mineral environment (Boyar, *et al.*, 2003).

It is known that there is a close relationship and important balance between lipid peroxidation, bone physiology and degenerative diseases. However, the effects of antioxidants on bone metabolism have not been well characterized, yet. The results of the previous studies are not always in agreement with each other (Xu *et al.*, 1995,

Leveille *et al.*, 1997, Melhus *et al.*, 1999, Ima-Nirwana *et al.*, 1999, Arjmandi, *et al.*, 2002). The study of Leveille *et al.* (1997) showed that vitamin E or beta-carotene intake was not associated with femoral neck bone density in postmenopausal women. Similarly, Melhus *et al.* (1999) also demonstrated that an adequate intake of dietary vitamin E did not reduce the risk of hip fracture in current smokers.

On the other hand, contradictory to the above results vitamin E stimulated trabecular bone formation, reduced bone resorption, and altered epiphyseal cartilage morphometry as a result of lipid peroxidation in thyrotoxic rats and/or in growing chicks (Xu *et al.*, 1995, Ima-Nirwana *et al.*, 1999). Similarly, rats given red palm olein, that is rich in vitamin E and other antioxidants, exhibited increased endosteal bone mineral apposition rate and bone formation rate in tibia (Watkins, *et al.*, 2001). In another study, it was also shown that vitamin E improved bone quality in the aged but not in young adult male mice (Arjmandi, *et al.*, 2002). It was also reported that an adequate intake of vitamin E and vitamin C was protective against the hip fracture risk in female smokers (Melhus *et al.*, 1999).

Similar to vitamin E, one of the major physiological roles of Se is to function as a general antioxidant. Selenium interacts with vitamin E in protecting the cell membrane against oxidative damage caused by peroxides produced from lipid metabolism. In the present study, for Se treated diabetic samples it was observed that, the changes in the intensities of C-H stretching bands approached to control values (Figure 24) indicating the restoring effect of Se. Furthermore, the presence of higher amount of protein and the disorderliness in the lipid environment as compared with diabetic group bones may indicate the presence of higher amount of proteolipids rather than other lipids. In addition, it also indicates the promotion of hydroxyapatite formation and bone remodeling (Boskey, *et al.*, 1988) due to possible improvement in antioxidant action in the presence of Se treatment. On the other hand, after oxidation, fatty acids can breakdown to a variety of reactive aldehydes. Di-aldehydes derived from lipid peroxidation can make cross-links with collagen. Therefore, these cross-links can have a direct effect on collagen function

and may also act as a link between glycation and further lipid peroxidation (Bailey *et al.*, 1998). This peroxidation can be lowered in the presence of selenium and may lead to improvement in mineral and organic structure of diabetic bones. It was also reported that sodium selenate has insulin like effects in vitro in fat cells in that it caused the translocation of glucose transporters to the plasma membrane in adipocytes and resulted in phosphorylation of some proteins (Ezaki, 1990). Similar effects might be seen in bone cells and help new bone formation. Actually, Delilbaşı *et al* reported that the mandibles of diabetic rats treated with sodium selenite were found to be healthier than untreated diabetic group mandibles (2002). In a recent study Turan *et al* reported that when sodium selenite was given together with vitamins E and C to the heparin induced osteoporotic model rabbits, the femurs had almost the same structure as in normal rabbits and this combination seemed to be more efficient than sole vitamin E and C combination (2003).

Another point that is necessary to discuss is the variation in the types of the long bones under investigation. In the current study more prominent alterations were noted with diabetic femurs rather than tibias. Similarly, Reddy *et al.* reported that a significant reduction in the breaking strength of STZ-induced diabetic rat bones occurred and this effect was greater in the femurs as compared with the tibias (2001). Therefore, in this study the femurs of control and experimental group rats were used for light microscopic and electron microscopic studies in order to investigate the histological changes in experimental group rats in comparison to control groups.

The electronmicrograph of a bone section taken from diabetic group bones showed that the microstructure of these bones affected negatively. For these bones one of the observations was that there was increased amount of adipocytes. As mentioned before, parallel to this observation FTIR analyses also revealed that lipid to protein ratio increased in diabetic bones.

The light microscopic examinations revealed that unlike control group rat bones, diabetic bones had heterogeneous appearance in the mineralized matrix. Upon sodium selenite treatment, newly formed trabeculae with different shapes and sizes were observed in diabetic group bone. Moreover, in Se treated diabetic bones the calcification was not complete in trabecular matrix and it was still continuing. As a supportive observation, active osteoblasts around the trabecules were determined in the electronmicrograph of selenium treated diabetic group bone. The increase in the density of the osteoblasts causes a parallel increase in the new bone formation. These results support the findings obtained from FTIR spectroscopic analysis. All of these microscopic and spectroscopic analysis results can imply that Se may play a preventive role for the formation of pathological structures in diabetic bone tissues by reducing the oxidative stress associated with diabetes.

On the other hand, the light microscopic investigation showed that treatment of the normal rats with sodium selenite did not affect the structure of the long bones significantly but led to enlargement in the unmineralized matrix and mineralized matrix. This observation is also in agreement with FTIR spectroscopic analysis results (Figure 19). Moreover, in a previous histological study Delilbaşı et al reported that there was a progressive resorption, trabecular and cortical irregularity and vascular proliferation in the mandibles of diabetic and selenium given control group rats and the mandibles of diabetic rats treated with sodium selenite were healthier (2002). Similarly, in the present study some irregularities in Se treated control group rat bones were determined. Therefore, unexpected results in the selenium given control group necessitate further studies on the mechanism of the effects of selenium in organisms.

In the present study x-ray diffraction analysis was also carried out. In the x-ray diffraction patterns, the peak broadening is inversely related to both crystal size and internal lattice perfection (i.e., the broader the peak, the smaller and / or more strained the crystals). Therefore, with this analysis the poor crystallinity of control and experimental group bone samples was clearly determined. However, according

to the analysis of the x-ray diffraction patterns there were slight variations between the crystal sizes of control and experimental group bones. For FTIR spectroscopic analysis a small piece of bone sample was always taken from the center of diaphysis. However, as 3-4 grams of bone powder was necessary for powder x-ray diffraction analysis, whole of the diaphysis was ground. Therefore, the bone powder used for x-ray diffraction analysis was more heterogenous as compared with that used for FTIR spectroscopic analysis. The difference in the variations of the crystal sizes obtained by two different biophysical techniques can be due to the level of heterogeneity in the bone samples.

In the current study the second aim was to investigate the effects of combined deficiency of dietary selenium and vitamin E and/or of sole selenium excess on bone mineral and organic matrix of rat femurs and tibias at molecular level. Although various effects of Se excess or deficiency have been reported in animals and humans (Young *et al.*, 1981, Anundi *et al.*, 1982, Sokoloff, 1985, Lin-Shiau, *et al.*, 1989, Yang, *et al.*, 1993a, 1993b, Turan *et al.*, 1996, 1997a, 1997b, 1997c, 2000; Reyes, *et al.*, 2001), most of the studies give limited information about the status of vitamin E in Se deficiency and the effect of Se excess on bone structure and function. In our research group's previous studies the effects of combined deficiency of dietary selenium and vitamin E and/or of sole selenium excess on rat bone mineral properties and biomechanical strength were investigated in where only the virtual comparison of FTIR spectra together with atomic absorption, X-ray diffraction analysis and biomechanical tests were reported (Turan *et al.*, 2000). In the present study a detailed FTIR spectroscopic analysis was carried out to determine the properties of the mineral and matrix environment of these bones.

In the present study, the curve-fitting analysis of the ν_1 , ν_3 PO_4^{3-} stretching band revealed an increase in the crystal size of experimental group bones [Table 17]. This increase seemed to be more pronounced in the case of the Se deficiency. Our data for both experimental groups implied that there were changes in the ionic substitutions of the local environment, since a change in crystal size is closely related to the stoichiometry and the solubility properties of biological apatites

(Arsenault and Grynpas, 1988). In order to obtain more information about the mineral environment, curve-fitting analysis was also performed in the ν_4 phosphate bending region. The results of this analysis revealed that selenium deficiency in diet led to a decrease in nonapatitic HPO_4^{2-} as well as a slight decrease in the non-apatitic PO_4^{3-} content of both femur and tibia [Figure 30, Table 16]. Unlike deficiency, the excess of Se led to an increase in the relative amount of acid phosphate content in both femur and tibia. This indicates the presence of newly formed mineral crystals in these tissues (Huang *et al.*, 2002).

From the investigation of the $\nu_2 \text{CO}_3^{2-}$ domain, it can be seen that a decrease in type B carbonate content occurred for both of femur and tibias of the deficient group, whereas, for the excess group an opposite result was found [Figure 31, Table 18]. It is known that the presence of carbonate can reduce the destabilizing effect of some ions, such as magnesium, on HA structure (Baravelli, *et al.*, 1984). For this reason, in the bones of the deficient group, a decrease in the amount of CO_3^{2-} ions occupying B sites may be affected by destabilizing effect of Mg^{2+} or other ions. The relative amount of type A carbonate was found to increase in the femurs of the deficient group whilst, a decrease was observed for the excess group. Phosphate, carbonate, and pH can influence the location of the carbonate ions during the formation and maturation of apatitic crystals. Since the non-apatitic HPO_4^{2-} group is easily exchangeable by carbonate species, in our case under Se deficiency, carbonate ions most probably substitute for OH^- and exchange with HPO_4^{2-} in a mineral environment. In the case of Se excess, the increase in the relative amount of HPO_4^{2-} might influence the pH of the environment and cause an increase in osteoclast action and, in turn, bone resorption. These findings were further supported by our light microscopy investigation in which Se and vitamin E deficiency and Se excess caused irregularities in overall bone structure.

Carbonate is also adsorbed onto the apatite surface. It gives rise to a broad non-apatitic, labile carbonate band at 866 cm^{-1} in the curve-fit FTIR spectrum [Figure 21]. Curve-fitting analysis of the $\nu_2 \text{CO}_3^{2-}$ domain revealed that, in tibias of

deficient group and in both femurs and tibias of the excess group, the relative amount of labile CO_3^{2-} content increased with respect to the control groups [Figure 31, Table 18]. This may imply the presence of newly formed mineral crystals (Rey *et al.*, 1989), besides the presence of large crystals as deduced by the curve-fitting analysis of the ν_1 , $\nu_3 \text{PO}_4^{3-}$ stretching band.

The information about collagen cross-links, that are abundant in bone tissue, was derived from the Amide I region of the FTIR spectra. The results revealed that the deficiency and excess of antioxidants led to an increase in the relative ratio of Pyr/DHLNL for femurs, whereas they led to a decrease in this ratio for tibias. This shows an increase in the relative amount of reducible DHLNL for tibias. In our research group's previous study (Turan *et al.*, 2000) it was reported that both a selenium and vitamin E-deficient diet and a selenium rich diet significantly decreased the biomechanical strengths of femurs and tibias while the bones belonging to the control group always had the highest modulus of elasticity. In that study the modulus of elasticity of tibia was reported as greater than that of femurs for both control and experimental groups. This may imply the greater biomechanical strength of tibias as compared with femurs. It is known that both collagen content and collagen cross-linking can affect the mechanical strength of bones (Burr, 2002). The covalent cross-links are essential in providing the tensile strength and mechanical stability of the collagen fibrils. Therefore, observed increase in the strength of the tibias as compared with the femurs might be resulted from an increase in the relative amount of reducible DHLNL. DHLNL is converted to the trivalent hydroxylysyl and lysylpyridinolines and pyrroles. It has previously been shown that the mechanical properties of bone correlate with the pyrrole content rather than with the pyridinoline content (Knott and Bailey, 1998). As mentioned before, though with our present knowledge the changes in the relative pyrrole content could not be determined from the FTIR spectra, the contribution of pyrrole to FTIR bands must be taken into consideration as well.

The mineral : matrix ratio can reflect the relative changes in both total phosphate and protein matrix. For both of the experimental groups' femurs, this ratio decreased whereas it increased in the tibias [Table 20]. On the other hand, the carbonate : phosphate ratios increased for the bones of both of the experimental groups [Table 20]. It is known that in normal calcified tendons and bone, acid phosphate content decreases, whereas carbonate content, Ca/P molar ratio, crystallite sizes, and stability of HA increases with increasing calcification. As it was stated in a previous study, according to atomic absorption measurements, in Se and vitamin E deficient femurs the Ca/P molar ratio decreased whereas in tibia this ratio slightly increased (Turan *et al.*, 2000). The differences observed in the present study in the distribution of carbonate and phosphate contents and in relative amounts of reducible and non-reducible cross-links in collagen might explain the variations in biomechanical strength between femurs and tibias observed in a previous study (Turan *et al.*, 2000). As noted before, the anatomical location of the bones is important and different types of bones can be affected at different extends. This is in agreement with a previous study in which the decrease in bone mineral density of femur of second-generation Se deficient rats was determined to be 2 % greater than that of tibia (Reyes *et al.* 2001).

Overall results showed that FTIR spectroscopy is a powerful technique due to its high sensitivity in detecting the changes in the functional groups belonging to tissue components, such as minerals, proteins and lipids (Boyar *et al.*, 2003, 2004, Toyran *et al.*, 2004). Together with microscopic studies it can provide valuable information about the effects of therapeutic agents on normal and pathological tissues at molecular level (Bohic *et al.*, 2000, Grynpas and Rey, Mendelsohn *et al.*, 2000, Huang *et al.*, 2002).

CHAPTER 5

CONCLUSION

The first part of the present study revealed that the changes observed in the mineral and matrix phases of diabetic bones, briefly, the increase in the mineral crystal size, the decrease in the acid phosphate and carbonate content, the increase in the non-reducible pyridinoline [Pyr] to reducible dihydroxylysinonorleucine [DHLNL] cross-links present in collagen I of the bone tissue as well as the increase in the lipid to protein ratio of the matrix are quite similar to those seen in osteoporotic patients and osteoporotic animal models and confirms the evidence of diabetic osteoporosis. Histologic studies carried out with light and electronmicroscopy supported these findings. FTIR spectroscopic analysis revealed that sodium selenite treatment had some restoring effects on the deviated properties of the microstructure of diabetic bones. Therefore, in addition to biomechanical and biochemical analysis, FTIR spectroscopic technique can be used as a diagnostic tool for the investigation of diseased bone tissues and to follow the effects of different therapeutic agents on bone microstructure.

It is known that the diabetic fracture callus demonstrates reduction in cell proliferation and collagen synthesis (content as well as type) during the early stages of the fracture healing. Insulin appears to have a key role in fracture healing. Insulin receptors have been identified in rat osteoblastic cells and it stimulates nucleotide synthesis of osteoblasts, proliferation of osteoblastic cells. It is also involved in collagen production in the rat. Moreover, it was also determined that the fracture healing in STZ-induced diabetes mellitus model appeared to be improved by the application of exogenous insulin. As mentioned before selenium can have dual effects in the treatment of diabetic bones. One of these effects can be due to its

antioxidative properties. The other one can be due to its insulin-like properties. As mentioned before Se deficiency can lead to development of glucose intolerance (Asayama *et al.*, 1986). The results of the present study revealed that the deficiency of selenium led to increase in the crystal size of the bone minerals, decreases in acid phosphate and labile carbonate content and increase in the ratio of the non-reducible pyridinoline [Pyr] to reducible dihydroxylysinonorleucine [DHLNL] cross-links present in collagen I of the bone tissue as in the case of diabetic bones. These results can be indicative of the importance of selenium in glucose metabolism. On the other hand, the results for Se toxicity are similar to those for deficiency except that the toxic amount of selenium led to increase in the relative amount of acid phosphate due to its pro-oxidant action on the living cells. This can affect the pH of the mineral environment and lead to deformation of the bone tissue. From the second part of the study it can be concluded that both antioxidant deficient and excess diets cause almost similar structural defects in the mineral and matrix phases of bone tissues. The results of this study on rats may reflect the importance of adequacy of antioxidants in diet for human life and if they are used in proper amounts they can be preventive for the complications of diabetes seen in bones as well as other organs. However, further investigations are necessary for the therapeutic usage of selenium, since the treatment of control group rat femurs with sodium selenite led to some structural alterations.

REFERENCES

- 1-Alexander, L. E. (1969) X-ray diffraction methods in polymer science, Wiley, New York.
- 2-Anderson, H. C. (1989) Biology of disease: Mechanism of mineral formation in bone. *Laboratory Invest* 60:320-330.
- 3-Anundi, I., Hogberg, J. and Stahl, A. (1982) Involvement of glutathione reductase in selenite metabolism and toxicity, studied in isolated rat hepatocytes. *Arch Toxicol* 50:113-23.
- 4-Apfelbaum, F., Mayer, I. and Featherstone, J. D. B. (1990) The role of HPO_4^{2-} and CO_3^{2-} ions in the transformation of synthetic apatites to $\beta\text{-Ca}_3(\text{PO}_4)_2$. *J Inorganic Biochem* 38:1-8.
- 5-Arjmandi, B. H., Juma, S., Beharka, A., Bapna, M. S., Akhter, M. and Meydani, S. N. (2002) Vitamin E improves bone quality in the aged but not in young adult male mice. *J of Nutritional Biochemistry* 13:543-549.
- 6-Armstrong, A. M., Chestnutt, J. E., Gormley, M. J. and Young, I. S. (1996). The effect of dietary treatment on lipid peroxidation and antioxidant status in new diagnosed non-insulin dependent diabetes. *Free Radical Biol Med* 21:719–726.
- 7-Arsenault, A. L. and Grynpas, M. D. (1988) Crystals in calcified epiphyseal cartilage and cortical bone of the rat. *Calcif Tissue Int* 43:219-225.
- 8-Asayama, K., Kooy, N. W. and Burr, I. M. (1986) Effect of vitamin E deficiency and selenium deficiency on insulin secretory reserve and free radical scavenging systems in islets: decrease of islet manganosuperoxide dismutase. *J Lab Clin Med* 107:459-464.
- 9-Atti, E., Gomez, S., Wahl, S. M., Mendelsohn, R., Paschalis, E. and Boskey, A. L. (2002) Effects of Transforming Growth factor- β deficiency on bone development: A Fourier Transform-Infrared imaging analysis. *Bone* 31:675-684.
- 10-Auwerx, J., Dequeker, J., Bouillon, R., Geusens, P. and Nijs, J. (1988) Mineral metabolism and bone mass at peripheral and axial skeleton in diabetes mellitus. *Diabetes* 37:8-12.

- 11-Ayaz, M., Özdemir, S., Ugur, M., Vassort, G. and Turan, B. (2004) Effects of selenium on altered mechanical and electrical cardiac activities of diabetic rat. *Arch Biochem and Biophys* 426:83-90.
- 12-Baddiel, C. B. and Berry, E. E. (1966) Spectra structure correlations in hydroxy and fluorapatite. *Spectrachimica Acta* 22:1407-1416.
- 13-Bailey, C. C. (1949) Alloxan diabetes. *Vit Horm* 7:365-382.
- 14-Bailey, A. J., Paul, R. G. and Knott, L. (1998) Mechanisms of maturation and ageing of collagen (Review). *Mechanism of Ageing and Development* 106:1-56.
- 15-Banse, X., Devogelaer, J. P., Lafosse, A., Sims, T. J., Grynpas, M. and Bailey, A. J. (2002) Cross-link profile of bone collagen correlates with structural organization of trabeculae. *Bone* 31:70-76.
- 16-Baravelli, S., Bigi, A., Ripamonti, A., Roveri, N. and Foresti, E. (1984) Thermal behavior of bone and synthetic hydroxyapatites submitted to magnesium interaction in aqueous medium. *J Inorg Biochem* 20:1-12.
- 17-Baron, R. D. D. S. (1999) Anatomy and ultrastructure of bone. In: Primer on the metabolic bone disease and disorders of mineral metabolism. An official publication of the American Society for Bone and Mineral Research. Favus, M. J. (Ed.). Lippincott Williams and Wilkins, Philadelphia, USA.
- 18-Battell M. L., Delgatty, H. L., McNeill, J. H. (1998) Sodium selenate corrects glucose tolerance and heart function in STZ diabetic rats. *Mol Cell Biochem*. 179:27-34.
- 19-Baud, C. A., Pouezat, J. A. and Tocho-Danguuy, H. J. (1976) Quantitative analysis of amorphous and crystalline bone tissue mineral in women with osteoporosis. *Calcif Tissue Int* 21S:452-456.
- 20-Baynes, J. W. (1991) Role of oxidative stress in development of complications in diabetes. *Diabetes* 40:1675-1678.
- 21-Beaten, V., Hourant, P., Morales, M. T. and Aparicio, R. (1998) Oil and fat classification by FT-raman spectroscopy. *J Agric Food Chem* 46:2638-2646.
- 22-Becker, D. J., Reul, B., Özçelikay, A. T., Buchet, J. P., Henquin, J. C. and Brichard, S. M. (1996). Oral selenate improves glucose homeostasis and partly reverses abnormal expression of liver glycolytic and gluconeogenic enzymes in diabetic rats. *Diabetologia* 39:3-11.

- 23-Bell, R. H. and Hye, R. J. (1983) Animal models of diabetes mellitus:physiology and pathology. *J Surg Res* 35:433-460.
- 24-Bennett, J. H., Joyner, C. J., Triffitt, J. T. and Owen M. E. (1991) Adipocytic cells cultured from marrow have osteogenic potential. *J Cell Science* 99: 131-139.
- 25-Beresford, J. N., Bennett, J. H., Devlin, C., Leboy, P., and Owen, M. E. (1992) Evidence for an inverse relationship between the differentiation of adipocytic and osteogenic cells in rat marrow stromal cell cultures. *J Cell Science* 102:341-351.
- 26-Berg, E. A., Wu, J. Y., Campbell, L., Kagey, M. and Stapleton, S. R. (1995) Insulin-like effects of vanadate and selenate on the expression of glucose-6-phosphate dehydrogenase and fatty acid synthesis in diabetic rats. *Biochimie* 77:919-924.
- 27-Berly, E. J. and Gillian, L. (1988) Direct determination of selenium of graphite furnace atomic absorption spectrometry with deuterium back ground correction and a reduced palladium modifier:Age-specific reference ranges. *Clin. Chem.* 34:709-714.
- 28-Bettger, W. J. (1992) Zinc and selenium, site-specific versus general antioxidation. *Can J Physiol Pharmacol* 71:721-724.
- 29-Block, N. E. Komori, K., Robinson, K. A., Dutton, S. L., Lam, C. F. and Buse, M. G. (1991) Diabetes-associated impairment of hepatic insulin receptor tyrosine kinase activity: a study of mechanisms. *Endocrinology* 128:312-322.
- 30-Bohic, S., Rey, C., Legrand, A., Sfihi, H., Rohanizadeh, R., Martel, C., Barbier, A. and Daculsi, G. (2000) Characterization of the trabecular rat bone mineral: Effect of ovariectomy and bisphosphonate treatment. *Bone* 26:341-348.
- 31-Boskey, A. L. and Posner, A. S. (1976) Extraction of a calcium-phospholipid-phosphate complex from bone. *Calcif Tissue Res* 19:273-283.
- 32-Boskey, A. L. and Marks, S. C. Jr. (1985) Mineral and matrix alterations in the bones of incisors-absent (ia/ia) osteopetrotic rats. *Calcif Tissue Int* 37:287-292.
- 33-Boskey, A. L., Di Carlo, E. F., Gilder, H., Donnelly, R. and Weintraub, S. (1988) The effect of short-term treatment with vitamin D metabolites of bone lipid and mineral composition in healing vitamin D-deficient rats. *Bone* 9:309-318.
- 34-Boskey, A. L., Gadeleta, S., Gundberg, C., Doty, S. B., Ducy, P. and Karsenty, G. (1998) Fourier transform infrared microspectroscopic analysis of bones of osteocalcin-deficient mice provides insight into the function of osteocalcin. *Bone* 23:187-196.

- 35-Boskey, A. L., Moore, D. J., Amling, M., Canalis, E. and Delany A. M. (2003) Infrared analysis of the mineral and matrix in bones of osteonectin-null mice and their wildtype controls. *J Bone Miner Res* 18:1005-1011.
- 36-Bouillon, R. (1991) Diabetic bone disease. *Calcif Tiss Int* 49:155-160.
- 37-Bouillon, R. (1992) Diabetic bone disease. Low turnover osteoporosis related to decreased IGF-I production. *Verh K Acad Geneeskd Belg* 54:365-392.
- 38-Bouillon, R., Bex, M., Herck, E. V., Laureys, J., Dooms, L., Lesaffre, E., Ravussin, E. (1995) Influence of age, sex, and insulin on osteoblast function: Osteoblast dysfunction in diabetes mellitus. *J Clin Endocrinol Metab* 80:1194-1202.
- 39-Boyar, H. and Severcan, F. (1997) Oestrogen-phospholipid membrane interactions: an FTIR study. *J Molecular Structure* 408/409:269-272.
- 40-Boyar, H., Turan, B. and Severcan, F. (2003) FTIR spectroscopic investigation of mineral structure of streptozotocin induced diabetic rat femur and tibia. *Spectroscopy: An International J* 17:627-633.
- 41-Boyar, H., Mut, M., Zorlu, F. and Severcan, F. (2004) The effects of chronic hypoperfusion on rat cranial bone mineral and organic matrix: A Fourier transform infrared spectroscopy study. *Analytical and Bioanalytical Chem* 379:433-438.
- 42-Burkhardt, R., Kettner, G., Bohm, W., Schmidmeir, M., Schlag, R., Frisch, B., Mallmann B., Eisenmenger, W., and Gilg, T. H. (1987) Changes in trabecular bone, hematopoiesis and bone marrow vessels in aplastic anaemia, primary osteoporosis and old age: a comparative histomorphometric study. *Bone* 8:157-164.
- 43-Burr, D. B. (2002) The contribution of the organic matrix to bone's material properties. *Bone* 31:8-11.
- 44-Camacho N. P., Rimnac, C. M., Meyer, R. A., Doty, S. B. and Boskey, A. L. (1995) Effect of abnormal mineralization on the mechanical behavior of x-linked hypophosphatemic mice femora. *Bone* 17:271-278.
- 45-Camacho N. P., Landis, W. J. and Boskey, A. L. (1996) Mineral changes in a mouse model of osteogenesis imperfecta detected by Fourier transform infrared microspectroscopy. *Connective Tissue Research* 35:259-265.

- 46-Camacho N. P., Rinnerthaler, S., Paschalis, E. P., Mendelson, R., Boskey, A. L. and Fratzl, P. (1999) Complementary information on bone ultrastructure from scanning small angle x-ray scattering and Fourier transform infrared microspectroscopy. *Bone* 25:287-293.
- 47-Campbell, J. D. (1984) In: *Biological Spectroscopy*. Elias, P. (Ed). Chapters 3 and 4. The Benjamin /Cummings Publishing Company, Inc.
- 48-Canalis, E. (1983) Effect of hormones and growth factors on alkaline phosphatase activity and collagen synthesis in cultured rat calvariae. *Metabolism* 32:14-20.
- 49-Casal, H. L. and Mantsch, H., H (1984) Polymorphic phase behaviour of phospholipid membranes studied by infrared spectroscopy. *Biochim Biophys Acta* 779:381-401.
- 50-Chen, X., Yang, G., Chen, J., Chen, X., Wen, Z. and Ge, K. (1980) Studies on the relations of selenium to Keshan disease. *Biol Trace Elem Res* 2:91-104.
- 51-Ci, X. Y., Gao, T. Y., Feng, J. and Guo, Z. Q. (1999) Fourier transform infrared characterization of human breast tissue: Implications for breast cancer diagnosis. *Applied Spectroscopy* 53:312-315.
- 52-Clark, R. F., Strukle, E., Williams, S. R. and Manoguerra, A. S. (1996) Selenium poisoning from a nutritional supplement. *J Am Med Assoc* 275:1087-1088.
- 53-Colthup, N. B., Daly, L. H. and Wiberley, S. E. (1975) *Introduction to infrared and raman spectroscopy*. New York: Academic Press.
- 54-Cozen, L. (1972) Does diabetes delay fracture healing? *Clin Orthop* 82:134-140.
- 55-Cser, A., Sziklai-Laszlo, I., Menzel, H. and Lombeck, I. (1993) Selenium status and lipoproteins in healthy and diabetic children. *J Trace Elem Electrolytes Health Dis* 7: 205-210.
- 56-Currey, J.D. (1984) Effects of differences in mineralization on the mechanical properties of bone. *Phil Trans R Soc London B* 304:509-518.

- 57-Çakmak G., Togan, İ, Uğuz, C., Severcan, F. (2003) FT-IR spectroscopic analysis of rainbow trout liver exposed to nonylphenol. *Appl Spectrosc* 57:835-841.
- 58-Daculsi, G., Bouler, J. M. and LeGeros R. Z. (1997) Adaptive crystal formation in normal and pathological calcifications in synthetic calcium phosphate and related biomaterials. *Int Rev Cytol* 172:129-191.
- 59-Deleeuw, I. and Abs, R. (1977) Bone mass and bone density in maturity-type diabetes measured by the ^{125}I photon absorption technique. *Diabetes* 26:1130-1135.
- 60-Delilbaşı, Ç., Demiralp, S. and Turan, B. (2002) Effects of selenium on the structure of the mandible in experimental diabetics. *J Oral Sci* 44:85-90.
- 61-Diascro, D. D. Jr, Vogel, R. L., Johnson, T. E., Witherup, K. M., Pitzenberger, S. M., Rutledge, S. J., Prescott, D. J., Rodan, G. A. and Schmidt, A. (1998) High fatty acid content in rabbit serum is responsible for the differentiation osteoblasts into adipocyte-like cells. *J Bone Miner Research* 25:1827-1832.
- 62-Dixit, P. K. and Ekstrom, R. A. (1980) Decreased breaking strength of diabetic rat bone and its improvement by insulin treatment. *Calcif Tissue Int* 32:195-199.
- 63-Douillet, C., Tabib, A., Bost, M., Accomintti, M., Borson-Chazot, F. and Ciavatti, M. (1999) Selenium in Diabetes: Effects of selenium on nephropathy in type I streptozotocin-induced diabetic rats. *J Trace Elements in Exper Medic* 12:379-392.
- 64-Duthie, G. G., Wahle, K. W. K. and James, W. P. T. (1993) Oxidants, antioxidants and cardiovascular disease. *Nutr Res Rev* 2:51.
- 65-Eanes, E. D. and Hailer, A. W. (2000) Anionic effects on the size and shape of apatite crystals grown from physiological solutions. *Calcif Tissue Int* 66:449-455.
- 66-Einhorn, T. A., Gundberg, C. M., Devlin, V. J. and Warman J (1988) Fracture healing and osteocalcin metabolism in vitamin K deficiency. *Clin Orthop.* 237:219-225.
- 67-El-Bayoumy, K. (2001) The protective role of selenium on genetic damage and on cancer. *Mutation Research* 475:123-139.

68-El-Feki, H., Rey, C. and Vignoles, M. Carbonate ions in apatite infrared investigations in the ν_4 CO_3 domain. *Calcif Tissue Int* 49: 269-274.

69-El-Miedany, Y. M., El Gaafary, S. and El Baddini, M. A. (1999) Osteoporosis in older adults with non-insulin-dependent diabetes mellitus: Is it sex related? *Clinical and Experimental Rheumatology* 17: 561-567.

70-Epand, R. M., Stafford, A. R., Tyers, S. M. and Nieboer, E. (1985) Mechanisms of action of diabetogenic zinc-chelating agents: model system studies. *Mol Pharmacol* 27:366-374.

71-Eyre, D. R., Koob, T. J., Van Ness, K. P. (1984) Quantitation of hydroxypyridinium cross-links in collagen by high-performance liquid chromatography. *Anal Biochem* 137:380-388.

72-Ezaki, O. (1990) The insulin-like effects of selenate in rat adipocytes. *J Biol Chem* 265: 1124-1128.

73-Fein, F. S., Kornstein, L. B., Strobeck, J. E., Capasso, J. M., Sonnenblick (1980) Altered myocardial mechanics in diabetic rats. *Circ Res* 47:922-933.

74-Felsenfeld, A. J., Iida-Klein, A. and Hahn, T. J. (1992) Interrelationship between parathyroid hormone and insulin: Effects on DNA synthesis in UMR-106-01 cells. *J Bone Miner Res* 7:1319-1325.

75-Foster, L. H. and Sumar, S. (1997) Selenium in health and disease: a review. *Crit Rev Food Sci Nutr* 37:211-228.

76-Fowler, B. O., Moreno, E. C. and Brown, W. E. (1966) Infrared spectra of hydroxyapatite, octacalcium phosphate and pyrolyzed octacalcium phosphate. *Arch Oral Biol* 11:477-496.

77-Frazer, T. E., White, N. H., Hough, S., Santiago, J. V., McGee, B. R., Bryce, G., Mallon, J. and Avioli, L. V. (1981) Alterations in circulating vitamin D metabolites in the young insulin-dependent diabetic. *J Clin Endocrinol Metab* 53: 1154-1159.

78-Freifelder, D. (1982) In: *Physical Chemistry. Applications to biochemistry and molecular biology*. Chapter 14. Freeman, W. H. (Ed), New York.

- 79-Funk, J. R., Hale, J. E., Carmines, D., Gooch, H. L. and Hurwitz, S. R. (2000) Biomechanical evaluation of early fracture healing in normal and diabetic rats. *J Orthopae Res* 18:126-132.
- 80-Gadeleta, S. J., Paschalis, E. P., Betts, F., Mendelsohn, R. and Boskey, A. L. (1996) Fourier transform infrared spectroscopy of the solution-mediated conversion of amorphous calcium phosphate to hydroxyapatite: New correlations between X-ray diffraction and infrared data. *Calcif Tissue Int* 58:9-16.
- 81-Gadeleta, S. J., Boskey, A. L., Paschalis, E. P., Carlson, C., Menschik, F., Baldini, T., Peterson, M. and Rimnac, C. M. (2000) A physical, chemical, and mechanical study of lumbar vertebrae from normal, ovariectomized, and nandrolone decanoate-treated cynomolgus monkeys (*Macaca fascicularis*). *Bone* 27:541-550.
- 82-Garrett, I. R., Boyce, B. F., Oreffo, R. O., Bonewald, L., Poser, J. and Mundy, G. R. (1990) Oxygen free radicals stimulate osteoclastic bone resorption in rodent bone in vitro and in vivo. *Jclin Invest* 85:632-639.
- 83-Garvey, W. T., Huecksteadt, T. P. and Birnbaum, M. J. (1989) Pretranslational suppression of an insulin responsive glucose transporter in rats with diabetes mellitus. *Science (Wash D. C.)* 245:60-63.
- 84-Gasmi, A., Garnier, R., Galliot-Guilley, M., Gaudillat, C., Quartenoud, B., Buisine, A. and Djebbar, D. (1997) Acute selenium poisoning. *Vet Hum Toxicol* 39:304-308.
- 85-Ge, K. and Yang, G. (1993) The epidemiology of selenium deficiency in the etiological study of endemic diseases in China. *Am J Clin Nutr Suppl* 57:259S-263S.
- 86-Gebre-Medhin, M., Ewald, U., Plantin, L. O. and Tuvemo, T. (1984) Elevated serum selenium in diabetic children. *Acta Pediatr Scand* 73:109–114.
- 87-Ghosh, R., Mukherjee, B. and Chatterjee M. (1994) A novel effect of selenium on streptozotocin-induced diabetic mice. *Diabetes Res* 25:165-171.
- 88-Giacca, A., Fassina, A., Caviezel, F., Cattaneo, A. G., Caldriola, G. and Pozza, G. (1988) Bone mineral density in diabetes mellitus. *Bone* 9:29-36.
- 89-Goodman, W. G. and Hori, M. T. (1984) Diminished bone formation in experimental diabetes. Relationship to osteoid maturation and mineralization. *Diabetes* 33:825-831.

- 90-Griesmacher, A., Kindhauser, M., Andert, S. E., Schreiner, W., Toma, C., Knoebl, P., Pietschmann, P., Prager, R., Schnack, C., Schernthaner, G. and Mueller, M. M. (1995) Enhanced serum levels of thiobarbituric acid reactive substances in diabetes mellitus. *Am J Med* 98:469-475.
- 91-Griffiths, P. R. and De Haseth, J. A. (1986) In: Fourier transform infrared spectrometry. New York: Wiley.
- 92-Grigoriadis, A. E., Heersche, J. N. and Aubin, J. E. (1988) Differentiation of muscle, fat, cartilage and bone from progenitor cells present in a bone-derived clonal cell population: effect of dexamethasone. *J Cell Biol* 106:2139-2151.
- 93-Grynpas, M.D. and Holymard, D. (1988) Changes in quality of bone mineral on aging and in disease. *Scanning Microsc* 2:1045-1054.
- 94-Grynpas, M.D. and Rey, C. (1992) The effect of fluoride treatment on bone mineral crystals in the rat. *Bone* 13:423-429.
- 95-Gundberg, C. M., Hauschka, P. V., Lian, J. B. and Gallop, P. M. (1984) Osteocalcin: Isolation, characterization and detection. *Methods Enzymol* 107:516-544.
- 96-Gunnarson, R., Berne, C. and Hellerström, C. (1974) Cytotoxic effects of streptozotocin and N-nitrosomethylurea on the pancreatic β cells with special regard to the role of nicotinamideadenine dinucleotide. *Biochem J* 140:487-494.
- 97-Hakkainen, J., Lindberg, P., Bengtsson, G., Jonsson, L. and Lannek, N. (1978) Requirement for selenium (as selenite) and vitamin E (as α -tocopherol) in weaned pigs. III. The effect on the development of the VESD syndrome of varying selenium levels in a low-tocopherol diet. *J Anal Sci* 46:1001-1008.
- 98-Hamlin, C. R., Kohn, R. R. and Luschin, J. H. (1975) Apparent accelerated aging of human collagen in diabetes mellitus. *Diabetes* 24:902-904.
- 99-Heap, J., Murray, M. A., Miller, S. C., Jalili, T., Moyer-Mileur, L. J. (2004) Alterations in bone characteristics associated with glycemic control in adolescents with type 1 diabetes mellitus. *J Pediatr* 144:56-62.
- 100-Hei, Y. J., Farahbakhshian, S., Chen, X., Battell, M. L. and McNeill, J. H. (1998) Stimulation of MAP kinase and S6 kinase by vanadium and selenium in rat adipocytes. *Mol Cell Biochem* 178:367-375.

- 101-Herbsman, H., Powers, J. C., Hirschman, A. and Shaftan G. W. (1968) Retardation of fracture healing in experimental diabetes. *J Surg Res* 8:424-431.
- 102-Hiramatsu, K. and Arimori, S. (1980) Increased superoxide production by mononuclear cells of patients with hypertriglyceridemia and diabetes. *Diabetes* 29:251.
- 103-Hock, J. M., Centrella, M. and Canalis, E. (1988) Insulin-like growth factor 1 has independent effects on bone matrix formation and cell replication. *Endocrinology* 122:254-260.
- 104-Hoekstra, W. G. (1975) Biochemical function of selenium and its relation to vitamin E. *Fed Proc* 34:2083-2089.
- 105-Holecek, V., Racek, J. and Jarabek, Z. (1995) Administration of multivitamin combination and trace elements in diabetes. *Cas Lek Cesk* 134:80-83.
- 106-Hosoya, S., Suzuki, H., Yamamoto, M., Kobayashi, K., and Abiko, Y. (1998) Alkaline phosphatase and type I collagen gene expression were reduced by hydroxyl radical-treated fibronectin substratum. *Mol Genet Metab* 65:31-34.
- 107-Hou, J. C. H., Zernicke, R. F. and Barnard R. J. (1993) Effects of severe diabetes and insulin on the femoral neck of the immature rat. *J Orthop Res* 11:263-271.
- 108-Hough, S., Avioli, L. V., Bergfeld, M. A., Fallen, M. D., Slatopolsky, E. and Teitelbaum, S. L. (1981) Correction of abnormal bone and mineral metabolism in chronic streptozotocin-induced diabetes mellitus in the rat by insulin therapy. *Endocrinology* 108:2228-2234.
- 109-Hough, F. S. (1987) Alterations of bone and mineral metabolism in diabetes mellitus. II. Clinical studies in 206 patients with type I diabetes mellitus. *South African Med J* 72:120-126.
- 110-Huang, R. Y., Miller, L. M., Carlson, C. S. and Chance, M. R. (2002) Characterization of bone mineral composition in the proximal tibia of Cynomolgus monkeys: Effect of ovariectomy and nandrolone decanoate treatment. *Bone* 30:492-497.
- 111-Huang, R. Y., Miller, L. M., Carlson, C. S. and Chance, M. R. (2003) In situ chemistry of osteoporosis revealed by synchrotron infrared microspectroscopy. *Bone* 33:514-521.

- 112-Hui, S. L., Epstein, S. and Johnston, C. C. (1985) A prospective study of bone mass in patients with type I diabetes. *J Clin Endocrinol Metab* 60:74-80.
- 113-Hunter, G. K., Heersche, J. N. M., Aubin, J. E. (1983) Isolation of three species of proteoglycans synthesized by cloned bone cells. *Biochem*, 22:831-837.
- 114-Ima-Nirwana, S., Kiftiah, A., Sariza, T., Gapor, M. T.A. and Khalid, B. A. K. (1999) Palm vitamin E improves bone metabolism and survival rate in thyrotoxic rats. *General Pharmac* 32:621-626.
- 115-Ingberg, C. M., Palmer, M., Aman, J., Arvidsson, B., Schvarcz, E. and Berne C. (2004) Body composition and bone mineral density in long-standing type 1 diabetes. *J Intern Med* 255:392-398.
- 116-Ingle, D. J. (1948) The production of experimental glycosuria in the rat. *Recent Prog Horm Res* 2:229-253.
- 117-Kao, W. H., L., Kammerer, C. M., Schneider, J. L., Bauer, R. L. and Mitchell, B. D. (2003) Type 2 diabetes is associated with increased bone mineral density in Mexican-American women. *Archives of Medical Research* 34:399-406.
- 118-Karten, T., Colein-Osdoby, P., Patel, N. *et al.* (1994) Potentiation of osteoclast bone resorption activity by inhibition of nitric oxide synthase. *Proc Natl Acad Sci USA* 91:3569-3573.
- 119-Kasra, M. and Grynpas, M. D. (1994) Effect of long-term ovariectomy on bone mechanical properties in young female cynomolgus monkeys. *Bone* 15:557-561.
- 120-Keaveny, T. M., Wachtel, E. F., Ford, C. M. and Hayes W. C. (1994) Differences between the tensile compressive strengths of bovine tibial trabecular bone depend on modulus. *J Biomech* 27:1137-1146.
- 121-Khan, M., Yamauchi, M., Srisawasdi, S., Stiner, D., Doty, S., Paschalis, E.P. and Boskey, A. L. (2001) Homocysteine decreases chondrocyte-mediated matrix mineralization in differentiating chick limb-bud mesenchymal cell micro-mass cultures. *Bone* 28:387-398.
- 122-Kimura, K. (1996) Role of essential trace elements in the disturbance of carbohydrate metabolism. *Nippon Rinsho* 54:79-84.

- 123-Kissler, H. J., Hofmann, G., Gepp, H., Erben, R. G. and Schwille, P. O. (2000) High insulin and low IGF-I plasma levels following pancreas transplantation in rats. Implications for bone and mineral metabolism. *Scand J Clin Lab Invest* 60:175-188.
- 124-Klein, E. A., Thompson, I. M., Lippman, S. M., Goodman, P. J., Albanes, D., Taylor, P. R. and Coltman, C. (2003) Select: the selenium and vitamin E cancer prevention trial. *Urologic Oncology: Seminars and Original Investigations* 21:59-65.
- 125-Kneipp, J., Lasch, P., Baldauf, E., Beekes, M. and Naumann, D. (2000) Detection of pathological molecular alterations in scrapie-infected hamster brain by Fourier transform infrared (FT-IR) spectroscopy. *Biochim Biophys Acta* 1501:189-199.
- 126-Knott, L., Whitehead, C. C., Fleming, R. H. and Bailey, A. J. (1995) Biochemical changes in the collagenous matrix of osteoporotic avian bone. *Biochem J* 310:1045-1051.
- 127-Knott, L. and Bailey, A. J. (1998) Collagen cross-links in mineralizing tissues: A review of their chemistry, function and clinical relevance. *Bone* 22:181-187.
- 128-Köhrle, J. (1996) Thyroid hormone deiodinases-a selenoenzyme family acting as gate keepers to thyroid hormone action. *Acta Med Austriaca* 23:17-30.
- 129-Krakauer, J. C., McKenna, M. J., Buderer, N. F., Rao, D. S., Whitehouse, F. W. and Parfitt, A. M. (1995) Bone loss and bone turnover in diabetes. *Diabetes* 44:775-782.
- 130-Kumpulainen, J. T. (1993) Selenium in foods and diets of selected countries, J Trace Elem, Electrolytes Health Dis 7:107.
- 131-Landis, W. J., (1995) The strength of a calcified tissue depends in part on the molecular structure and organization of its constituent mineral crystals in their organic matrix. *Bone* 16:533-544.
- 132-Lazarev, Y. A., Grishkovsky, B. A. and Khromova, T. B. (1985) Amide I band of IR spectrum and structure of collagen and related polypeptides. *Biopolymers* 24:1449-1478.
- 133-Leon, M., Larrodera, L., Lledo, G. and Hawkins, F. (1989) Study of bone loss in diabetes mellitus type I. *Diabetes Res Clin Pract* 6:237-242.

- 134-Leveille, S. G., LaCroix, A. Z., Koepsell, T. D., Beresford, S., Belle, G. V. and Buchner, D. M. (1997) Do dietary antioxidants prevent postmenopausal bone loss? Nutrition Research 17:1261-1269.
- 135-Levin, M. E., Boisseau, V. C. and Avioli, L. V. (1976) Effects of diabetes mellitus on bone mass in juvenile and adult-onset diabetes. N Engl J Med 294:241-245.
- 136-Lewis, M., Boisseau, V. C. and Avioli, L. V. (1976) New England Journal of Medicine 294:241-245.
- 137-Lin, S. Y., Li, M. J., Liang, R. C. and Lee, S. M. (1998) Non-destructive analysis of the conformational changes in human lens lipid and protein structures of the immature cataracts associated with glaucoma. Spectrochimica Acta Part A 54:1509-1517.
- 138-Lin-Shiau S. Y., Liu, S. H. and Fu, W. M. (1989) Studies on the contracture of the mouse diaphragm induced by sodium selenite. Eur J Pharmacol 167:137-146.
- 139-Lithell, H. and Berne, C. (1991) Diabetogenic Drugs. In: Pharmacology of Diabetes: Present Practice and Future Perspectives. Mogensen, C. E. and Standl, E. (Eds) 3:57-74. Walter de Gruyter, Berlin.
- 140-Loder, R., T. (1988) The influence of diabetes mellitus on the healing of closed fractures. Clin Orthop 232:210-216.
- 141-Loong, C. K., Rey, C., Kuhn, L. T., Combes, C., Wu, Y., Chen, S. H. and Glimcher, M. J. (2000) Evidence of hydroxyl-ion deficiency in bone apatites: an inelastic neutron-scattering study. Bone 26:599-602.
- 142-Macey, L. R., Kana, S. M., Jingushi, S., Terek, R. M., Borretos, J. and Bolander, M. E. (1989) Defects of early fracture-healing in experimental diabetes. J Bone Joint Surg (Am) 71:722-733.
- 143-Magnuson, M. A., Andreone, T. L., Printz, R. L., Koch, S. and Granner, D. K. (1989) Rat glucokinase gene:structure and regulation by insulin. Proc Natl Acad Sci USA 86:4838-4842.
- 144-Mandrup-Poulsen, T. (1990) Cytokine-mediated beta-cell destruction: the molecular effector mechanism causing IDDM? J Autoimmun Suppl 1:121-122.

- 145-Manoharan, R., Baraga, J. J., Rava, R. P., Dasari, R. R., Fitzmaurice, M. and Feld, M. S. (1993) Biochemical analysis and mapping of atherosclerotic human artery using FTIR microspectroscopy. *Atherosclerosis* 103:181-193.
- 146-Martin, R. B. and Ishida, J. (1989) The relative effects of collagen fiber orientation, porosity, density, and mineralization on bone strength. *J Biomechan* 22:419-426.
- 147-May, J. M., Mendiratta, S., Hill, K. E. and Burk, R. F. (1997) Reduction of dehydroascorbate to ascorbate by the selenoenzyme thioredoxin reductase. *J Biol Chem* 272:22607-22610.
- 148-McMurray, C., H. and Blanchflower, W., J. (1979) Application of a high-performance liquid chromatographic fluorescence method for the rapid determination of α -tocopherol in the plasma of cattle and pigs and its comparison with direct fluorescence and high-performance liquid chromatography-ultraviolet detection methods. *J Chromatogr* 178:525-531.
- 149-McFarlane, S. I., Muniyappa, R., Shin, J. J., Bahtiyar, G. and Sowers, J. R. (2004) Osteoporosis and cardiovascular disease: brittle bones and boned arteries, is there a link? *Endocrine* 23:1-10.
- 150-McNair, P., Madsbad, S., Christiansen, C., Christensen, M., S., Faber, O. K., Binder, C. and Transbol, I. (1979a) Bone loss in diabetes: Effects of metabolic state. *Diabetologia* 17:283-286.
- 151-McNair, P., Madsbad, S. and Christiansen, C. (1979b) Bone mineral loss in insulin treated diabetes mellitus; studies on pathogenesis. *Acta Endocrinol (Copenh)* 90:463-472.
- 152-McNair, P., Christiansen, C., Christensen, M. S., Madsbad, S., Faber, O. K., Binder, C. and Transbøl, I. (1981) Development of bone mineral loss in insulin-treated diabetes: a 1 $\frac{1}{2}$ years follow-up study in sixty patients. *Eur J Clin Invest* 11:55-59.
- 153-McNair, P., (1988) Bone mineral metabolism in human type 1 (insulin dependent) diabetes mellitus. *Dan Med Bull* 35:109-121.
- 154-McNeill, J. H. Delgatty, H. L. M. and Battel, M. L. (1991) Insulin-like effects of sodium selenate in STZ-induced diabetic rats. *Diabetes* 40:1675-1678.
- 155-Meema M. E. and Meema, S. (1967) The relationship of diabetes mellitus and body weight to osteoporosis in elderly females. *Can Med Ass J* 96:132-139.

- 156-Melhus, H., Michaelsson, K., Holmberg, L., Wolk, A. and Ljunghall, S. (1999) Smoking, antioxidant vitamins, and the risk of hip fracture. *J Bone Miner Res* 14:129-135.
- 157-Melin, A., Perromat, A. and Déléris, G. (2000) Pharmacologic application of Fourier transform IR spectroscopy: In vivo toxicity of carbon tetrachloride on rat liver. *Biopolymers (Biospectroscopy)* 57:160-168.
- 158-Mendelsohn, R. and Mantsch, H. H. (1986) Fourier transform infrared studies of lipid protein interaction. In: *Progress in Protein-Lipid Interactions*, Watts, A. and De Pont, J. J. H. M. (Eds) 2:103-147. Elsevier Science Publishers, BV (Biomedical Division) Amsterdam, Netherlands.
- 159-Mendelsohn, R. Paschalis, E. P., Sherman P. J. and Boskey A. L. (2000) IR microscopic imaging of pathological states and fracture healing of bone. *Applied Spectroscopy* 54:1183-1191.
- 160-Meunier, P., J., Aaron, J., Edouard, C. and Vignon, G. (1971) Osteoporosis and the replacement of cell populations of the marrow by adipose tissue. *Clin Orthop Rel Res* 80:147-154.
- 161-Miller, L. M., Vairavamurthy, V., Chance, M. R., Mendelsohn, R., Paschalis, E. P., Betts, F. and Boskey, A. L. (2001) In situ analysis of mineral content and crystallinity in bone using infrared micro-spectroscopy of the $\nu_4 \text{PO}_4^{3-}$ vibration. *Biochimica et Biophysica Acta* 1527:11-19.
- 162-Miller, L. M. and Tague, J. T. Jr. (2002) Development and biomedical applications of fluorescence-assisted synchrotron infrared micro-spectroscopy. *Vibrational Spectroscopy* 28:159-165.
- 163-Mody, N., Parhami, F., Sarafian, T. A. and Demer, L. L. (2001) Oxidative stress modulates osteoblastic differentiation of vascular and bone cells. *Free Radical Biol Medic* 31:509-519.
- 164-Mohan, I. K. and Das, U. N. (1997) Oxidant stress, anti-oxidant and nitric oxide in non-insulin dependent diabetes mellitus. *Med Sci Res* 25:55.
- 165-Moreau, M. F., Chappard D., Lesourd, M., Montheard J., P. and Basle, M., F. (1998) Free radicals and side products released during methylmethacrylate polymerization are cytotoxic for osteoblastic cells. *J Biomed Mater Res* 40:124-131.

- 166-Moustaid, N., Beyer, R. S. and Sul, H. S. (1994) Identification of an insulin response element in the fatty acid synthase promoter. J Biol Chem 269:5629-5634.
- 167-Mueller, A. S., Pallauf, J. and Rafael, J. (2003) The chemical form of selenium affects insulinomimetic properties of the trace element:investigaiton in type II diabetic dbdb mice. J Nutritional Biochemistry 14:637-647.
- 168-Navarro, A. M., Lopez, G., de la Serrana, H., Perez,V., V. and Lopez, M. M. C. (1999) Serum and urine selenium concentrations as indicators of body status in patients with diabetes mellitus. Sci Total Environ 228:79-85.
- 169-Newman, E., Turner, A. S. and Wark, J. D. (1995) The potential of sheep for the study of osteopenia: Current status and comparison with other animal models. Bone 16 (Suppl.):277S-284S.
- 170-Nightingale, J. P. and Lewis, D. (1971) Pole figures of the orientation of apatites in bones. Nature 232:334-335.
- 171-Nuttall, M.E., Paton, A.J., Olivera, D.L., Nadeau, D. P. and Gowen, M. (1998) Human trabecular bone cells are able to express both osteoblastic and adipocytic phenotype: implications for osteopenic disorders, J. Bone Miner Res. 13:371-382.
- 172-Nyomba, B. L., Bouillon, R., Lissens, W., Van Baelen, H. and De Moor, P. (1985) 1,25-Dihydroxy vitamin D and vitamin D-binding protein are both decreased in streptozotocin-diabetic rats. Endocrinology 116:2483-2488.
- 173-Nyomba, B. L., Verhaeghe, J. Thomasset, M., Lissens, W. and Bouillon, R. (1989) Bone mineral homeostasis in spontaneously diabetic BB rats. 1. Abnormal vitamin D metabolism and impaired active intestinal calcium absorption. Endocrinology 124:565-572.
- 174-O'Brien, R. M., Lucas, P. C., Forest, C., Magnuson, M. A., and Granner, D. K. (1990) Identification of a sequence in the PEPCK gene that mediates a negative effect of insulin on transcription. Science 249:533-537.
- 175-O'Brien, R. M. and Granner, D. K. (1996) Regulation of gene expression by insulin. Physiol Rev 76:1109-1161.
- 176-Okuna, Y, Nishizawa, Y., Sekiya, K. *et al.* (1991) Total and regional bone mineral content in patients with non-insulin dependent diabetes mellitus. J Nutr Sci Vitaminol 37:S43-S49.

- 177-Ou-Yang, H., Paschalis, E. P., Boskey A. L. and Mendelsohn, R. (2000) Two-dimensional vibrational correlation spectroscopy of in vitro hydroxyapatite maturation. *Biopolymers (Biospectroscopy)* 57:129-139.
- 178-Öztürk, Y., Altan, V. M. and Ari, N. Y. (1996) Effects of experimental diabetes and insulin on smooth muscle functions. *Pharmacol Rev* 48:1-44.
- 179-Paschalis, E. P., DiCarlo, E., Betts, F., Sherman, P., Mendelsohn, R. and Boskey, A. L. (1996) FTIR microspectroscopic analysis of human osteonal bone. *Calcif Tissue Int.* 59:480-487.
- 180-Paschalis, E. P., Betts, F., DiCarlo, E., Mendelsohn, R. and Boskey, A. L. (1997) FTIR microspectroscopic analysis of normal human cortical and trabecular bone. *Calcif Tissue Int* 61:480-486.
- 181-Paschalis, E. P., Ilg, A., Verdelis, K., Yamauchi, M., Mendelsohn, R. and Boskey, A. L. (1998) Spectroscopic determination of collagen cross-links at the ultrastructural level and its application to osteoporosis. *Bone* 23:S342.
- 182-Paschalis, E. P., Verdelis, K., Doty, S. B., Boskey, A. L., Mendelsohn, R. and Yamauchi, M. (2001) Spectroscopic characterization of collagen cross-links in bone. *J Bone and Mineral Res* 16:1821-1828.
- 183-Passeri, M. and Provvedini, D. (1983) Vitamin E in geriatric physiopathology. *Acta Vitaminol Enzymol* 5:53-63.
- 184-Piepkorn, B., Kann, P., Forst, T., Andreas, J., Pfutzner, A. and Beyer, J. (1997) Bone mineral density and bone metabolism in diabetes mellitus. *Horm Metab Res* 29:584-591.
- 185-Pleshko, N. L., Boskey, A. L. and Mendelsohn, R. (1991) Novel infrared spectroscopic method for the determination of crystallinity of hydroxyapatite minerals. *Biophys. J.* 60:786-793.
- 186-Pleshko, N. L., Boskey, A. L. and Mendelsohn, R. (1992) An FT-IR microscopic investigation of the effect of tissue preservation on bone. *Calcif. Tissue Int.* 51:72-77.
- 187-Posner, A. S. (1987) Bone mineral and the mineralization process. *Bone Min Res* 5:65-116.

- 188-Potmis, R. A., Nonavinakere, V. K., Rasekh, H. R. and Early, J. L. (1993) Effect of selenium (Se) on plasma ACTH, beta endorphine, corticosterone and glucose in rats: influence of adrenal enucleation and metapyrone treatment. *Toxicology* 79:1-9.
- 189-Rabinovitch, A. and Baquerizo, H. (1990) Immunological mechanisms of pancreatic β -cell destruction: effects of cytokines (Abstract). *J Autoimmun* 3:85.
- 190-Raggio, C. L., Boyan, B. D. and Boskey, A. L. (1986) In vitro hydroxyapatite formation by lipids. *J Bone Min Res* 1:409-416.
- 191-Rai, D. V. and Behar, J. (1986) Biophysical characterization of osteoporotic bone. *Environ Res* 40:68.
- 192-Raisz, L. G. (1988) Local and systemic factors in the pathogenesis of osteoporosis. *N Engl J Med* 318:818-828.
- 193-Rasekh, H. R., Potmis, R. A., Nonavinakere, V. K., Early, J. L., Iszard, M. D. (1991) Effect of selenium on plasma glucose of rats: the role of insulin and glucocorticoids. *Toxicol Lett* 58:199-207.
- 194-Raskin, P., Stevenson, M. R., Barilla, D. E. and Pak, C. Y. (1978) The hypercalciuria of diabetes mellitus: its amelioration with insulin. *Clin Endocrinol (Oxf)* 9:329-335.
- 195-Reddi, A. S. and Bollineni, J. S. (2001) Selenium-deficient diet induces renal oxidative stress and injury via TGF- β 1 in normal and diabetic rats. *Kidney International* 59:1342-1353.
34. Rey, C., Collins, B., Goehl, T., Dickson, I. R. and Glimcher, M. J. (1989) The carbonate environment in bone mineral: A resolution-enhanced Fourier transform infrared spectroscopy study. *Calcif. Tissue Int* 45:157-164.
- 196-Reddy, G. K., Stehno-Bittel, L. Hamade, S. and Enwemeka, C. S. (2001) The biomechanical integrity of bone in experimental diabetes. *Diabetes Res. and Clinic Pract* 54:1-8.
- 197-Reilly, D. T. and Burstein, A. H. (1974). The mechanical properties of cortical bone. *J B J S* 56A:1001-1022.
- 198-Rey, C., Collins, B., Goehl, T., Dickson, I. R. and Glimcher, M. J. (1989) The carbonate environment in bone mineral: A resolution-enhanced Fourier transform infrared spectroscopy study. *Calcif Tissue Int* 45:157-164.

- 199-Rey, C., Shimizu, M., Collins, B. and Glimcher, M. J. (1990) Resolution-enhanced Fourier transform infrared spectroscopy study of the environment of phosphate ions in the early deposits of a solid phase of calcium-phosphate in bone and enamel, and their evolution with age: I: Investigation in the ν_4 PO_4 domain. *Calcif Tissue Int* 46:384-394.
- 200-Rey, C., Renugopalakrishnan, V., Shimuzu, M., Collins, B. and Glimcher, M. J. (1991a) A resolution-enhanced Fourier transform infrared spectroscopic study of the environment of the CO_3^{2-} ion in the mineral phase of enamel during its formation and maturation. *Calcif Tissue Int* 49:259-268.
- 201-Rey, C., Shimizu, M., Collins, B. and Glimcher, M. J. (1991b) Resolution-enhanced Fourier transform infrared spectroscopy study of the environment of phosphate ions in the early deposits of a solid phase of calcium-phosphate in bone and enamel and their evolution with age: 2. Investigation in the ν_3 PO_4 domain. *Calcif Tissue Int* 49:383-388.
- 202-Rey, C., Renugopalakrishnan, V., Collins, B. and Glimcher, M. J. (1991c) Fourier transform infrared spectroscopic study of the carbonate ions in bone mineral during aging. *Calcif Tissue Int* 49:251-258.
- 203-Rey, C., Miquel, J. L., Facchini, L., Legrand, A. P. and Glimcher, M. J. (1995) Hydroxyl groups in bone mineral. *Bone* 16:583-586.
- 204-Reyes, R. M., Egrise, D., Nève, J., Pasteels, J. L. and Schoutens, A. (2001) Selenium deficiency-induced growth retardation is associated with an impaired bone metabolism and osteopenia. *J Bone and Mineral Res* 16:1556-1563.
- 205-Rico, H., Hernandez, E. R., Cabranes, J. A. and Gomez-Castresana, F. (1989) Suggestion of a deficient osteoblastic function in diabetes mellitus: the possible cause of osteopenia in diabetics. *Calcif Tissue Int* 45:71-73.
- 206-Rigas, B., Morgello, S., Goldman, I. S. and Wong, P. T. T. (1990) Human colorectal cancers display abnormal Fourier transform infrared spectra. *Proc Natl Aca Sci USA* 87:8140-8144.
- 207-Rosenbloom, A. L., Lezotle, D. C., Weber, F. T., Gudat, J., Heller, D. R., Weber, M. L., Klein, S. and Kennedy, B. B. (1977) Diminution of bone mass in childhood diabetes. *Diabetes* 26:1052-1055.
- 208-Rosenfeld, I. and Beath, O. A. (1964) Selenium, Geobotany, Biochemistry, Toxicity and Nutrition. Academic Press New York, p. 294.

- 209-Rotruck, J. T., Pope, A. L., Ganther, H. E., Swanson, A. B., Hafeman, D. G. and Hoekstra, W. G. (1973) Selenium: Biochemical role as a component of the glutathione peroxidase. *Science* 179:588-590.
- 210-Santiago, J. V., McAlister, W. H., Ratzan, S. K., Bussman, Y., Haymond, M. W., Shakelford, G. and Weldon, V. V. (1977) Decreased cortical thickness and osteopenia in children with diabetes mellitus. *J Clin Endocrinol Metab* 45:845-848.
- 211-Sasaki, S., Iwata, H., Ishigura, N., Habuchi, O and Miura, T. (1994) Low selenium diet, bone and articular cartilage in rats. *Nutrition* 10:538-543.
- 212-Schlienger, J. L., Grunenberger, F., Maier, E. A., Simon, C., Chabier, G. and Leroy, M. J. F. (1988) Perturbation des oligoéléments plasmatiques dans la diabète. Relation avec le quilibre glycémique. *Presse Med* 17:1076–1079.
- 213-Schneider, L. E. and Schedl, H. P. (1972) Diabetes and intestinal calcium absorption in the rat. *Am J Physiol* 223:1319-1323.
- 214-Schneider, L. E., Schedl, H. P., McCain, T. and Haussler, M. R. (1977) Experimental diabetes reduces circulating 1,25-dihydroxy-vitaminD in the rat. *Science* 196:1452-1454.
- 215-Schwarz, K. and Foltz, C. M. (1957) Selenium as an integral part of factor 3 against dietary necrotic liver degeneration. *J Am Chem Soc* 79: 3292-3293.
- 216-Scott, M. L., Olson, G., Krook, L. and Brown, W. R. (1967) Selenium-responsive myopathies of myocardium and of smooth muscle in the young poult. *J Nutr* 91:573-583.
- 217-Seeley, R. R., Stephens, T. D. and Tate, P. (1996) The skeletal system-Bones and joints. In: *Essentials of Anatomy and Physiology*. Smith, J. M., Callanan, R. J., Shahane, K. M. (Eds). WCB/The McGraw Hill Companies Inc., USA.
- 218-Severcan, F. and Haris, P. I. (1999) FTIR spectroscopic characterization of protein structure in aqueous and non-aqueous media. *Journal of Molecular Catalysis B. Enzymatic* 7:207-221.
- 219-Severcan, F., Toyran, N., Kaptan, N. and Turan, B. (2000) Fourier transform infrared study of the effect of diabetes on rat liver and heart tissues in the C-H region. *Talanta* 53:55-59.

- 220-Shah, K. M., Goh, C. H., Karunanithy, R., Low, L. S., Das De, S. and Bose, K. (1995). Effect of decalcification on bone mineral content and bending strength of feline femur. *Calcif Tissue Int* 56:78-82.
- 221-Shepherd, P. R., Navé, B. T. and Siddle, K. (1995) Insulin stimulation of glycogen synthesis and glycogen synthase activity is blocked by wortmannin and rapamycin in 3T3-L1 adipocytes: evidence for the involvement of phosphoinositide-3kinase and p70 ribosomal protein-S6 kinase. *Biochem J.* 305:25-28.
- 222-Shires, R., Teitelbaum, S. L., Bergfeld, M. A., Fallen, M. D., Slatopolsky, E. and Avioli, L. V. (1981) The effect of streptozotocin-induced chronic diabetes mellitus on bone and mineral homeostasis in the rat. *J Lab Clin Med* 97:231-240.
- 223-Shore, R. M., Chesney, R. W., Mazess, R. B., Rose, P. G. and Bargman, G. J. (1981) Osteopenia in juvenile diabetes. *Calcif Tissue Int* 33:455-457.
- 224-Short, J. M., Wynshaw-Boris, A., Short, H. P. and Hanson, R. W. (1986) Characterization of the phosphoenolpyruvate carboxykinase (GTP) promoter-regulatory region. *J Biol Chem* 261:9721-9726.
- 225-Silberberg, R. (1986) The skeleton in diabetes mellitus: a review of the literature. *Diabetes Res* 3:329-338.
- 226-Silverton, S. F. and Mesaros, S. (1975) Osteoclast radical interactions: NADPH causes pulsatile release of NO and stimulates superoxide production. *Endocrinology*, 136:5244-5247.
- 227-Simpson, H. C. R., Sturley, R., Stirling, C. A. and Reckles, J. P. D. (1990) Combination of insulin with glipizide increases peripheral glucose disposal in secondary failure type 2 diabetic patients. *Diabet Med* 7: 143-147.
- 228-Slieker, L. J., Roberts, E. F., Shaw, W. N. and Johnson, W. T. (1990) Effect of streptozotocin-induced diabetes on insulin-receptor tyrosine kinase activity in obese zucker rats. *Diabetes* 39: 619-625.
- 229-Sokoloff, L. (1985) Endemic forms of osteoarthritis. *Clin Rheum Dis* 11:187-212.
- 230-Souness, J. E., Stouffer, J. E. and Chagoya de Sanchez, V. (1983) The effects of selenium deficiency on rat fat cell glucose oxidation. *Biochem J* 214:471-477.

- 231-Spalohlz, J. E. (1994) On the nature of selenium toxicity and carcinostatic activity. *Free Rad Biol Med* 1 45-64.
- 232-Stapleton, S. R., Mitchell, D. A., Salati, L. M. and Goodridge, A. G. (1990) Triiodothyronine stimulates transcription of the fatty acid synthase gene in chick embryo hepatocytes in culture. *J Biol Chem* 265:18442-18446.
- 233-Stapleton, S. R., Garlock, G. L., Foellmi-Adams, L. and Kletzien, R. E. (1997) Selenium potent stimulator of tyrosyl phosphorylation and activator of MAP kinase. *Biochim Biophys Acta* 1355:259-260.
- 234-Stapleton, S. R. (2000) Selenium: an insulin-mimetic. *Cellul Molec Life Sci* 57:1874-1879.
- 235-St Germain, D. L. and Galton, V. A. (1997) The deiodinase family of selenoproteins. *Thyroid* 7:655-668.
- 236-Strout, H. V., Vicario, P. P., Biswas, C., Saperstein, R., Brady, E. J., Pilch, P. F. and Berger, J. (1990) Vanadate treatment of streptozotocin diabetic rats restores expression of the insulin-responsive glucose transporter in skeletal muscle. *Endocrinology*. 126:2728-2732.
- 237-Stuart, B. (1997) In: *Biological Applications of Infrared Spectroscopy*. Chapters 1 and 2. Ando, D. J. (Ed.), John Wiley and Sons, Ltd., England.
- 238-Suetens, C., Moreno-Reyes, R., Chasseur, C., Mathieu, F., Begaux, F., Haubrûge, E., Durand, M. C., Nève, J. and Vanderpas, J. (2001) Epidemiological support for a multifactorial aetiology of Kashin-Beck disease in Tibet. *International Orthopaedics* 25:180-187.
- 239-Suzuki, H., Hayakawa, M., Kobayashi, K., Takiguchi, H. and Abiko, Y. (1997) H₂O₂-derived free radicals treated fibronectin substratum reduces the bone nodule formation of rat calvarial osteoblast. *Mech Ageing Dev* 98:113-125.
- 240-Szalontai, B., Nishiyama, Y., Gombos, Z. and Norio, M. (2000) Membrane dynamics as seen by Fourier transform infrared spectroscopy in a cyanobacterium, *Synechocystis PCC 6803*. The effects of lipid unsaturation and the protein-to-lipid ratio. *Biochimica et Biophysica Acta* 1509: 409-419.
- 241-Tamayo, R., Goldman, J., Villanneva, A., Walczak, N., Whitehouse, F. and Parfitt, M. (1981) Bone mass and bone cell function in diabetes. *Diabetes* 30 Suppl.1:31A.

- 242-Tawardowska-Saucha, K., Grzeszczak, W., Lacka, B., Froehlich, J. and Krywult, D. (1994) Lipid peroxidation, antioxidant enzyme activity and trace element concentration in II and III trimester of pregnancy in pregnant women with diabetes. *Pol Arch Med Women* 92:313–321.
- 243-Taylor, M. G., Parker, S. F., Simkiss, K. and Mitchell, P. C. H. (2000) Inelastic neutron scattering of bone. Highlights of ISIS Science: www.isis.rl.ac.uk/isis2000/highlights/boneScatteringH14.htm.
- 244-Terada, M., Inaba, M., Yano, Y., Hasuma, T., Nishizawa, Y. Morii; H. and Otani, S. (1998) Growth-inhibitory effect of a high glucose concentration on osteoblast-like cells. *Bone* 22:17-23.
- 245-Termine, J. D., Eanes, E. D., Greenfield D. J. and Nylen M. U. (1973) Hydrazine deproteinated bone mineral. *Calcif Tissue Res* 12:73-90.
- 246-Termine, J. D. and Robey, P. G. (1996) Bone matrix proteins and the mineralization process. In:Primer on the Metabolic Bone Diseases and Disorders of Mineral Metabolism, Favus, M. J. (ed.) 3rd edit. An Official Publication of the American Society of Bone and Mineral Research. Lippincott-Raven Publishers, New York, N, USA, pp.24-28.
- 247-Thompson, D. D., Posner, A. S., Laughlin, W. S. and Blumenthal N. C.(1983) Comparison of bone apatite in osteoporotic and normal Eskimos. *Calcif Tissue Int.* 35:392-393.
- 248-Tinggi, U. (2003) Essentiality and toxicity of selenium and its status in Australia: a review. *Toxicology letters* 137:103-110.
- 249-Tomlinson, K. C., Gardiner, S. M., Hebden, R. A. and Bennett, T. (1992) Functional consequences of streptozotocin-induced diabetes mellitus, with particular reference to the cardiovascular system. *Pharmacol Rev.* 44:103-150.
- 250-Toyran, N., Zorlu, F., Dönmez, G., Öge, K. and Severcan, F. (2004) Chronic hypoperfusion alters the content and structure of proteins and lipids of rat brain homogenates: a Fourier transform infrared spectroscopy study. *Eur Biophys J* (in press).
- 251-Turan, B., Desilets, M., Açı̄an, L. N., Hotamaroğlu, Ö., Vannier, C. and Vassort, G. (1996) Oxidative effects of selenite on rat ventricular contractility and Ca movements. *Cardiovasc Res* 32:351-361.

- 252-Turan, B., Balçık, C. and Akkaş, N. (1997a) Effect of dietary selenium and vitamin E on the biomechanical properties of rabbit bones. Clinical Rheumatol 16:441-449.
- 253-Turan, B., Koç, E. and Zaloğlu, N. (1997b) Deficiency and toxicity of selenium alter the acetylcholine stimulated contraction of isolated rabbit ileum. Trace Elem Electrolytes 14:13-18.
- 254-Turan, B., Zaloğlu, N., Koç, E., Saran, Y. and Akkaş, N. (1997c) Dietary selenium and vitamin E induced alterations in some rabbit tissues. Biol Trace Elements Res 58:237-253.
- 255-Turan, B., Hotamaroğlu, Ö., Kılıç, M. and Yılmaz, E. D. (1999) Cardiac dysfunction induced by low and high diet antioxidant levels comparing selenium and vitamin E in rats. Regulatory Tox Pharmacol 29:142-150.
- 256-Turan, B., Bayarı, S., Balçık, C., Severcan F. and Akkaş, N. (2000) A Biomechanical and spectroscopic study of bone from rats with selenium deficiency and toxicity. Biometals 13:113-121.
- 257-Turan, B., Can, B. and Delilbaşı E. (2003) Selenium combined with vitamin E and vitamin C restores structural alterations of bones in heparin-induced osteoporosis. Clin Rheumatol. 22:432-436.
- 258-Umemura, J., Cameron, D., G. and Mantsch, H., H. (1980) A Fourier-transform infrared spectroscopic study of the molecular interaction of cholesterol with 1,2-dipalmitoyl-sn-glycero-3-phosphocholine. Biochim Biophys Acta 602:32-44.
- 259-Veis, A. (1997) Collagen fibrillar structure in mineralized and nonmineralized tissues Current Opin Solid State Mater Sci 2:370-378.
- 260-Verhaeghe, J., Bouillon, R., Lissens, W., Visser, W. J. and Van Assche, F. A. (1988) Diabetes and low Ca-P diet have opposite effects on adult and fetal bone mineral metabolism. Am J Physiol 254:E496-E504.
- 261-Verhaeghe, J., Suiker, A. M. H., Nyomba, B. L., Visser, W. J., Einhorn, T.A., Dequeker, J. and Bouillon, R. (1989) Bone mineral homeostasis in spontaneously diabetic BB rats. II. Impaired bone turnover and decreased osteocalcin synthesis. Endocrinology 124:573-582.

- 262-Verhaeghe, J. Van Herck, E. Visser W. J., Suiker, A. M. H., Thomassel, M., Einhorn, T. A. Faierman, E. and Bouillon, R. (1990) Bone and mineral metabolism in BB rats with long-term diabetes: decreased bone turnover and osteoporosis. *Diabetes* 39:477-482.
- 263-Verhaeghe, J., Suiker, A. M. H., Van Bree, R. Van Herck, E., Jans, L., Visser, W. J. Thomasset, M., Allewaert, K. and Bouillon, R. (1993) Increased clearance of 1,25-(OH)₂D₃ and tissue-specific responsiveness to 1,25-(OH)₂D₃ in diabetic rats. *Am J Physiol* 265:E215-E223.
- 264-Wagle, A., Jivraj, S., Garlock, G. and Stapleton, S. R. (1998) Insulin regulation of glucose-6-phosphate dehydrogenase gene expression is rapamycin sensitive and requires phosphatidylinositol 3-kinase. *J Biol Chem* 273:14968-14974.
- 265-Wagner, H. D. and Weiner, S. (1992) On the relationship between the microstructure of bone and its mechanical stiffness. *J Biomech*.25:1311-1320.
- 266-Walters, M. A., Leung, Y. C., Blumenthal, N. C., LeGeros, R. Z. and Konsker, K. A. (1990) A raman and infrared spectroscopic investigation of biological hydroxyapatite. *J Inorganic Biochemistry* 39:193-200.
- 267-Wang, W. C., Makela, A. L., Nanto, V. and Makela, P. (1995) Serum selenium levels in diabetic children. A followup study during selenium-enriched agricultural fertilization in Finland. *Biol Trace Elem Res* 47:335-364.
- 268-Watkins, B. A., Yong, L., Rogers, L. L., Hoffmann, W. E., Iwakiri, Y., Allen, K. G. D. and Seifert M. F. (2001) Effect of red palm olein on bone tissue fatty acid composition and histomorphometric parameters. *Nutrition Research* 21:199-213.
- 269-Watrous, D., A. and Andrews, B. S. (1989) The metabolism and immunology of bone. *Seminars in Arthritis and Rheumatism*, 19:45-65.
- 270-Weinger, J. M. and Holtrop, M. E. (1974) An ultrastructural study of bone cells: The occurrence of microtubules, microfilaments and tight junctions. *Calcif Tissue Res* 14:15-29.
- 271-Wiske, P. S., Wentworth, S. M., Norton, J. A., Epstein, S. and Johnston, C. C. (1982) Evaluation of bone mass and growth in young diabetics. *Metabolism* 31:848-854.

272-Wood, R. J., Alien, L. H. and Bronner, F. (1984) Regulation of calcium metabolism in streptozotocin-induced diabetes. *Am J Physiol* 247:R120-R123.

273-www.biologycorner.com/bio3/rat_external.html.

274-Xu, H., Watkins, B. A. and Seifert, M. F. (1995) Vitamin E stimulates trabecular bone formation and alters epiphyseal cartilage morphometry. *Calcif Tissue Int* 57:293-300.

275-Yamauchi, M. (1996) Collagen: The major matrix molecule in mineralized tissues. In: Calcium and Phosphorus in Health and Disease. Anderson, J. J. B. and Garner, S. C. (eds); CRC Press, New York, NY, USA, pp.127-141.

276-Yang, C., Niu, C., Bodo, M., Gabriel, E., Notbohm, H., Wolf, E. and Muller, P. K. (1993a) Fulvic acid supplementation and selenium deficiency disturb the structural integrity of mouse skeletal tissue. An animal model to study the molecular defects of Kashin-Beck disease. *Biochemical J* 289:829-835.

277-Yang, C., Wolf, E., Roser, K., Delling, G. and Muller, P. K. (1993b) Selenium deficiency and fulvic acid supplementation induces fibrosis of cartilage and disturbs subchondral ossification in knee joints of mice: an animal model study of Kashin-Beck disease. *Virchows Arch A Pathol Anat Histopathol* 423:483-491.

278-Yang, S., Ries, W. L., and Key, Jr, L. L. (1998) NADP oxidase in the formation of superoxide in osteoclasts. *Calcif Tissue Int* 63:346-350.

279-Yono, K., Ohoshima, S., Shimuzu, Y., Moriguchi, T. and Katayama, H. (1996) Evaluation of glycogen level in human lung carcinoma tissues by an infrared spectroscopic method. *Cancer Letters* 110:29-34.

280-Young, J. D., Crowley, C. and Tucker, E. M. (1981) Haemolysis of normal and glutathione-deficient erythrocytes by selenite and tellurite. *Biochem Pharmacol* 30:2527-2530.

281-Ytrehus, K., Ringstad, J., Myklebust, R., Norheim, G. and Mjos, O. D. (1988) The selenium-deficient rat heart with special reference to tolerance against enzymatically generated oxygen radicals. *Scand J Clin Lab Invest* 48:289-295.

CURRICULUM VITAE

Name, Surname: Handan BOYAR

Date of Birth : 16.05.1970

Place of Birth : İstanbul, TURKEY

Address: Başbakanlık DPT ABEGPM Hüseyin Rahmi Sok. No: 2
06680 Çankaya / Ankara / TURKEY

Telephone: +90 312 409 61 37 **e-mail:** hboyar@ua.gov.tr

Education:

Ph.D. : June **2004**- Middle East Technical University, Department of Biology, Ankara, Turkey. Thesis title: "*Biophysical investigation of the effects of antioxidants on normal and diabetic rat bone tissues at molecular level.*"

M.S. : August, **1995**, Middle East Technical University, Department of Biology, Ankara, Turkey. Thesis title: "*Interaction of estrogen and tamoxifen with phospholipid membranes: An FTIR study*"

B.S. : July, **1992**, Middle East Technical University, Department. of Biology, Ankara, Turkey.

High School: **1987**, Kırıkkale High School, Kırıkkale, Turkey.

Work Experience:

01.04.2004- State Planning Organisation European Union Education and Youth Programmes Center (EU EYPC), Youth Department; enrolled as Action 2 European Voluntary Service Specialist.

27.09.2000-01.04.2004 Ministry of National Education (MNE), Education Research and Development Directorate (ERDD), Department of Project; enrolled in implementation of the following international student assessment projects:

1-Third International Mathematics and Science Study-Repeat (TIMSS-R, 1999) and **2**-Progress in International Reading Literacy Study (PIRLS, 2000-2001) carried out by International Organization of Education for Student Assessment (IEA).

3- Program of International Student Assessment (PISA, 2002-2003) project carried out by OECD.

She was responsible for: i) translation of test booklets and questionnaires used in these projects, ii) preparation of test booklets and questionnaires for publication at computer media, iii) application of tests and questionnaires at schools, iv) coordination of marking processes of constructed response items, v) data entry and data cleaning.

06.07.1998-27.09.2000 Science and English item writer for national student assessment projects implemented by MNE, ERDD, Department of Measurement and Evaluation.

01.05.2000-01.04.2004 English Teacher at Distance Education High School, MNE, General Directorate of Education Technology.

06.11.1992 - 01.05.2000 English Teacher at MNE, Ankara Gaziçiftliği High School.

International meetings she attended:

A-Meetings related with her academic studies:

- 1) 12-15 October, 2003, Kuşadası, Aydın, **TURKEY**, 13th Balkan Biochemical, Biophysical Days and Meeting on Metabolic Disorders.
- 2) 7-12 September, 2003, Granada, **SPAIN**, Colloquium Spectroscopicum Internationale CSI XXXIII.
- 3) 5-8 July, 2003, London, **U.K.** Second International Conference on Biomedical Spectroscopy.
- 4) 7-10 July 2002, Cardiff, WALES, **U. K.** First International Conference on Biomedical Spectroscopy: From Molecules to Men.
- 5) 10-13 May, 2001, Bucharest, **ROMANIA**, 12th Balkan Biochemical, Biophysical Days.

B- Meetings related with her studies in MNE, ERDD:

- 1) 1-5 March, 2004, Athens, **GREECE**; OECD PISA-2006 1st National Project Managers meeting
- 2) 16-22 February, 2003, Madrid, **SPAIN**; OECD PISA-2003 National Project Managers meeting and seminar for marking of constructed response items used in PISA-2003 Main Survey.
- 3) 8-12 December, 2002, İstanbul, **TURKEY**; IEA-PIRLS-2001 Project, 8th National Research Coordinators Meeting.
- 4) 17-23 February, 2002, Salzburg, **AUSTRIA**; OECD PISA National Project Managers meeting and seminar for marking of constructed response items used in PISA2003 Field Trial.
- 5) 20-27 May, 2001, Budapest, **HUNGARY**; IEA-PIRLS-2001 National Project Managers meeting and seminar for marking of constructed response items used in PIRLS 2001 Main Survey.

Academic Studies

A) Publications:

1-Handan Boyar, Faruk Zorlu, Melike Mut and Feride Severcan “The effects of chronic hypoperfusion on rat cranial bone mineral and organic matrix: A Fourier transform infrared spectroscopy study. Anal Bioanal Chem **2004**, 379:433-438.

2-Handan Boyar, Belma Turan and Feride Sevencan “FTIR spectroscopic investigation of mineral structure of streptozotocin induced diabetic rat femur and tibia”. Spectroscopy: An International Journal **2003**, 17: 627-633.

3-Handan Boyar and Feride Sevencan “Tamoxifen-model membrane interactions: An FTIR study” Journal of Molecular Structure, **1997**, 408/409: 265-268.

4-Handan Boyar and Feride Sevencan, “Oestrogen-Phospholipid Membrane Interactions: An FTIR study” Journal of Molecular Structure, **1997**, 408/409: 269-272.

5-Feride Sevencan, Erhan Süleymanoğlu and **Handan Boyar** “Turbidity studies of the effect of divalent cations on tamoxifen-model membrane interactions” Biochemical Society Transactions, **1997**, 25, S493.

6-Handan Boyar, Sevgi Bayarı, Feride Sevencan and Belma Turan, “Investigation of the effect of selenium-vitamin E deficiency and selenium excess on bone tissue by Fourier transform infrared spectroscopy.” (Turkish title: Selenyum-vitamin E eksikliğinin ve selenyum fazlalığının kemik doku üzerindeki etkisinin Fourier transform kızıl ötesi (FTIR) spektroskopı teknigi ile incelenmesi.) XIIth National Biophysics Congress (7-9 September, 2000) Panel, Conferences and Presentations Booklet, 6 pages, **2000**.

B) Presentations

I- Oral Presentations

1- Handan Boyar and Feride Sevencan “*Interaction of oestrogen-tamoxifen-phospholipid membrane*”(Turkish title: Östrojen-tamoksifen-fosfolipid membran etkileşmesi.) VIIIth National Biophysics Congress, 26-28 September **1996**, Gebze, Kocaeli, **TURKEY**.

2- Handan Boyar and Feride Sevencan., “*FTIR investigation of interaction of oestrogen with model cell membrane*”(Turkish title: Östrojenin model hücre membranı ile etkileşmesinin FTIR ile incelenmesi.) VIIth National Biophysics Congress, 11-13 October, **1995**, Balcalı, Adana, **TURKEY**.

3-Handan Boyar and Feride Sevencan “*FTIR investigation of interaction of tamoxifen with model cell membrane*” (Turkish title: Tamoksifenin model hücre membranı ile etkileşmesinin FTIR ile incelenmesi.) VIIth National Biophysics Congress, 11-13 October, **1995**, Balcalı, Adana, **TURKEY**.

II-Poster Presentations

II-A) Posters Presented at International Meetings

1- Neslihan Toyran, **Handan Boyar**, Faruk Zorlu, Melike Mut and Feride Sevencan “*FTIR spectroscopic analysis of chronic hypoperfusion on rat brain and cranial bone proteins.*” 13th BBB (Balkan Biochemical Biophysical Days) and Meeting on Metabolic Disorders, 12-15 October, **2003**, Kuşadası, Aydin, **TURKEY**.

2- Handan Boyar, Faruk Zorlu, Melike Mut and Feride Severcan “*The effects of chronic hypoperfusion on rat cranial bone mineral and organic matrix: A Fourier transform infrared spectroscopy study*” Colloquium Spectroscopicum Internationale, CSI XXXIII, 7-12 September, **2003**, Granada, **SPAIN**.

3- Handan Boyar and Feride Severcan “*Temperature induced effect of 17 β -estradiol at low and high concentrations, on phospholipid model membranes: An FTIR study*” Second International Conference on Biomedical Spectroscopy, 5-8 July, **2003**, London, **U.K.**

4- Handan Boyar, Belma Turan and Feride Severcan “*FTIR spectroscopic investigation of the effects of selenium on streptozotocin induced diabetic rat femur and tibia in the C-H stretching region*” Second International Conference on Biomedical Spectroscopy, 5-8 July, **2003**, London, **U.K.** (**Awarded as the 2nd poster in the best poster competition.**)

5- Handan Boyar, Belma Turan and Feride Severcan “*Investigation of the effects of selenium on streptozotocin induced diabetic rat femur by x-ray diffraction and FTIR spectroscopic analysis*” First International Conference on Biomedical Spectroscopy: From Molecules to Men. 7-10 July, **2002**, Cardiff, **Wales, U.K.**

6- Handan Boyar, Sevgi Bayarı, Belma Turan and Feride Severcan “*Detailed spectroscopic analysis of phosphate and carbonate bands in FTIR spectra of bones of rats fed with selenium and vitamin E deficient diet.*” 20th International Physics Congress, 10-13 September, **2001**, Bodrum, Muğla, **TURKEY**.

7- Handan Boyar, Belma Turan and Feride Severcan “*Comparison of streptozotocin-induced diabetic and control rat bones by Fourier transform infrared spectroscopy*” 12th Balkan Biochemical Biophysical Days (BBBD), 10-13 May, **2001**, Bucharest, **ROMANIA**.

8- Sevgi Bayarı, Handan Boyar, Belma Turan and Feride Severcan “*The effect of selenium-vitamin E deficiency and selenium excess on bone mineral and amide matrix, measured by Fourier transform infrared spectroscopy.*” XXV EUCMOS, European Congress on Molecular Spectroscopy, 27 August-1 September, **2000**, Coimbra, **PORTUGAL**.

9- Can. Ali.Yücesoy, Handan Boyar, Mehmet Uğur, Belma Turan, Feride Severcan and Nuri Akkaş “*Biomechanical and spectroscopical investigations of streptozotocin-induced diabetic rat bones*” Federation of European Physiological Society Meeting, 29 June-4 July, **1999, Prague, **CZECH REPUBLIC**.**

10- Handan Boyar and Feride Severcan “*Tamoxifen-model membrane interactions: An FTIR study*” EUCMOS XXIII European Congress on Molecular Spectroscopy, 25-30 August, **1996, Balatonfüred, at the lake Balaton, **HUNGARY**.**

11- Handan Boyar and Feride Sevencan “Concentration and temperature induced effect of 17- β estradiol on phospholipid model membranes: An FTIR study” EUCMOS XXIII European Congress on Molecular Spectroscopy, 25-30 August, **1996**, Balatonfüred, at the lake Balaton, **HUNGARY**.

12-. Feride Sevencan, Erhan Süleymanoğlu and **Handan Boyar** “Turbidity studies of the effect of divalent cations on the thermotropic phase behaviour of phospholipid model membranes containing tamoxifen” EUCMOS XXIII European Congress on Molecular Spectroscopy, 25-30 August, **1996**, Balatonfüred, at the lake Balaton, **HUNGARY**.

II-B) Posters Presented at National Meetings

1- Handan Boyar, Belma Turan and Feride Sevencan “FTIR spectroscopic investigation of the effects of selenium on diabetic rat bones in the C-H stretching region” (Turkish title: Selenyumun diyabetik sıçan kemikleri üzerindeki etkilerinin FTIR spektroskopisi ile C-H gerilme bölgesinde incelenmesi.) XVth National Biophysics Congress, 8-12 October, **2003**, Pamukkale University, Denizli, **TURKEY**.

2- Handan Boyar, H. Kamil Öge, Faruk Zorlu and Feride Sevencan “Investigation of the effects of hypoperfusion and stereotactic radiosurgery, which is used for therapy, on rat cranial bones by FTIR spectroscopy technique” (Turkish title: Hipoperfüzyonun ve tedavi amaçlı kullanılan stereotaktik radyocerrahinin sıçan kafatası kemiği dokusundaki etkilerinin FTIR spektroskopisi tekniği ile incelenmesi.) XIVth National Biophysics Congress, 4-6 September, **2002**, Gülhane Military Medicine Academy, Ankara, **TURKEY** (**Awarded as the 3rd poster in the best poster competition**).

3- Handan Boyar, Belma Turan and Feride Sevencan “X-ray diffraction and detailed Fourier transform infrared spectroscopic analysis of streptozotocin-induced diabetic rat bones” (Turkish title: Streptozotocin ile induklenmiş diyabetli sıçan kemiklerinin x-işını kirinimi ve detaylı Fourier transform infrared spectroskopik analizi.) XIIIth National Biophysics Congress, 5-7 September, **2001**, Osmangazi University, Eskişehir, **TURKEY**.

4- Handan Boyar, Sevgi Bayarı, Belma Turan and Feride Sevencan “Investigation of the effects of selenium-vitamin E deficiency and selenium excess on rat bones by Fourier transform infrared spectroscopy.” (Turkish title: Selenyum-vitamin E eksikliğinin ve selenyum fazlalığının kemik doku üzerindeki etkisinin Fourier transform kızıl ötesi (FTIR) spektroskopisi tekniği ile incelenmesi.) XIIth National Biophysics Congress, 7-9 September **2000**, Silivri, İstanbul, **TURKEY** (**Awarded as the 2nd poster in the best poster competition**).

5- Feride Severcan, **Handan Boyar**, Neslihan Toyran, Belma Turan and Faruk Zorlu “The investigation of the effect of disease and radiation on bone and soft tissues of rat by Fourier transform infrared spectroscopy.” (Turkish title: Hastalık ve radyasyon gibi faktörlerin sıçan kemik ve yumuşak dokularındaki etkilerinin FTIR spektroskopisi ile incelenmesi.) VIIth National Medical Physics Congress, 11-13 November **1999**, Dokuz Eylül University, İzmir, **TURKEY**.

6- Selçuk Muratoğlu, Fatma Eker, **Handan Boyar** and Feride Severcan “Investigation of the interaction of oestrogen and progesteron with phospholipid model membranes.” (Turkish title: Östrojen ve progesteronun fosfolipid model membranlar ile etkileşmesinin incelenmesi.) IXth National Biophysics Congress, 5-6 September **1997**, Middle East Technical University, Ankara, **TURKEY** (**Awarded as the 3rd poster in the best poster competition**).

Citations for her publications

I- **Handan Boyar** and Feride Severcan *Oestrogen-Phospholipid Membrane Interactions: An FTIR Study* Journal of Molec Structure, 408/409:269-272, **1997**.

Cited by:

1-Severcan, F., Kaptan, N. and Turan, B. “Fourier Transform Infrared Spectroscopic Studies of Diabetic Rat Heart Crude Membranes” Spectroscopy:An International Journal (**2003**) 17:569-577.

2-Severcan, F., Kazancı, N. and Zorlu, F. “ Tamoxifen Increases Membrane Fluidity at High Concentrations ” Bioscience Reports **2000**, 20: (3) 177-184.

3-Severcan, F., Durmuş, H. O., Eker, F., Akinoğlu, B. G. and Haris, P. I. "Vitamin D₂ Modulates Melittin-Membrane Interactions" Talanta, **2000**, 53: (1) 205-211.

4- Shumilina, E. V., Khromova, Y. L. and Shchipunov, Y. A., "A Study of the Structure of Lecithin Organic Gels by Fourier Transform IR Spectroscopy" Russian Journal of Physical Chemistry, **2000**, 74: (7) 1083-1092.

5- Dicko, A., Morissette, M., Ben Amur, S., Pezolet, M. and Di Paola, T. "Effect of Estradiol and Tamoxifen on Brane Membranes: Investigation by Infrared and Fluorescence Spectroscopy." Brain Research Bulletin, **1999**, 49: (6) 401-405.

6- Institut für Analytische Chemie, Year Overview 1997, **Trend Report: Infrared and Raman Spectroscopy 1997** <http://analyt.chm.tu-dresden.de/analyt/english/forschung/jahr97k.html>

II- Handan Boyar and Feride Sevencan *Tamoxifen-Model Membrane Interactions: An FTIR Study*" Journal of Molecular Structure, **1997**, 408/409:265-268.

Cited by:

- 1-** Engelke, M., Tykhnova, S., Zorn-Kruppa M, Diehl, H. "Tamoxifen Induces Changes in the Lipid Composition of the Retinal Pigment Epithelium Cell Line D407." Pharmacology and Toxicology **2002**, 91(1):1.
- 2-** Engelke, M., Bojarski, P., BloB, R. and Diehl, H. " Tamoxifen Perturbs Lipid Bilayer Order and Permeability: Comparison of DSC, Fluorescence Anisotropy, Laurdan Generalized Polarization and Carboxyfluorescein Leakage Studies" Biophysical Chemistry **2001**, 90:157-173.
- 3-** Sevencan, F., Kazancı, N. and Zorlu, F. "Tamoxifen Increases Membrane Fluidity at High Concentrations" **2000**, 20: (3) 177-184.
- 4-** Dicko, A., Morissette, M., Ben Amur, S., Pezolet, M. and Di Paola T., "Effect of Estradiol and Tamoxifen on Brane Membranes: Investigation by Infrared and Fluorescence Spectroscopy." Brain Research Bulletin, **1999**, 49: (6) 401-405.

III- Handan Boyar, Belma Turan and Feride Sevencan "FTIR spectroscopic investigation of mineral structure of streptozotocin induced diabetic rat femur and tibia". Spectroscopy: An International Journal **2003**, 17: 627-633.

Cited by:

- 1-Handan Boyar**, Faruk Zorlu, Melike Mut and Feride Sevencan "The effects of chronic hypoperfusion on rat cranial bone mineral and organic matrix: A Fourier transform infrared spectroscopy study. Anal Bioanal Chem **2004**, 379:433-438.